METABOLIC ENGINEERING OF *ESCHERICHIA COLI* ATCC 8739 FOR PRODUCTION OF BIOELECTRICITY

By

JONATHAN C. MOORE

A DISSERTATION PRESENTED TO THE GRADUATE SCHOOL
OF THE UNIVERSITY OF FLORIDA IN PARTIAL FULFILLMENT
OF THE REQUIREMENTS FOR THE DEGREE OF
DOCTOR OF PHILOSOPHY

UNIVERSITY OF FLORIDA

2009

To Negarre and Murv Moore

ACKNOWLEDGMENTS

I thank my family for their encouragement and support and Dr. Lonnie Ingram and the other members of my Supervisory Committee for their guidance. I also thank members of the Ingram Lab, past and present, for their helpful discussions. I am indebted to Dr. Xuan Wang for his helpful comments and suggestion during preparation of this manuscript. I thank Dr. Andrew Rinzler and Dr. Zhuangchun Wu for providing the single-walled carbon nanotubes and the micro-scale carbon fibers for our study and for their collaboration on microbial fuel cell electrode optimization. I am grateful for the assistance of Ms. Marjorie Chow and of Dr. Matthew Humbard with the proteomic comparisons. I thank Dr. Donald Court of the National Cancer Institute for the gift of plasmid pEL04 and Dr. Linda Thony-Meyer for the gift of pEC86. I thank Dr. Robert H. Fillingame of the University of Washington for the kind gift of antisera.

TABLE OF CONTENTS

page

LIST OF TABLES

LIST OF FIGURES

LIST OF ABBREVIATIONS

α-KGDH	alpha-ketoglutarate dehydrogenase
ACK	acetate kinase
ADP	adenosine diphosphate
AMP	adenosine monophosphate
ArcA-P	phosphorylated response regulator of redox-sensitive two-component system
ATP	adenosine triphosphate
BCA	bicinchoninic acid
BCIP	bromochloroindolyl phosphate
BEC	bulk electrolysis cell
cAMP-CRP	cyclic AMP-catabolism repressor protein
C_E	Coulombic efficiency
CF	carbon fiber
CoA	coenzyme A
DCM	dry cell mass
DMRB	dissimilatory metal-reducing bacteria
DMSO	dimethyl sulfoxide
d-NADH	deamino-nicotinamide adenine dinucleotide (reduced)
EC	electrochemical cell
EMP	Embden-Meyerhoff Pathway
ETS	electron transport system
FNR	transcriptional regulator named for role in fumarate and nitrate reduction
FRT	FLP recombinase recognition target
HGA	homogentisic acid
H-NS	histone-like nucleoid structuring protein

HPLC	high pressure liquid chromatography
KCN	potassium cyanide
MB	methylene blue
MFC	microbial fuel cell
MOPS	4-morpholinopropanesulphonic acid
MtrA	periplasmic cytochrome *c*
MtrB	outer membrane protein associated with OmcA and MtrC
MtrC	outer membrane cytochrome *c*
MV	membrane vesicle
$NADH/NAD^+$	nicotinamide adenine dinucleotide (reduced/oxidized)
NapC	cytoplasmic (cytochrome *c*) subunit of periplasmic nitrate reductase
NBSM	New Brunswick Scientific MOPS mineral salts medium
NBT	nitro blue tetrazolium
NDH	NADH dehydrogenase
NOX	NADH oxidase
OM	outer membrane
OmcA	outer membrane cytochrome *c*
PCR	polymerase chain reaction
PDH	pyruvate dehydrogenase
PMF	proton motive force
PTA	phosphotransacetylase
PTFE	polytetrafluoroethylene
PVDF	polyvinylidene fluoride
RVC	reticulated vitreous carbon
SDS-PAGE	sodium dodecyl sulfate polyacrylamide gel electrophoresis

SS	stator stalk of the F_1F_O ATP synthase
T2SS	type II secretion system
TCA	tricarboxylic acid cycle
TMAO	trimethylamine N-oxide
TMPD	N,N,N',N'-tetramethyl-phenylenediamine
v_{redMB}	specific rate of methylene blue reduction

Abstract of Dissertation Presented to the Graduate School
of the University of Florida in Partial Fulfillment of the
Requirements for the Degree of Doctor of Philosophy

METABOLIC ENGINEERING OF *ESCHERICHIA COLI* ATCC 8739 FOR PRODUCTION OF BIOELECTRICITY

By

Jonathan Moore

December 2009

Chair: Lonnie O. Ingram
Major: Microbiology and Cell Science

Escherichia coli ATCC 8739 was genetically engineered to increase electric current and Coulombic yield from glucose in a microbial fuel cell (MFC). Initial testing of strains was done using aerobic batch cultures. Deletion of genes for the ATP synthase stator stalk (*atpFH*) resulted in a 44% increase in rate of glucose utilization. With the higher rate of glucose catabolism, NADH reoxidation by the electron transport system (ETS) became limiting, despite increased levels of ETS proteins. The change in redox ratio led to acetate production as part of an overflow metabolism. To increase the rate of NADH oxidation and to minimize acetate production, *ackA* (encoding acetate kinase) was replaced by *naoX* from *Streptococcus mutans*, encoding a cytoplasmic, water-forming NADH oxidase. The *arcA* gene was deleted to remove redox sensitive controls. These modifications enabled the complete oxidation of glucose in aerobic cultures. In a poised potential MFC with a chemical mediator, the maximum current produced by the engineered strain JC93 was 19% higher than the wild type, with a Coulombic efficiency (percent theoretical yield of electrons) of 76% (versus 49% for wild type). The *arcA* deletion did not significantly affect current or Coulombic efficiency. However, deletion of *arcA* in an $naoX_{Sm}^{+}$ background increased flux through the tricarboxylic acid (TCA) cycle during aerobic glucose metabolism.

Genes (*omcA* and *mtrCAB*) encoding *c*-type cytochromes of the *Shewanella oneidensis* MR-1 extracellular ETS were integrated into the chromosome of the engineered strain. Heterologous expression of these genes was investigated to allow mediatorless MFC operation and to establish the minimal sufficient set for extracellular electron transfer. Current production by the *omcA-mtrCAB* integration strains was low and further study is required.

Successful optimization of the MFC biocatalyst is likely to shift the rate limiting steps back to the design of the MFC. An enhanced anode was designed to increase active surface area and decrease concentration overpotentials. The design incorporated single-wall carbon nanotubes and mixed-length carbon fibers and resulted in up to 3-fold higher average MFC current output. The practical adoption of MFC technology requires higher power densities, which can be achieved by combining MFC design optimization with biocatalyst improvement.

CHAPTER 1
INTRODUCTION

Bioelectricity

Electrical energy production from renewable feedstocks and organic wastes has great potential as a component of a comprehensive strategy to offset the use of fossil fuels. Microorganisms are capable of transforming the stored chemical energy in organic materials such as cellulosic biomass and animal wastes to useful electrical energy. The most direct and theoretically efficient strategy to harvest microbially derived electrical energy is the use of a microbial fuel cell (MFC). Other strategies include microbially catalyzed production of liquid biofuels, methane or hydrogen. All of these biofuels require additional steps to convert the stored energy to electricity, thus lowering the overall efficiency of the process. Alternately, the stored energy in biofuels may be used to do work through combustion. A thorough lifecycle analysis of biofuel production and combustion for transportation shows this process to be less efficient than direct combustion of biomass to supply an electrical infrastructure (18). Most abiotic transformations of biomass to electricity involve combustion and other significant process losses. Even the promising route to bioelectricity from gasification combined with solid oxide fuel cells (105), while avoiding the inefficiency of combustion, requires significant energy inputs. In the context of a global energy economy that is shifting towards increased efficiency and sustainability, the preferred process is one that is able to convert solar energy and waste streams to electrical energy most directly.

Most of the effort in MFC research has been focused upon MFC design optimization, extracellular electron transfer and the microbial ecology of consortia colonizing the electrodes of wastewater-fed MFCs. Substantial gains in MFC electrical power output have been made (1, 23, 141). However, few studies have reported attempts to complement these approaches with genetic

engineering of the MFC biocatalysts. No natural environments have been studied that are similar to that of an MFC. An ideal MFC biocatalyst is capable of rapidly and completely oxidizing any fuel and of efficiently transferring the liberated electrons to an electrode. While certain organisms have evolved to do some of these things well, no known ecological niche appears to select for all of the desired attributes. The greatest strength of genetic engineering is the ability to modify biocatalysts for tasks for which there has been no natural selection. Production of bioelectricity can only achieve its potential through metabolic optimization of the biocatalysts, in conjunction with MFC design efforts.

Microbial Fuel Cells

Microbial fuel cells employ microorganisms to convert stored chemical energy into useful electrical energy. The electrons liberated from the oxidation of organic material through the metabolic activity of these microbes are transferred to an anode in an MFC. The electrons flow through an external circuit across a load (such as a resistor, a motor, or a light) to the cathode, where they combine with an oxidant in the balancing half-cell reaction (Figure 1-1). Protons from the anodic reaction are conducted through the electrolyte and across a proton exchange membrane (or salt bridge, etc.) to the cathode, where they are reunited with the electrons in the cathode oxidation reaction. Figure 1-1 depicts a simple, two-chambered MFC using glucose as an electron donor. If the glucose is completely oxidized to CO_2 by the microbial biocatalyst in the anode chamber, the anode half-cell reaction would be:

$$C_6H_{12}O_6 + 6H_2O \rightarrow 6CO_2 + 24H^+ + 24e^- \quad (1\text{-}1)$$

If oxygen was used as the oxidant in the cathode half-cell reaction (potassium ferricyanide is shown in the figure and is frequently used in laboratory experiments because of improved electrode kinetics) :

$$24e^- + 24H^+ + 6O_2 \rightarrow 12H_2O \quad (1\text{-}2)$$

The overall reaction in the MFC is the same as the one for the complete catabolism of glucose by a respiring cell:

$$C_6H_{12}O_6 + 6O_2 \rightarrow 6CO_2 + 6H_2O \quad (1\text{-}3)$$

Figure 1-1 shows a mediator (a diffusible electron carrier) carrying electrons from the bacterial inner membrane electron transport chain to the anode. MFCs reroute electrons from microbial metabolism through an external circuit to capture a portion of the stored energy in the fuel as electricity.

In heterotrophic organisms, the oxidation of organic material is coupled to storage of the released energy in high group-transfer potential compounds such as adenosine triphosphate (ATP). These compounds are subsequently used in cellular biosynthetic processes. This energy transformation involves the stepwise transfer of electrons up a reduction potential gradient to a terminal electron acceptor. This terminal electron acceptor can be an endogenous metabolite, as in fermentation, or an exogenous acceptor, in respiration. In an MFC, electrons can be transferred from the respiratory chain to the anode (as the terminal electron acceptor), or fermentation products may be oxidized by the anode. When electrons are captured from the respiratory chain, the transfer can be direct or indirect (via a soluble mediator). The soluble mediators involved in the indirect electron transfer can be endogenously produced or exogenous, supplied compounds.

Since the discovery of microbes that are capable of electron transfer to an electrode (electrode reducers) without requiring added mediators (59), most MFC studies have used mediatorless MFCs to avoid the expense and toxicity issues associated with the use of added mediators. Much of the research has focused on MFC design and the mechanisms of electron transfer. However, low power density is the greatest challenge for the widespread adoption of MFCs as a means of

sustainable energy transformation (24, 36). The largest remaining gains in MFC power density are to be made through studying and engineering of microbial metabolism (88) to increase the rate of electron transfer (current) as well as the conversion efficiency from the fuel.

History of MFC Research

M. C. Potter is generally recognized as publishing the first study of the microbially catalyzed production of electricity from organic material in 1911 (96). In that study, he measured the electrical potential developed from the fermentation of sugars by *Saccharomyces cerevisiae* and by *E. coli* in a simple electrochemical cell with platinum electrodes. While Potter's preliminary experiments provided a proof of concept, few subsequent MFC studies were published for over half a century. In the 1960s, several MFC studies were published including an article describing the operation of a methane-oxidizing bacterial fuel cell employing *Psuedomonas methanica* at the anode (122). In 1993, Allen and Bennetto studied redox dye-mediated MFCs using various bacterial strains and conditions (3). Kim *et al*. (59) revolutionized the field by describing a microbial fuel cell which used *Shewanella putrefaciens* (later changed to *S. oneidensis*) MR-1 to oxidize lactate with transfer of electrons to the electrode without the need for any added mediator. Many other microbes were subsequently found to be capable of this extracellular electron transfer. These organisms have been termed exoelectrogens (73). There is extensive but not complete overlap of the exoelectrogen group with the dissimilatory metal reducers, microorganisms capable of energy coupling electron transfer to metal oxides and oxyhydroxides.

MFC Design and Applications

All fuel cells share the same fundamental components: an anode, to which electrons from the fuel are transferred, a cathode, where the oxidation reaction occurs, and an electrolyte, which conducts positively-charged ions (cations) from the anode to the cathode for the completion of

the circuit. Electrons flow through the external circuit across the load to the cathode, but do not flow through an electrically insulating electrolyte polymer or membrane. MFCs are generally categorized as one or two-chambered. Biological fuel cells have aqueous anode chambers, whereas other fuel cells generally have solid electrolytes, sandwiched between the two electrodes. The liquid in the anode chamber (anolyte) of an MFC contains the nutrients required by the electron-providing microbes. It is kept anaerobic to prevent direct electron transfer to oxygen, which would decrease MFC power output and efficiency. Furthermore, many of the microbes used in MFCs are obligate anaerobes. The fuel (electron donor) is added to the anolyte, which may be stirred and operated in batch mode, or operated in flowthrough mode. Anaerobic conditions (and sometimes mixing) can be maintained by flowing gases such as argon or nitrogen/carbon dioxide into the anode chamber. A diffusible electron carrier (mediator) can be added to the anolyte, if necessary.

A two-chambered MFC (Figure 1-1) has separate cathode chamber that is generally filled with an aqueous catholyte. The catholyte contains the oxidant. The oxidant can be oxygen, or it can be a surrogate such as the potassium ferricyanide (Figure 1-1), frequently used because of its favorable electrode kinetics. The two compartments and their contents may be separated by an ion permeable membrane, such as the proton-permeable Nafion from DuPont, or simply by a salt bridge.

Single-chambered MFCs have an anode chamber and a direct air cathode. They commonly use a membrane electrode assembly, similar to those used in other types of fuel cells (68). The proton exchange membrane is laminated onto the cathode, which is exposed to the air outside the assembly. Single-chambered MFCs can also be membraneless. Membraneless MFCs are not separated from the anolyte by a membrane or a salt bridge. This design is made possible by the

unique properties of MFCs that use microbes that form a biofilm on the anode and do not require the addition of a mediator. Thus, electrons are primarily transferred to the anode and do not significantly decrease MFC efficiency by traveling to the cathode through the anolyte.

MFC design has focused upon maximizing Coulombic efficiency and power density. Coulombic efficiency (C_E, Eq. 1-4) is the percentage of total electrons in the fuel (theoretical Coulombic yield) that are recovered by the MFC (experimental Coulombic yield).

C_E = Coulombic yield (experimental)/ Coulombic yield (theoretical) (1-4)

The theoretical Coulombic yield from 1 mol glucose is 24 mol electrons (or 2.32×10^6 C, based upon Faraday's constant (Eq. 1-5)

$F = 96{,}485 \text{ C mol}^{-1}$ (1-5)

Experimental Coulombic yield is calculated by measuring current produced over time by the MFC with a known quantity of fuel added. Integration of the area under the peak gives the total charge transferred to the electrode, which can be divided by the theoretical value to give the C_E. The C_E of an MFC is never 100%, due to biological and non-biological losses. Microbial biosynthesis and cellular maintenance reactions can require reduced cofactors and therefore decrease MFC Coulombic yields. Any incomplete microbial fuel catabolism resulting in fermentation or other side products further decreases Coulombic yield. In addition, any diffusion of competing electron acceptors into the anode chamber (oxygen, nitrate, etc.) from the cathode chamber or from outside the MFC will result in a lower C_E. Therefore it is important to consider both the metabolic pathways used by the microbial biocatalyst and the MFC design when attempting to optimize electron recovery.

Total energy recovery by an MFC is ultimately more informative than C_E, because C_E neglects the potential difference between anode and cathode. The total MFC energy recovery is

the electrical energy produced as a percentage of the total energy content of the fuel (heat of combustion). MFC power integrated over time gives the MFC energy recovery, just as MFC current integrated over time provides the Coulombic yield. Power is the product of the potential difference (MFC voltage) and the current produced. As the primary focus of our study was on improvement of current production and of Coulombic yield through metabolic engineering of the microbial biocatalyst, a poised potential electrochemical cell was used for most of the experiments. With this type of system, MFC voltage and power output (and by extension, total energy recovered) are not considered.

As mentioned above, MFC power density is a critical factor for useful application of MFC technology. Power densities of MFCs have frequently been reported as a function of electrode surface area (W/m^2). Many studies have reported current densities (mA/m^2). The lack of convention has made direct comparison of MFC designs difficult. Some MFC researchers have agreed upon volumetric power (W/m^3) as the most useful measure of MFC power density (21, 71). Volumetric power takes into account most of the relevant factors involved in MFC operation, but notably ignores C_E and operational longevity. These are very important parameters, as they constitute the primary advantages that MFC offer over enzymatic fuel cells, for example (along with lower cost). Enzymatic fuel cells (133) can achieve higher power densities than existing MFCs, but are subject to fouling from products and are not capable of self-repair and enzyme replenishment. Furthermore, enzymatic fuel cells cannot recover much of the energy present in more complex fuels. For example, a glucose oxidase fuel cell (57) recovers only two electrons per glucose (maximum theoretical C_E is 8.3%). While these additional factors must be considered, volumetric power is an important MFC operational metric by which to compare different MFCs for most applications.

MFC power output is dependent upon the voltage (potential difference) across the load. The open circuit voltage is not simply the difference between the reduction potentials for the two half-cell reactions. For example, in the glucose-fed MFC with an oxygen cathode, the difference between the reduction potentials of the O_2/H_2O (Eq. 1-2) and glucose/CO_2 (Eq. 1-1) couples is approximately 1.2 V (0.805 V - (-0.414 V), both vs. normal hydrogen electrode (116)). However, the actual MFC voltage would be lower. First, the anode chamber redox potential is ultimately determined not by the fuel, but by the potential of the immediate electron donor to the anode. That is the mediator, or perhaps an outer membrane cytochrome in a mediatorless MFC. Next, there are several reasons for voltage losses (ohmic losses and overpotentials) in an MFC (21, 24). Polarization curves are routinely used to evaluate MFC performance. Since voltage is inversely proportional to resistance, the external resistance can be changed to vary the voltage. The current is plotted as a function of voltage. A power curve can then be plotted based upon the the polarization curve (and the relationship between power, voltage and current, Eq. 1-6).

$$P = V \times I \tag{1-6}$$

These types of curves provide both the maximum power production and the effect of the MFC internal resistance. Current varies in a nonlinear manner with voltage because of current-dependent overpotentials. The relationship would be linear if there were no internal resistance (Eq. 1-7).

$$I = V/ R \tag{1-7}$$

However, the total resistance is the sum of external and internal resistance and it is the total resistance that must be used in the calculations. Internal resistance is dependent upon ohmic (conductive) losses as well as anodic and cathodic overpotentials . Types of overpotentials include activation overpotentials (due to electron transfer kinetics), losses due to bacterial

metabolism, and mass transfer losses (concentration overpotentials) due to substrate limitation of biocatalysis or at the electrode. Part of our study focused on overcoming anodic overpotentials due to metabolism and due to activation overpotentials using metabolic engineering and improvement of electron transfer kinetics. Activation overpotentials are greatest at lower current, while concentration overpotentials become a factor when current increases (72, 138). Our study also investigated optimization of anode design to minimize ohmic losses and concentration overpotentials.

There are many potential applications for MFC technology. MFCs offer unique benefits for niche applications such as power for remote sensing equipment, power and waste recycling for space travel, small-scale distributed power generation in areas lacking infrastructure, and for use as biosensors. The larger scale applications that are currently being developed include MFCs for processing of wastewater and of food processing wastes.

MFCs have been developed for use in providing electricity to low-power sensing and communications equipment in remote locations. Benthic unattended generators (BUGs) are examples of sediment MFCs (74, 115). BUGs have an anode, buried in seafloor sediment, that harvests electrons from the metabolic processes of the natural microbial ecosystem and couples the anodic half-reaction to the oxidation of a cathode located in the oxygenated seawater above. One could also imagine MFCs powering telemetry equipment in a forest or jungle, using tree sap or other readily and continuously available fuel to allow long-term, low-cost, maintenance-free operation.

Exotic niche applications such as MFCs for space travel (83) and in foraging robotic systems (132) may be somewhat limited in scale, but these research efforts can help fund further MFC research for more widespread practical usage. Projects such as the gastrobot research effort

(131) and the slugbot, an autonomous (carnivorous) pest contol sytem (58), both powered by MFCs, generated headlines and awareness of the possibilities for MFC technology. Another MFC application that is attracting attention is the use of very simple, inexpensive MFCs (9) in third-world countries for small-scale distributed power. Several non-profit organizations are distributing plans and teaching the people in these areas to make these MFCs from cheap and locally available materials.

Initial MFC applications that benefit from economies of scale include the treatment of industrial, agricultural, municipal and domestic sewage wastes. The organic material content of these wastes is currently released directly into the environment, or pretreated before release. These processes involve significant costs, both financial and environmental. As an example, treatment of sewage wastewater (generally by aerobic bacteria in staged mixing tanks) in the United States costs over $25 billion annually (71). The energy in the organic wastes is not currently recovered. Removal of organic material via large-scale flowthrough MFCs could offset energy (and therefore operational) costs through the recovery of this stored energy as electricity. Progress is being made in MFC scale-up design and operation. Recently, a 1 m^3 pilot MFC system began operation at a Foster's brewery in Queensland, Australia. The system was designed by and is operated by a group from the Advanced Water Management Centre at the University of Queensland, in cooperation with the brewery. A collaboration between the Center for Environmental Sciences and Engineering at the University of Connecticut and a private environmental engineering company has received funding to build and operate pilot-scale wastewater treatment MFCs in New York. These types of projects mark a new phase for MFC research, which is still quite young compared with most other energy harvesting technologies.

Dissimilatory Metal Reducing Bacteria

The number of MFC studies increased dramatically after the discovery that some dissimilatory metal reducing bacteria were able to reduce an MFC anode (59). Some microorganisms are capable of transferring electrons to insoluble metal oxides and oxyhydroxides in an energy coupling manner (43, 75, 85). The use of extracellular metals as terminal electron acceptors to support growth is known as dissimilatory metal reduction. Bacteria that can respire on these metals are known as dissimilatory metal reducing bacteria (DMRB). Many DMRB can transfer electrons to an MFC electrode (70). While some archaea are capable of dissimilatory metal reduction (56), we will focus on dissimilatory metal reduction by eubacteria.

Limitations of DMRB for Use in MFC

Although DMRB possess desirable attributes for MFC application in that most are capable of reducing an electrode without requiring addition of an electron carrying mediator, these organisms have significant limitations. The DMRB can be present as isolates in MFCs, or more commonly, as members of a consortium in the anode containing chamber. DMRB such as *Shewanella* or *Geobacter* have a very limited substrate range and are incapable of using sugars as electron donors. MFCs using *Shewanella* are inefficient because they can only partially oxidize the fuel (primarily lactate is oxidized to acetate). Other DMRB have very low metabolic rates and grow slowly. One example of a DMRB that is capable of completely oxidizing sugars and transferring electrons to an electrode with a high Coulombic yield is *Rhodoferax ferrireducens* (22). Despite its ability to efficiently transform the chemical energy of sugars into electrical energy and to transfer electrons directly without the need for a mediator, the doubling time for this organism is more than a week and sugars are catabolized very slowly (22). This low catabolic rate translates to low current and power production. DMRB generally live in an

environment of low substrate availability and the electron donors present are often inorganic compounds or breakdown products from the catabolism of more complex organic substances by other organisms. Therefore, high metabolic rates and fast growth would not seem to offer a survival advantage, nor would complete oxidation of complex carbohydrates or other organic compounds. It is possible that these traits could be introduced and improved through genetic engineering and directed evolution. However, the necessary genetic tools have not been readily available for long and in many cases they are still lacking for DMRB. Furthermore, many of these organisms have additional nutrient requirements and are obligate anaerobes, both of which make culturing and genetic manipulation more difficult.

The use of consortia in mediatorless fuel cells has been the most common approach since the first report of direct electron transfer to an electrode (59). The anodic chamber in these studies generally contains some type of organic wastewater with an ill-defined chemical composition and microbial flora already present in the source. A stable, electrical current-producing consortium is then selected for through prolonged MFC or poised potential bioelectrochemical cell operation. The optimization of MFC design and operation in these studies has led to considerable increases in power output and densities. The challenges associated with these black box MFCs are that their complex interactions and metabolic networks are difficult to study and lessons learned from researching one system may not be applicable to another. A poor understanding of the underlying metabolic processes might make stable and reproducible MFC performance difficult and certainly complicates efforts to increase microbial current production via metabolic engineering. MFCs employing isolated organisms may limit power output over the short term, but the ability to study simpler systems has been integral to the understanding of fundamental principles. Isolated DMRB such as *Shewanella oneidensis* are

being used as model systems in extracellular electron transfer research. This research can provide the basis for the combination of efficient, mediatorless electron transfer with increased substrate range and current production in a single organism, via a genetic engineering approach.

Shewanella oneidensis MR-1

S. oneidensis strain MR-1 is a model organism for the study of dissimilatory metal reduction. Its genome has been sequenced and many studies have focused on its system for transfer of electrons to insoluble extracellular acceptors. *S.oneidensis* is a Gram-negative, facultative anaerobe belonging to the *Gammaproteobacteria. S. oneidensis* was first isolated from Lake Oneida (New York) sediment (126). *Shewanella* species, while primarily aquatic, may be found in many environments, from soil and sediment, to spoiled fish, to Antarctic seawater (15). While *S. oneidensis* does not appear to use simple or complex sugars and incompletely oxidizes growth substrates (64), it is capable of transferring electrons to many soluble and insoluble acceptors, including electrodes, without the need for exogenous mediators (43, 78, 128).

S. oneidensis MR-1 central metabolism

S. oneidensis MR-1 contains most of the genes necessary for a complete Embden-Meyerhoff Pathway (EMP), but is missing phosphofructokinase (64). It contains the genes encoding the complete pentose phosphate and Entner-Doudoroff pathways. However, *S. oneidensis* MR-1 does not use hexose or pentose sugars. One and three-carbon compounds serve (primarily) as carbon sources for growth. *S. oneidensis* MR-1 has a complete tricarboxylic acid cycle (TCA) under some conditions, but flux is limited and it generally does not completely oxidize carbon sources to CO_2.

S. oneidensis MR-1 is a facultative anaerobe and is capable of aerobic respiration. It is not known to be fermentative, but has most of the fermentative pathway genes. Terminal electron

acceptors that *S. oneidensis* MR-1 can use in the absence of oxygen include: dimethyl sulfoxide (DMSO), trimethylamine N-oxide (TMAO), sulfate, elemental sulfur, nitrate, nitrite, various metal oxides and oxyhydroxides, and carbon electrodes (78, 126).

S. oneidensis extracellular electron transfer

The mechanism of extracellular electron transfer used by *S. oneidensis* has not been fully elucidated. An electron transport chain linking cytoplasmic membrane-embedded cytochromes to soluble periplasmic and outer membrane cytochromes has been shown (Figure1-2) (108), along with evidence of conductive pili, called nanowires (42). The outer membrane decaheme, *c*-type cytochromes OmcA and MtrC are terminal reductases in the *S. oneidensis* MR-1 extracellular electron transfer system (26). OmcA and MtrC form a complex with MtrB in the outer membrane (102). MtrB is not a cytochrome and no direct role in electron transfer has been reported. MtrA is a periplasmic decaheme *c*-type cytochrome (94) that associates with MtrB and transfers electrons to the terminal reductases. All of these proteins, along with the inner membrane-bound tetraheme c-type cytochrome CymA, have been reproted to be necessary for extracellular electron transfer (108). *S. oneidensis* MR-1 has 46 *c*-type cytochromes (108), making it difficult to determine which are sufficient for insoluble metal (or electrode) reduction. Indirect electron transfer to insoluble acceptors was also reported, but until recently, the endogenous mediators used in this process were unidentified. It has now been shown that flavins are used by *S. oneidensis* as soluble electron carriers (78, 128).

Escherichia coli

E. coli is a Gram-negative, heterotrophic, facultative anaerobe belonging to the *Gammaproteobacteria*. It is the best-studied prokaryote, with minimal nutrient requirements and a short generation time. Excellent genetic tools are available and several complete *E. coli* strain genome sequences have been published and well annotated. These characteristics all contribute

to making *E. coli* an ideal organism for basic and applied research projects. *E. coli* has been used extensively by all types of researchers as a molecular biology tool, by microbiologists as a model system, and by the biotechnology industry for production of everything from pharmaceuticals to fuels.

E. coli Central Metabolism

The primary central metabolic pathways of *E. coli* that are involved in aerobic glucose catabolism (Figure 1-3) consist of glycolysis (Embden-Meyerhof-Parnas pathway), intermediate (pyruvate) metabolism, and the tricarboxylic acid cycle (TCA cycle, also called the Krebs or citric acid cycle). *E. coli* has a wide substrate range and is capable, under aerobic conditions, of completely oxidizing a variety of organic compounds including: sugars (hexoses and pentoses), sugar alcohols, organic acids, fats, and proteins. *E. coli* can synthesize all amino acids, nucleic acids and cofactors needed for its growth and metabolism, and can be cultured in a mineral salts medium. It can respire anaerobically and can use nitrate, nitrite, DMSO, TMAO, or fumarate as terminal electron acceptors. However, *E. coli* is not generally capable of mediatorless extracellular electron transfer. There have been reports of strains of *E. coli* that have been serially transferred in MFCs to select for mediatorless extracellular electron transfer (97, 129), but further characterization of these strains has not been reported, nor have the initial reports been independently confirmed. In the absence of exogenous electron acceptors, *E. coli* metabolizes sugars via mixed acid fermentation. Primary fermentation products are lactate, acetate, formate and ethanol, accompanied by succinate and pyruvate as side products. Under these conditions, the TCA cycle is not complete and flux to succinate and α-ketoglutarate is via reductive and oxidative branches (respectively) of the split pathway. In addition, flux through the pyruvate dehydrogenase (PDH) complex, also important in aerobic catabolism, is greatly

diminished. The control of flux through these metabolic pathways is primarily exerted by the cellular ATP/ADP and NADH/NAD^+ ratios.

ATP/ADP ratio

The ratio of ATP to ADP has been shown to be largely responsible for control of flux through glycolysis. By overexpressing the genes of the F_1 sector (cytoplasmic ATPase portion) of the F_1F_O ATP synthase, Koebmann *et al*. determined that greater than 75% of glycolytic flux control is exerted by ATP/ADP (63). Therefore overexpression of genes encoding glycolytic enzymes had little effect upon glycolytic flux. Other groups have reported that futile metabolic cycles (gratuitously consuming energy) increase the rate of glucose catabolism as well (67, 91). Disruption of the *atp* operon (encoding the subunits of the F_1F_O ATP synthase) eliminates oxidative phosphorylation, decreasing the ATP/ADP ratio and increasing the rate of glycolysis (52). The ATP/ADP ratio affects the rate of glucose catabolism through substrate limitation and by allosteric control of key glycolytic enzymes (20). Manipulation of the ATP/ADP ratio by the abovementioned means has been successfully used to increase production rates of compounds such as acetate (20) and pyruvate (19) in *E. coli*, and glutamic acid in *Corynebacterium glutamicum* (5).

Cellular redox balance

The cellular NADH/NAD^+ ratio is another critical factor in determining metabolic flux and routing in *E. coli*. In the context of the complete and rapid oxidation of glucose, this ratio must be kept low. Increased glycolytic flux without a similar increase in the rate of NADH reoxidation will result in the incomplete catabolism of the glucose. In the absence of oxygen or other exogenous electron acceptors, respiration is not possible and the NADH/NAD^+ ratio is elevated (109). Fermentative pathways permit the reoxidation of the NADH via reduction of intracellular metabolites such as pyruvate and acetyl-CoA, but limit MFC yield and stable operation. Even in

the presence of an exogenous electron acceptor, the respiratory chain can become rate-limiting, leading to phenomena such as acetate overflow metabolism (76, 124). High glycolytic flux results in a high NADH production rate. If NADH cannot be reoxidized rapidly enough by the respiratory chain, NADH can limit flux through the TCA cycle and divert carbon to acetate via the phosphotransacetylase-acetate kinase (PTA-ACK) pathway. This shunting to acetate avoids the extra reducing equivalents that would otherwise be produced via the TCA cycle and helps to maintain redox balance. NADH exerts its negative control of TCA cycle flux primarily through transcriptional regulation, through allosteric inhibition of key enzymes, and through its inhibition of dihydrolipamide dehydrogenase (the E3 component of both PDH and α-KGDH). Overcoming the problem of rate and yield limitation due to redox imbalance requires either increasing the rate of NADH oxidation, or removing the negative controls of NADH over PDH and the TCA cycle. Both approaches have resulted in some success. Vemuri *et al*. have combined these approaches to address the problem of acetate overflow metabolism (124), using an engineered *arcA* deletion strain expressing a gene from *Streptococcus pneumoniae* encoding a water-forming NADH dehydrogenase. Veit *et al*. replaced the *sdhC* promoter region to eliminate repression of *gltA* (encoding citrate synthase) and of the *sdhCDAB-sucABCD* operon (123). The intergenic region between *gltA* and *sdhC* contains several ArcA-P binding sites (28), as well as binding sites for cAMP-CRP (cyclic AMP-bound catabolite repressor protein) and FNR. FNR and ArcA-P are redox sensitive (ArcA is the response regulator of the ArcAB system and is phosphorylated by ArcB under reducing conditions) transcriptional dual regulators (77). Kim *et al*. characterized an *lpd* (encoding dihydrolipoamide dehydrogenase) mutant whose PDH activity is less sensitive to NADH inhibition (62). Each of these strategies for increasing flux through intermediate metabolism and the TCA cycle has been shown to be beneficial and several are incorporated into

our study. However, the more global approach to solving this problem of increasing flux by directly addressing the reoxidation of NADH is simpler and may be more effective than trying to remove individual bottlenecks. This work will therefore focus upon maintaining a low $NADH/NAD^+$ ratio to enable higher electron yields from glucose while increasing the catabolic rate by keeping the ATP/ADP ratio low.

Electron Transport

Unlike the DMRB, *E. coli* is incapable of extracellular electron transfer in the absence of exogenous electron acceptors. The electron transport chain is confined primarily to the inner membrane, with a few periplasmic proteins that function in nitrate and nitrite reduction. There are no outer membrane cytochromes in *E. coli* and therefore no conduit for the electrons from glucose metabolism to cross the outer membrane. Nor are there any confirmed reports of native *E. coli* producing diffusible electron carriers (such as the flavins of *Shewanella* species) for extracellular electron transfer.

The electron transport chain of *E. coli* can contain several different dehydrogenases and terminal oxidases, connected by the quinone pool (17). Our study primarily discusses the components normally involved in aerobic (and nitrate) respiration, with NADH as the primary electron donor. It is important to note, however, the presence (under the appropriate conditions) of dehydrogenases that accept electrons from: glucose, lactate, pyruvate, succinate, formate hydrogen, and glycerol-3-phosphate. Also, DMSO, TMAO, nitrate, nitrite and fumarate reductases can accept electrons from the quinone pool.

With all of its dehydrogenases and terminal reductases, along with three types of quinones (ubiquinone, menaquinone, and dimethylmenaquinone) there are a number of possible combinations and therefore many possible electron transport chains. In reality, the cellular redox potential and energy state determine the path of the electrons. The greater the difference in

potential between the electron donor and the terminal electron acceptor, the more energy that is available from the overall reaction and the more proton-translocating coupling steps that are involved. Electron donor and acceptor pairs with small differences in potential, such as formate and DMSO, are not energy conserving transfer pathways, whereas NADH and oxygen (aerobic respiration) provide the greatest potential difference that can result in the most proton translocation for energy conservation. Therefore, when oxygen is available, the cell can derive more energy from using the aerobic respiratory chain than from respiration with any other acceptors.

Engineered *E. coli* as a Clean Background Model for Dissimilatory Metal Reduction and as a Biocatalyst for Increased MFC Power Output

Despite significantly improved models of extracellular electron transport systems in bacteria such as *Shewanella* and *Geobacter* species, much is still unknown about these systems. In particular, it has not been easy to determine which components are sufficient for the reduction of extracellular acceptors. This is primarily due to the large number of periplasmic and outer membrane cytochromes that are present in these DMRB. There is a complicated and redundant set of electron transfer pathways, with some leading to specific terminal electron acceptors and some pathways that can be used for reduction of many different types of acceptors. *E. coli* offers a clean background in which to assemble the minimal set of components to allow reduction of extracellular acceptors. The extracellular electron transport chain of *S. oneidensis* MR-1 is the best studied system and Pitts *et al*. have already demonstrated that the periplasmic MtrA, heterologously produced in *E. coli*, can accept electrons from the native NapC (94). Further, the outer membrane cytochromes OmcA and MtrC from *S. oneidensis* have been produced in *E. coli* and can localize to the outer face of the OM, permitting their reduction and oxidation by

chemical agents (34). However, the chain has not yet been completed and the minimal set of proteins (and other carriers) has not been determined.

The establishment of mediatorless extracellular electron transport in *E. coli* could also be useful for production of bioelectricity in an MFC. Combining the broad substrate range, ease of genetic manipulation and high productivity of *E. coli* with an extracellular electron transport system would provide an excellent biocatalyst for robust and versatile MFCs. Such a strain could be readily engineered and adapted to provide high power output and high Coulombic efficiency.

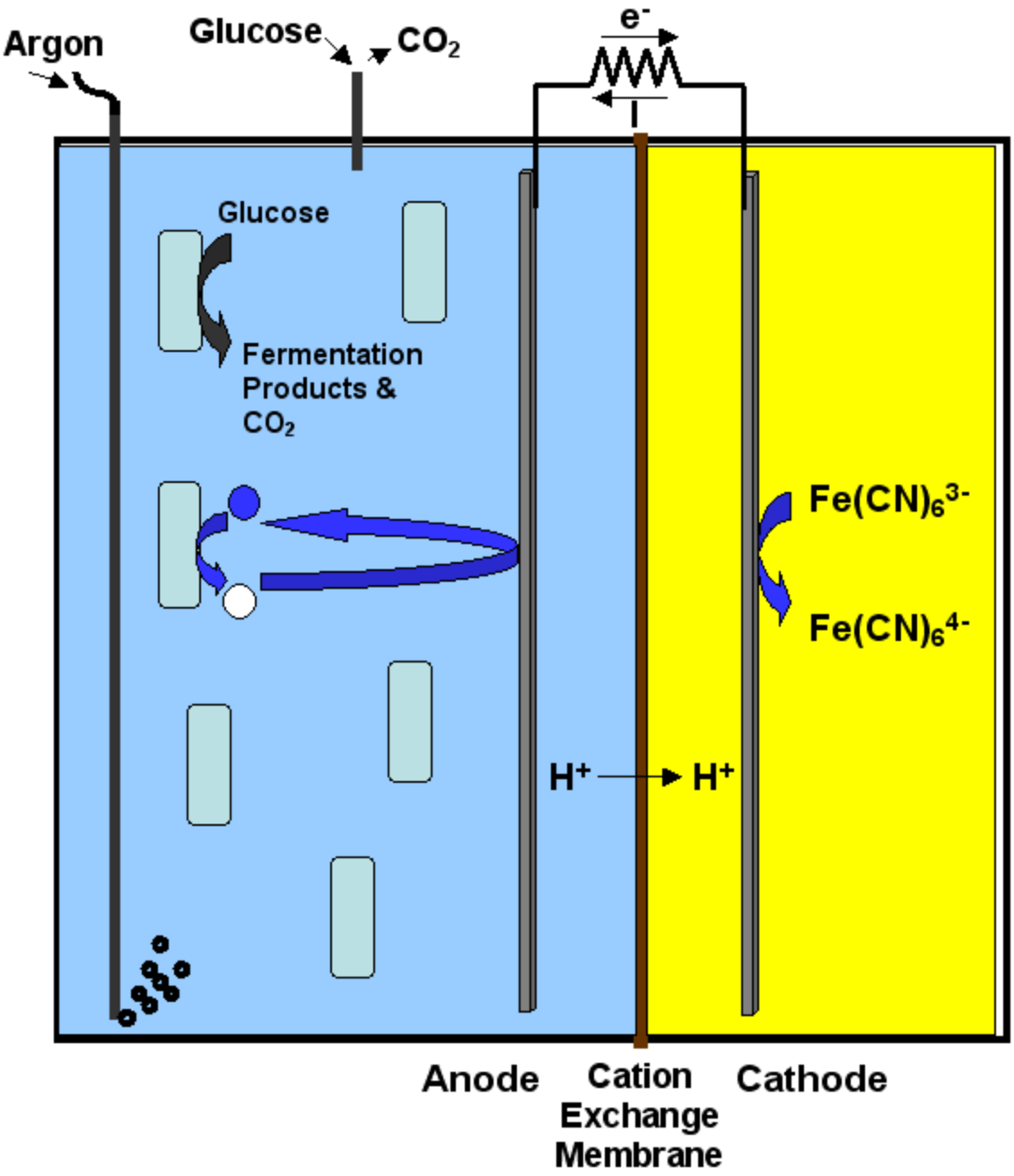

Figure 1-1. Example of a simple two-chambered microbial fuel cell. The current (I) is shown counter to the flow of electrons (e^-) by convention. Potassium ferricyanide is used as the oxidant in the cathode chamber in this example. Argon gas is used to maintain anaerobic anode chamber. Light rectangles represent microbial biocatalyst. Filled and open circles, oxidized and reduced diffusible mediator dye (respectively).

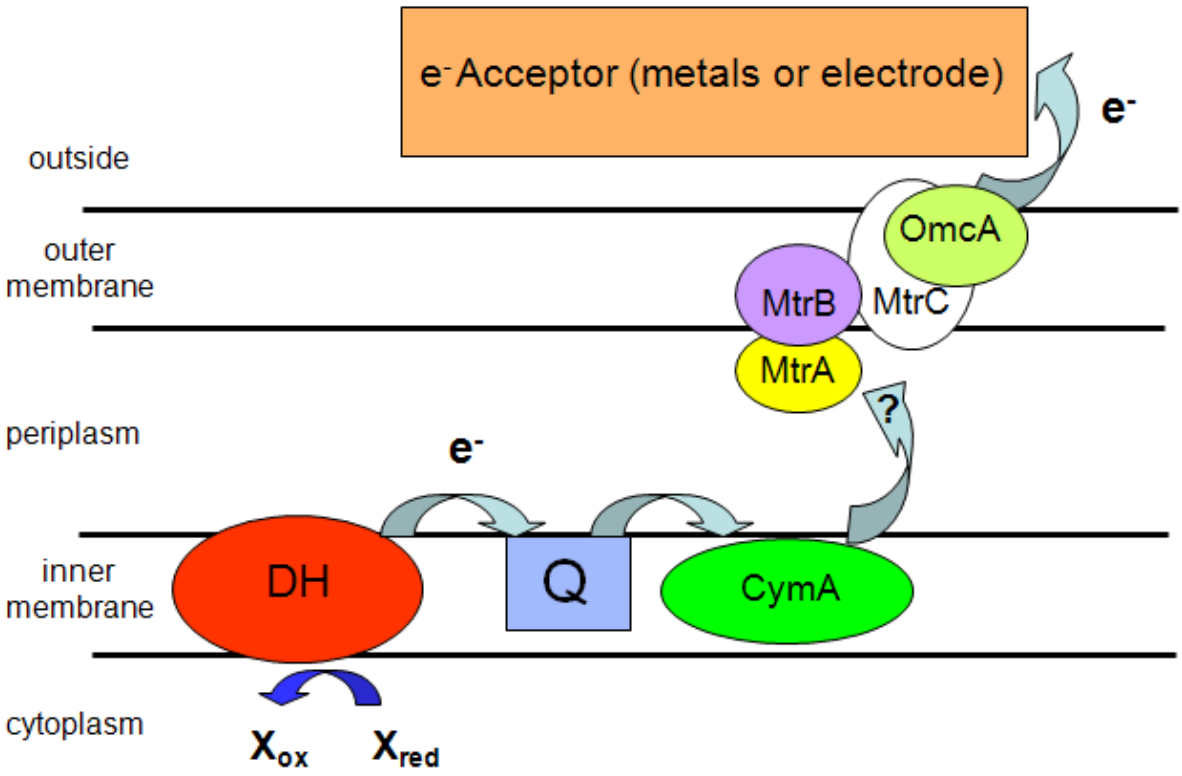

Figure 1-2. Simple model of extracellular electron transfer in *Shewanella oneidensis*. Light blue arrows represent electron transfer. X*red/ox*, reduced/oxidized dehydrogenase substrate; DH, formate (or other cytoplasmic membrane-associated) dehydrogenase; Q, quinone pool; CymA, cytoplasmic membrane associated *c*-type cytochrome; MtrA, periplasmic *c*-type cytochrome, OmcA and MtrC, outer membrane associated c-type cytochromes; MtrB, protein of unknown function (complexes with OmcA and MtrC). Electron transfer to MtrA may be directly from CymA or via an (unknown) intermediate. Some putative components of system omitted.

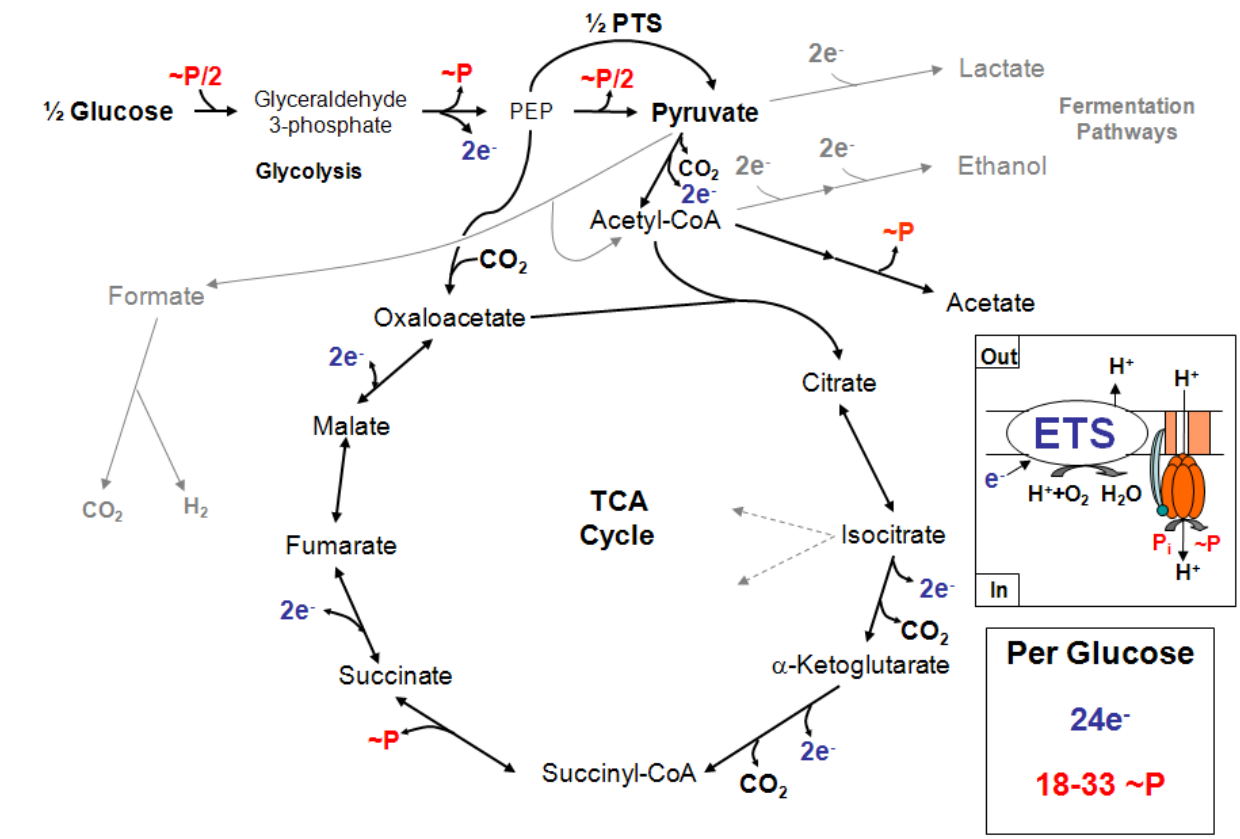

Figure 1-3. Simplified view of central metabolism of aerobically cultured *Escherichia coli* ATCC 8739. Glyoxylate shunt (grayed, dotted lines) is not active and is omitted. Major fermentation pathways are not active and are shown in gray, with dotted lines. Inset shows simplified oxidative phosphorylation with the electron transport system (ETS) driving the net translocation of protons into the periplasmic space (Out) and their return to the cytoplasm (In) through the F_1F_O ATP synthase. Reducing equivalents are shown as electrons (e^-) and ATP is shown as ~P for simplicity. P_i, inorganic phosphate.

CHAPTER 2
PHYSIOLOGY AND METABOLISM OF AN *E. COLI* ATCC 8739 STRAIN LACKING THE STATOR STALK OF THE ATP SYNTHASE

Introduction

The F_1F_O ATP synthase of *Escherichia coli* is a well-studied molecular motor which couples the proton potential generated by electron transport through the respiratory chain with the phosphorylation of ADP. The complex is composed of two sectors, a cytoplasmic membrane-bound F_O sector and a catalytic F_1 sector. The F_O sector is made up of an a subunit, a ring of c subunits and two b subunits. The γ, ε, α, β and δ subunits comprise the F_1 sector. The structure of the F_1F_O ATP synthase has been reviewed by others (41, 130).

Functionally, the F_O sector contains the channel (between the a and c subunits) through which protons are translocated across the membrane, causing the rotation of the c subunit rotor and its γ subunit shaft (16, 87). The b and δ subunits make up the stator stalk (112), which tethers the α and β subunit complex of the cytoplasmic F_1 sector to the a subunit of the F_O sector and holds it steady against the rotation of the γ subunit. This rotation drives the phosphorylation of ADP within the stator of the F_1 sector. The process is reversible, with ATP hydrolysis capable of pumping protons out of the cytoplasm (29). Thus the F_1F_O ATP synthase is able to tightly control the cytoplasmic pH over a wide range of conditions (140), in addition to its more commonly discussed role in oxidative phosphorylation.

The eight genes encoding the structural subunits of the *E. coli* F_1F_O ATP synthase are part of a nine gene operon (*atpIBEFHAGDC*), where *atpI* does not code for a structural subunit of the F_1F_O ATP synthase, but may have a regulatory function (37) or might assist in assembly of the complex (90). The other genes encode, respectively (with subunit stoichiometry): a_1, c_{10}, b_2, δ_1, α_3, γ_1, β_3 and ε_1 (Figure 2-1).

Flux through glycolysis is increased through overexpression of F_1 genes (63) or by disruption of the *atp* operon (20, 52, 86). The first approach lowers the cellular ATP/ADP ratio as a result of gratuitous cytoplasmic F_1 ATPase activity. Control of glycolytic flux is largely dependent upon this ratio (63). The lower ATP/ADP ratio in strains with deletions in the *atp* operon leads to an increase in glycolytic flux via activation of phosphofructokinase by ADP and AMP (32), AMP activation of pyruvate kinase (121) and inhibition of the gluconeogenic fructose bisphosphatase by AMP (7). The increase in ADP availability for phosphoglycerate kinase and pyruvate kinase is also stimulatory. This leads to an increased pyruvate pool and acetate overflow metabolism, since downstream steps become rate limiting (27). The primary reason for this rate limitation seems to be the inability of the respiratory chain to reoxidize the NADH produced by glucose catabolism (19). This respiratory limitation is partially alleviated because increased pyruvate levels inactivate the pyruvate dehydrogenase repressor (PdhR). PdhR has been found to negatively regulate transcription of *ndh* and *cyoABCDE* (encoding cytochrome bo_3) (89).

Mutation of the *atp* operon by insertion or deletion also lowers the ATP/ADP ratio by eliminating oxidative phosphorylation. Deletion of the *atpFH* genes physically uncouples the F_1 and F_O sectors through the elimination of the second stalk and can further lower the ratio through a combination of the abovementioned effects (20). Other *atp* operon deletion strains are partially complemented with the F_1 genes expressed from a plasmid (63). Previous work in our laboratory used *atpFH* deletion strains to produce acetate and pyruvate with high rates and yields (19, 20). These strains have high flux from glucose to acetate or to pyruvate when oxidative routes to acetate are eliminated.

Here I have made a detailed investigation of the physiology and metabolism of an *atpFH* deletion strain. Respiratory and overall electron transfer routes were examined by measurement of cytoplasmic membrane associated NADH oxidation and of dye reduction activities. Relative transmembrane proton conductance and membrane potentials were evaluated. I underscore the important role of the F_1F_O ATP synthase in pH homeostasis and in metabolic flux distribution for cellular redox balance.

Materials and Methods

Growth of Cultures and Media

The strains used in this study are derivatives of *E. coli* ATCC 8739 (Table 1-1). Unless otherwise specified, cells were grown aerobically in NBS mineral salts (20), containing MOPS (4-morpholinopropanesulphonic acid, 0.1 M, pH 7.4) and glucose (50 mM glucose), using baffled flasks (50 ml broth in 250 ml flasks, 250 rpm, 37°C). LB and LB agar plates were used only for plasmid and strain construction. Glucose was included (20 g/liter) for strains that contained deletions in the *atp* operon. Antibiotics were included as appropriate (kanamycin, 50 mg/liter; ampicillin, 100 mg/liter; chloramphenicol, 40 mg/liter). Arabinose (20 g/liter) was used to induce expression of Red recombinase genes (strain construction).

Anaerobic Batch Fermentation

Fermentations were done in 500 ml vessels (250 ml working volume, 37°C, 150 rpm) under argon. Cells were grown in NBSM mineral salts with glucose (50 mM glucose). Samples were removed for the measurement of pH, optical density (cell mass), and fermentation products (by high pressure liquid chromatography, HPLC).

Construction of ATP Synthase Gene Deletions

E. coli ATCC 8739 was used as the parental strain for all modifications. PCR primers, plasmids and strains used in this work are listed in Table 1-1. Standard methods (103) were used

in PCR amplification, plasmid construction, and transformations. Deletions were made by Red recombinase (30) catalyzed integration of an FRT (FLP recognition target)-flanked cassette containing a selective antibiotic marker. This cassette was excised by a FLP recombinase-catalyzed intramolecular recombination (95), leaving a single FRT-containing sequence artifact. FLP recombinase also enabled the removal of longer chromosomal sequences between similarly oriented FRT sites from two individual deletions.

A portion of *atpD* was deleted to produce JC10. Primers JM*atpC*-C*Kpn*I and JM*atpD*-N*Nde*I were used to amplify part of *atpC* through part of *atpD* from ATCC 8739 genomic DNA by PCR. The product was cloned into pCR2.1-TOPO (Invitrogen, Carlsbad, CA) to produce pLOI4135. The *Kpn*I/*Nde*I *atpCD*' fragment was inserted into the corresponding sites within the multiple cloning site of pFLAG-CTC to produce pLOI4123. The *Eco*RI/*Sma*I FRT-*kan*-FRT fragment from pLOI2511 was ligated into the *Stu*I/*Eco*RI-digested inside-out PCR product (JM*atpD*-*Stu*I/ JM*atpD*-*Eco*RI primers, pLOI4123 template). The resulting plasmid (pLOI4125) was digested with *Kpn*I/*Nde*I and used a template for PCR with JM*atpC*-C*Kpn*I and JM*atpD*-*NNde*I primers. Construction of JC07 was by Red recombinase facilitated, double-crossover homologous recombination with the PCR product and ATCC 8739 transformed with pKD46 (30). The successful integrants were selected for chloramphenicol resistance. The FRT-flanked chloramphenicol marker was removed via the FLP recombinase method previously described (79, 95) to produce JC10.

Replacement of *atpFH* with FRT-*cat*-FRT in ATCC 8739 and JC10, followed by FLP recombination, resulted (respectively) in strains JC27 (Δ*atpFH*) and JC25 (Δ*atpFHAGD*). JC25 resulted from an FLP recombinase-catalyzed excision of sequence between integration sites. JM*atpFH*down*Kpn*I and JM*atpFH*up*Nde*I primers were used for PCR cloning of *atpFH*

(pLOI4139) and for amplification of the fragment for integration (from pLOI4134). Primers JM*atpFH-Stu*I and JM*atpFH-Eco*RI were used for inside-out PCR. The *Stu*I/*Eco*RI FRT-*cat*-FRT fragment from pLOI4131 was ligated into the *Stu*I/*Eco*RI-digested inside-out PCR product (for pLOI4134).

Dye Reduction Assay

Electron transfer rates were determined during glucose catabolism using methylene blue (MB, colorless in reduced form) as the terminal electron acceptor (8, 84). Specific rates were measured using aerobically grown cultures (NBSM, 10 g/liter glucose) harvested in early exponential growth (approximately 0.33 gDCM/liter). Equal volumes (1.5 ml each) of culture and medium containing carboxymethylcellulose (10 g/liter) and MB (50 μM) were mixed in a stoppered cuvette. Carboxymethylcellulose was included to increase viscosity and minimize mixing of the oxidized surface. Change in A_{609nm} was monitored at 37°C and used to calculate the specific rate of dye reduction.

Enzyme Assays

Cells were lysed and fractionated for the determination of membrane-associated NADH dehydrogenase, NADH oxidase, and TMPD (N,N,N',N'-tetramethyl-phenylenediamine) oxidase activities. Aerobic cultures (50 ml) were harvested (0.33 gDCM/liter) by centrifugation and stored overnight at -20°C. Pellets were thawed on ice, washed with 10 ml ice-cold TM buffer (50 mM Tris-HCl, 10 mM $MgSO_4$, pH 7.5) and suspended to a cell density of 0.35 gDCM/liter in ice-cold TM buffer containing 10 μg/ml DNase I. Cells were disrupted by passage though a French pressure cell at 14,000 psi. Unbroken cells and debris were removed by two centrifugation steps (10 min each, 8,000×g, 4°C). Supernatant volumes were adjusted to 10 ml with TM buffer and membrane pellets prepared by ultracentrifugation (1 h, 165,000×g, 4°C). Membrane pellets were homogenized (vortex mixing and Teflon homogenizer) in 1 ml of TM

buffer. Both the supernatants (cytoplasmic fractions) and membrane fractions (membrane vesicles, MVs) were held on ice and used immediately for enzyme assays. Enzyme activities were measured at room temperature (22°C). Values reported are from triplicate determinations of two independent samples. Activities are expressed as nmol min^{-1} mg $protein^{-1}$.

Total membrane-bound NADH oxidation activity was determined spectrophotometrically (340 nm) using the molar extinction coefficient of NADH (6220 M^{-1} cm^{-1}). Reactions were initiated by adding MVs (30 μg protein) to a 1 ml assay mixture containing TM buffer and 0.25 mM NADH (110). Deamino-NADH (d-NADH) oxidation was used to measure the NADH oxidase activity from the proton-translocating NADH dehydrogenase (NDH-1) in a similar manner. Note that deamino-NADH is a substrate for NDH-1, but not for NDH-2 (81).

Membrane-bound NADH dehydrogenase activity was measured spectrophotometrically (110) using potassium ferricyanide as the electron acceptor. KCN was included in the reaction mix to inhibit cytochrome oxidase activity. NADH (0.5 mM, final) was used as substrate to measure combined NDH activities. The deamino-NADH (0.5 mM, final) was used to measure NDH-1. Reactions were initiated by addition of MVs (30 μg protein).

Cytochrome oxidase activity was measured as the oxidation of TMPD (53) at 609 nm using the molar extinction coefficient for oxidized TMPD (12,200 $M^{-1}\cdot cm^{-1}$). Reactions were initiated by adding MVs (30 μg protein).

SDS Electrophoresis and Immunoblotting

MVs (approximately 5 μg protein) were incubated for 1 h at room temperature in reducing SDS sample buffer (46) and resolved by electrophoresis using 12% polyacrylamide slabs (200 V for 35 min) with Tris-glycine running buffer (65). Protein was transferred to a polyvinylidene fluoride (PVDF, Hybond) membrane (44) and blocked with 5% (w/v) nonfat powdered milk. Primary rabbit antisera against subunits a and c (provided by Dr. Robert Fillingame) were diluted

(1:5,000 and 1:10,000, respectively), combined and incubated with the PVDF membrane (1 h at ambient temperature). Alkaline phosphatase-conjugated goat anti-rabbit secondary antibody was diluted (1:10,000 in TBS-Tween20) and incubated with the PVDF membrane (40 min at ambient temperature). The washed membrane was then developed as previously described (44) with bromochloroindolyl phosphate/nitro blue tetrazolium (BCIP/NBT) as a substrate, rinsed in deionized water and dried for imaging.

Analyses

Glucose and organic acids concentrations were measured by HPLC using an HP 1090 Series II equipped with refractive index and UV(210 nm) detectors, a Bio-Rad HPX-87H column and with a 4 mM H_2SO_4 mobile phase (20). Cell mass was estimated by measuring optical density at 550 nm using a Bausch & Lomb Spectronic 70 spectrophotometer (1 OD_{550} is equivalent to 0.33 gDCM/liter). Protein concentration was determined using the bicinchoninic acid method (BCA Protein Assay Kit, Thermo Scientific, Rockford, IL), with bovine serum albumin as a protein standard.

Results

Construction of JC25 and JC27 Through Targeted Deletions in *atp* Operon

Two isogenic strains were constructed using ATCC 8739 by making targeted deletions in the *atp* operon (Table 2-1, Figure 2-1). Both of the deletion strains lacked the genes encoding the b and δ subunits of the stator (peripheral) stalk (SS) of the F_1F_O ATP synthase (33 bp of *atpF*, encoding the first 11 amino acids of the b subunit, remained in JC25 and JC27). In addition, JC25 lacked the F_1 sector genes (*atpC* remained). These strains provided a clean genetic background and a means to compare the metabolic and physiological effects of removal of each of these major F_1F_O ATP synthase structural elements, *in vivo*.

The membrane proteins from aerobically grown ATCC 8739 and JC27 were electrophoretically separated by SDS-PAGE and subjected to immunoblotting to determine whether or not subunits a and c were present in the membrane of JC27 (Figure 2-2). Subunit c was present in the membrane fraction of JC27, but subunit a was absent. The band that migrated just above subunit a was due to nonspecific labeling, as confirmed by its presence in the membrane fraction of an F_O^- strain (Figure 2-2, lane 3). This result is consistent with previous reports of incomplete F_O assembly in the absence of the b subunit (46). In particular, JC27 lacks codons for residues that have been found to contact the a subunit (82). These results show that JC27 is functionally F_O^- and should not allow F_O sector-mediated proton transduction across the inner membrane. The F_O transmembrane proton channel has been reported to be at the interface between a and c subunits (113). While the JC25 membrane fraction was not analyzed, it likely contained only the c subunits of the F_O sector, since it (like JC27) was missing the b subunit. The only genotypic difference between JC27 and JC25 is the presence of the genes for the subunits of the F_1 (ATPase) sector in the former. Therefore, both stains were expected to lack oxidative phosphorylation and any phenotypic difference should have resulted from gratuitous ATP hydrolysis in JC27 (20).

Comparison of Aerobic Growth Rates and Yields

The maximum specific growth rates (μ), cell densities and biomass yields from glucose (Y_g) of the strains ATCC 8739, JC25, and JC27, grown aerobically in a mineral salts medium, were compared in order to characterize the effects of each deletion in the *atp* operon (Table 2-2). The growth rate and Y_g of JC27 were approximately 30% and 50% lower, respectively, than ATCC 8739. Growth rates and cell yields of the JC25 and JC27 strains were similar.

Product Formation and Specific Rates of Glucose Consumption

Both strains with deletions in the *atp* operon had approximately 44% higher specific rates of glucose consumption (J_{gluc}) vs. the wild type, when the cultures were grown aerobically (Table 2-2). The higher glucose consumption rates were consistent with those reported for other *atp* mutants (20, 52, 86).

There have been few studies of the product profiles of *E. coli* strains with targeted *atp* operon deletions grown aerobically in glucose mineral salts medium (20, 86). However, the accumulation of acetate by the modified strains (Figure 2-3) was not unexpected, given the increased glycolytic flux and the well-established phenomenon of overflow metabolism to acetate (123, 124). Furthermore, others have used engineered *atp* strains to produce high titers of acetate and pyruvate from glucose (20, 135). JC25 produced 22.3 mM acetate from 50 mM glucose by 11 h, after which the acetate levels decreased slightly to 14.3 mM by 24 h. JC27 accumulated 21.1 mM acetate by 11 h, which decreased to 15.5 mM by 24 h. In contrast, the wild type strain transiently produced a small amount of acetate (3.2 mM) by 8 h, which was undetectable by 9 h. JC25 and JC27 transiently produced a small amount of pyruvate and trace amounts of lactate. Most of the acetate produced in the mutant strains was not subsequently catabolized by the cells, presumably due to energetic constraints. Both of the primary acetate assimilation pathways require one ATP per acetate for conversion to acetyl-CoA. In the absence of oxidative phosphorylation, there is no net energetic benefit in catabolism of acetate, because a maximum of one ATP per acetyl-CoA can be gained via the TCA cycle.

Methylene Blue Reduction Rates

The rates of net electron transfer from glucose catabolism in aerobically grown cultures were evaluated on the basis of the specific rates of reduction of MB (v_{redMB}). MB is a membrane permeable, water-soluble phenothiazine redox dye with a standard biological midpoint potential

of +0.011V. It has been used as an indicator of bacterial metabolism in the food industry (2) and to quantitate viable *E. coli* cells on the basis of total reducing power (8). The dye changes from blue in its oxidized form (absorbance max at 609 nm) to colorless when reduced, in a two-electron transfer. The oxidative phosphorylation-deficient strains showed higher v_{redMB} values than the wild type strain (Figure 2-4). Strain JC27 (Δ*atpFH*) had a v_{redMB} that was over six-fold higher than that of the wild type (100.3 vs. 16.3 nmol min^{-1} $mgDCM^{-1}$, respectively). JC25 (Δ*atpFHAGD*) lacked the F_1 sector and exhibited a v_{redMB} that was five-fold higher (82.0 nmol min^{-1} $mgDCM^{-1}$) than ATCC 8739. These results suggest that elimination of oxidative phosphorylation is responsible for most of the increase in v_{redMB} observed for the strains with deletions in the *atp* operon. The slightly higher rate of MB reduction shown by JC27 (vs. JC25) may have been due to the effect of gratuitous ATP hydrolysis. While the glucose-dependent reduction of MB allowed the measurement of the rate of production of reducing equivalents, it did not show which pathways were used for reoxidation of reduced cofactors in these strains.

Anaerobic vs. Aerobic Growth Rates and Metabolism

Strains lacking oxidative phosphorylation were expected to grow similarly in the presence or absence of oxygen. To test this hypothesis, ATCC8739 (wild type) and JC27 (Δ*atpFH*) were grown anaerobically in glucose minimal medium and their growth rates compared with the aerobic cultures (Figure 2-5). As mentioned above, the absence of oxidative phosphorylation led to the lower growth rate of JC27 under aerobic conditions. As expected, the growth rate of the wild type was lower (0.604 h^{-1}, 59% of aerobic culture growth rate) in the absence of oxygen. However, a surprisingly lower growth rate (0.357 h^{-1}, 48% of aerobic culture growth rate) was seen in JC27 anaerobic cultures. The difference cannot be attributed to a lower ATP yield in JC27. Therefore, it is likely to be the result of limitations imposed by the lower cellular redox

potential and the need to maintain the PMF via ATP hydrolysis-driven proton pumping by the F_1F_O ATP synthase (ATPase).

Anaerobic growth, under tested conditions, was not glucose-limited for either of the strains. While ATCC 8739 consumed all glucose (50 mM initial conc.) by 30 h, it reached its maximum cell density of approximately 0.90 gDCM/liter by 13 h. JC27 cultures had only consumed 19 mM glucose and reached a maximum cell density of approximately 0.17 gDCM/liter by 30 h. The pH of the medium dropped from an initial value of 7.2 to 5.0 by 30 h in the ATCC 8739 culture, whereas the the pH of the medium in JC27 cultures only decreased to 6.7 by 30 h. By the time JC27 growth reached a maximum (16 h) the total concentration of reduced products measured (lactate, succinate and ethanol) was 8.5 mM. Total acids produced (pyruvate, succinate, lactate, formate and acetate) were 16.1 mM, from 7.1 mM of consumed glucose. These results indicate that the anaerobic growth of JC27 was limited by its inability to maintain an optimal cytoplasmic pH and the necessary proton motive force due to the lack of an ATP-driven proton pump.

NADH Oxidase and NADH Dehydrogenase Activities

Membrane vesicles were used to measure membrane-associated NADH oxidation (Table 2-3). The rate of oxidation of NADH by JC27 MVs was 2.5-fold higher than ATCC 8739. Rates of d-NADH oxidation were at least 30-fold lower than NADH oxidation, suggesting that very little NDH-1 activity was present and that NDH-2 (non-proton translocating) was primarily being used in the aerobic respiratory chains, under tested conditions.

As the rate of NADH oxidation by JC27 MVs was higher than the parent, it was important to measure NDH-2 NADH dehydrogenase activities in the MVs to determine whether higher NDH-2 levels were responsible for the elevated rate of NADH oxidtion by the entire electron transport chain. Potassium ferricyanide was used in the NADH dehydrogenase assays as the

electron acceptor and cyanide was included to inhibit the terminal oxidases. NADH dehydrogenase activity of JC27 MVs was 1.7-fold that of ATCC 8739 (Table 2-3). The higher NADH dehydrogenase activity in JC27 is consistent with previous findings with an *atpA* mutant (86).

Cytochrome Oxidase Activity

There are two types of enzymes of the *E. coli* aerobic respiratory chain that are involved in the transfer of electrons from NADH to molecular oxygen (54, 118). The first is an NADH dehydrogenase (NDH-1 or NDH-2) and the second is a cytochrome oxidase (cytochrome *bo*, cytochrome *bd*-I, or cytochrome *bd*-II). These two complexes represent the two energy coupling sites in the aerobic electron transport chain (Figure 2-6). Different levels of either type of enzyme could have been responsible for the higher rate of NADH oxidation observed for JC27. Having determined that NDH levels were likely to be a major factor in the difference, MV cytochrome oxidase activity was measured using TMPD as the substrate. TMPD oxidase activity in JC27 MVs was approximately 1.3-fold higher than that of the parent strain MVs (Table 2-3). The higher TMPD oxidase activity in JC27 MVs is probably due to higher levels of cytochrome *bd* (86).

Discussion

Deletions (or other disruptions) in the *atp* operon eliminate oxidative phosphorylation, lowering the ATP/ADP ratio and increasing the rate of glucose catabolism as a result. Targeted deletion of *atpFH* in ATCC 8739 increased the rate of glucose catabolism, but resulted in accumulation of acetate in aerobic batch cultures. Acetate overflow metabolism is thought to result from a redox imbalance, which makes additional flux through the TCA cycle (and its production of extra reducing equivalents) undesirable (124). Flux is shunted from acetyl-coA through the PTA-ACK pathway to acetate, providing one ATP per acetyl-CoA, but avoiding

production of additional reducing equivalents. This suggests that despite its higher rate of NADH oxidation, the respiratory chain of JC27 may still be rate-limiting. However, the experimental evidence presented here does not clearly support that hypothesis. The JC27 MV NADH oxidation rate (2.5-fold that of the parent) should be sufficient to reoxidize the elevated rate of glucose catabolism (1.4-fold that of the parent). Perhaps, *in vivo*, even the higher rate of reoxidation of NADH by the JC27 respiratory chain is rate-limiting. The absence of the F_1F_O ATP synthase in the proton circuit of JC27 (Figure 2-6) may allow a higher respiratory rate, as reported in other *atp* mutants (52, 86). Although there are other components of the transmembrane proton circuit (such as transporters and flagella) that can dissipate the gradient formed by electron transport, JC27 can be viewed as having a "short" circuit (or at least lower resistance) because the "load" (the F_1F_O ATP synthase) is missing. Higher NADH dehydrogenase activity provides a higher rate of electron transport, in conjunction with higher levels of terminal oxidase activity. Increases in NDH and cytochrome oxidase activity were reported to be primarily due to higher levels of non-proton translocating NDH (NDH-2) and cytochrome oxidase (cyt-*bd*) in another *atp* mutant (86). These changes could allow higher respiratory rates without being limited by an excessive proton gradient. However, in vivo electron transport may not be able to compensate for the higher rate of glucose catabolism in JC27.

Alternatively, pyridine nucleotide transhydrogenase (such as UdhA) activity (104) may limit the TCA cycle (NADP limitation of isocitrate dehydrogenase). The TCA cycle is subject to complex regulation and there may be other explanations for the observed flux to acetate in JC27. However, reports of using cofactor engineering (manipulating $NADH/NAD^+$) to overcome the acetate overflow problem (124, 125) support the hypothesis that respiratory chain NADH

reoxidation limits the TCA cycle. This work aims to test this hypothesis in ATCC 8739, as part of the overall goal to transform the stored energy in glucose to useful electrical energy, with high rate and yield.

Table 2-1. Strains, plasmids, and PCR primers

Strain/plasmid/primer	Relevant features	Reference/source
E. coli		
ATCC 8739	Parent strain	ATCC
JC07	ATCC 8739, Δ*atpD*::FRT-*kan*-FRT	This study
JC10	ATCC 8739, Δ*atpD*::FRT	This study
JC22	JC10, Δ*atpFH*::FRT-*cat*-FRT	This study
JC24	ATCC 8739, Δ*atpFH*::FRT-*cat*-FRT	This study
JC25	ATCC 8739, Δ*atpFHAGD*::FRT	This study
JC27	ATCC 8739, Δ*atpFH*::FRT	This study
Plasmids		
pCR2.1-TOPO	Cloning vector, *bla*, *kan*	Invitrogen
pKD46	pSC101 rep. (temp. cond.), *bla*, *gam*, *bet*, *exo*	(30)
pFTA	pSC101 rep. (temp. cond.), *bla*, *tetR*, *flp*	(79)
pLOI2511	*bla*, FRT-*kan*-FRT	(120)
pLOI4123	*bla*, '*atpDC*'	This study
PLOI4125	*bla*, '*atpDC*'::FRT-*kan*-FRT	This study
pLOI4131	*bla*, FRT-*cat*-FRT	(51)
pLOI4133	*bla*, *atpFH*'	This study
pLOI4134	*bla*, *atpFH*'::FRT-*cat*-FRT	This study
pLOI4135	*bla*, *kan*, '*atpDC*' (PCR) in pCR2.1-TOPO	This study
pLOI4139	*bla*, *kan*, *atpFH*' (PCR) in pCR2.1-TOPO	This study
Primers		
JM*atpC*-C*Kpn*I	AAGGTACCGCCGTGAGAGCTGCTAAT	This study
JM*atpD*-N*Nde*I	AACATATGCCGCGCAGCACCTTCCTA	This study
JM*atpD-Stu*I	AACAGGCCTTACATGGTCGGTTCCATC	This study
JM*atpD-Eco*RI	AACGAATTCCTGACGGCTCAGTACCAC	This study
JM*atpFH*down*Kpn*I	AAGGTACCGTCTGCAAGGCGCTCAAG	This study
JM*atpFH*up*Nde*I	AACATATGGAAGGCGCAGCGCGTCAA	This study
JM*atpFH-Stu*I	AACAGGCCTTGCCGCACTGAGTGAACA	This study
JM*atpFH-Eco*RI	AACGAATTCTGGCCTGGCCGAGGATTG	This study

Primer sequences are 5' to 3', with relevant restriction endonuclease recognition site underlined. Apostrophes before or after genes indicate truncation.

Table 2-2. Growth and glucose consumption of *atp* deletion strains

Strain	Growth rate (μ [h^{-1}])	Max. cell density ($gDCM \cdot L^{-1}$)	Biomass yield ($gDCM \cdot mmol^{-1}$)	Glucose flux ($mmol \cdot gDCM^{-1} \cdot h^{-1}$)
ATCC 8739	1.028 ± 0.013	4.75 ± 0.10	0.095 ± 0.002	10.82 ± 0.18
JC25 (F_1^-)	0.732 ± 0.014	2.34 ± 0.04	0.047 ± 0.001	15.61 ± 0.19
JC27 (SS^-)	0.746 ± 0.007	2.40 ± 0.02	0.048 ± 0.000	15.53 ± 0.02

All values are reported as mean ± SD, n = 3

Table 2-3. Respiratory chain activities

Strain	NADH oxidase ($nmol \cdot min^{-1} \cdot mg^{-1}$)	d-NADH oxidase ($nmol \cdot min^{-1} \cdot mg^{-1}$)	NADH dehydrogenase ($nmol \cdot min^{-1} \cdot mg^{-1}$)	d-NADH dehydrogenase ($nmol \cdot min^{-1} \cdot mg^{-1}$)	TMPD oxidase ($nmol \cdot min^{-1} \cdot mg^{-1}$)
ATCC 8739	458.8 ± 46.2	14.9 ± 5.3	1938.0 ± 90.6	467.2 ± 23.9	71.0 ± 11.1
JC27	1128.1 ± 35.8	24.7 ± 8.3	3315.8 ± 215.4	774.2 ± 37.2	94.7 ± 8.3

All values are reported as mean ± SD, n = 3

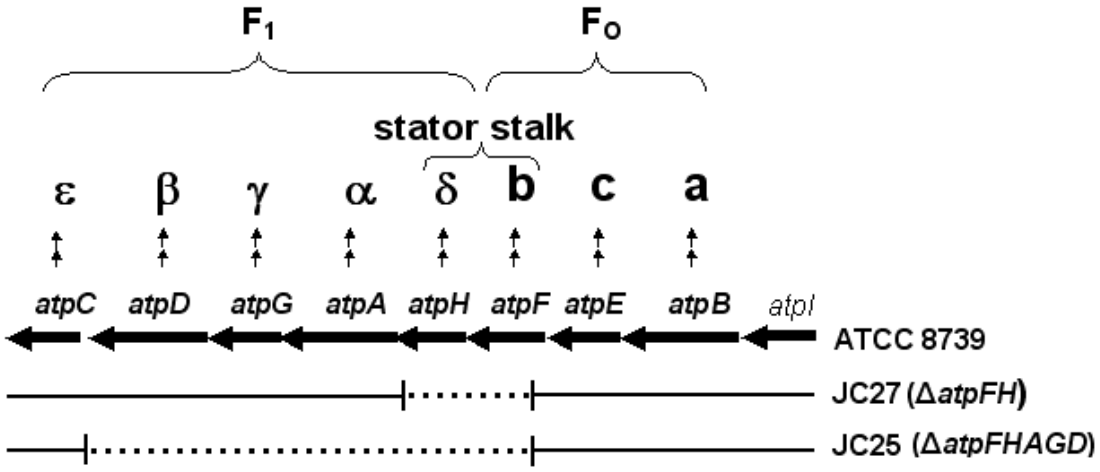

Figure 2-1. Genetic organization and gene products of the *atpIBEFHAGDC* operon with subunits shown above coding genes. Dotted lines represent region deleted from operon in the listed strains.

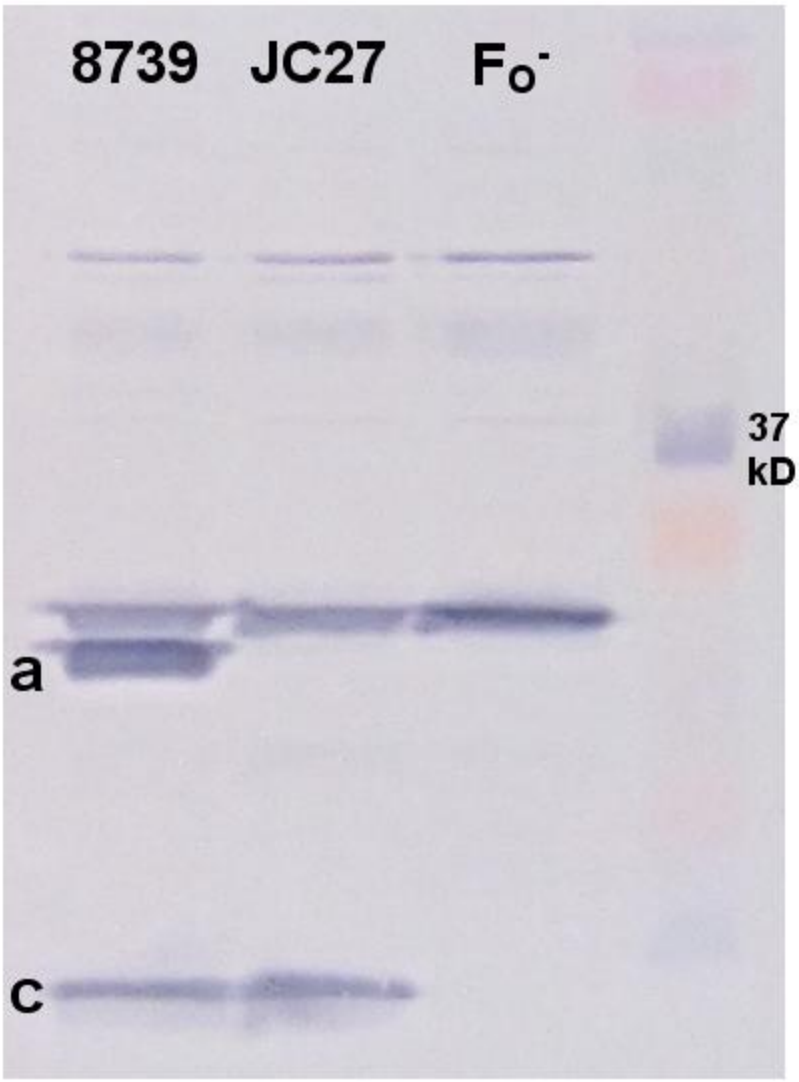

Figure 2-2. Immunoblot of membrane fractions separated by SDS-PAGE (12%, Tris-glycine). Rabbit antisera against subunits a and c were used together as 1° antibodies (1:5000, 1:10,000, respectively) and goat anti-rabbit-AP 2° antibody was used, with NBT/BCIP substrate for detection. Lane 4 contains BioRad Kaleidoscope prestained protein standards.

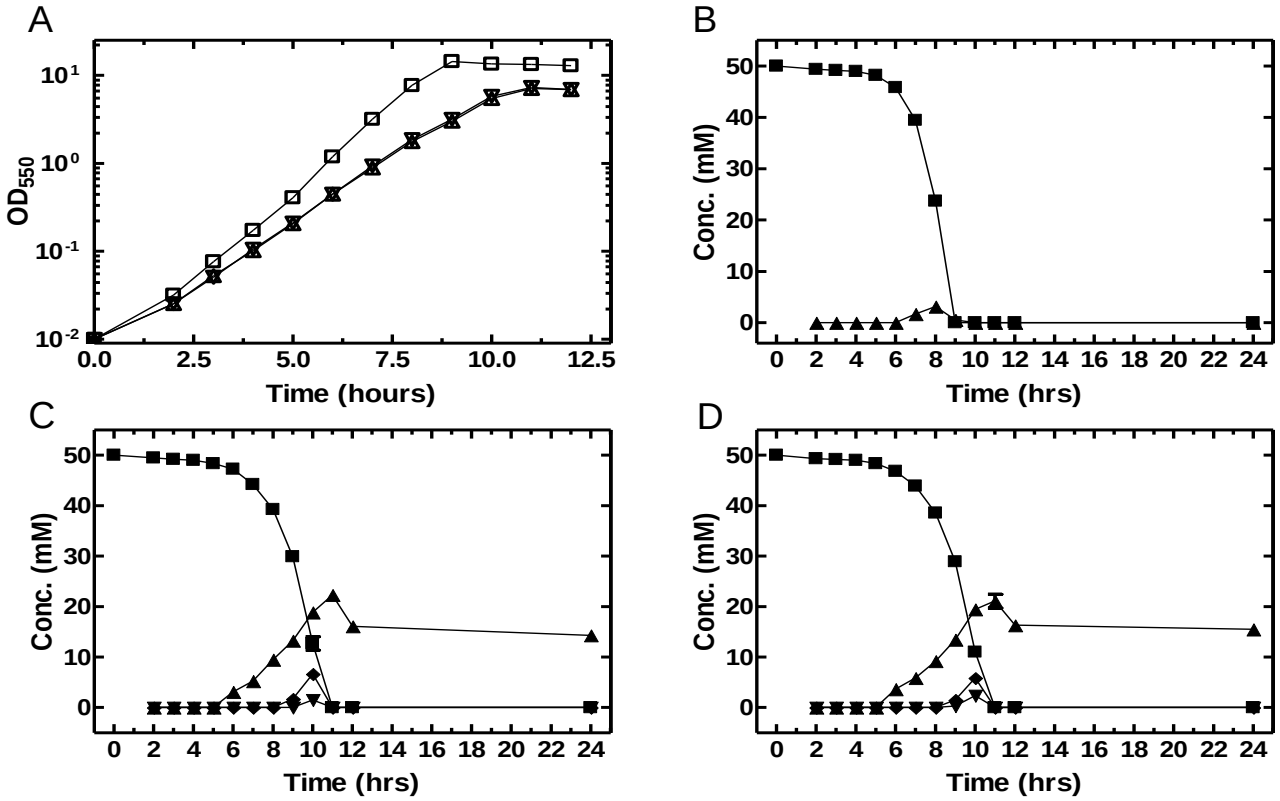

Figure 2-3. (A) Growth of aerobic cultures in glucose mineral salts medium. ATCC8739 (wild type), squares; JC25 (F_1^-), triangles; JC27 (SS^-), inverted triangles; JC16 (F_1^-, F_o^-), diamonds; JC29 (F_o^-), circles. Product formation and glucose consumption by (B) ATCC 8739, (C) JC25 and (D) JC27. In (B) through (D): glucose, squares; acetate, triangles; lactate, inverted triangles; pyruvate, diamonds; succinate, circles. Error bars represent standard error of the mean of triplicate values.

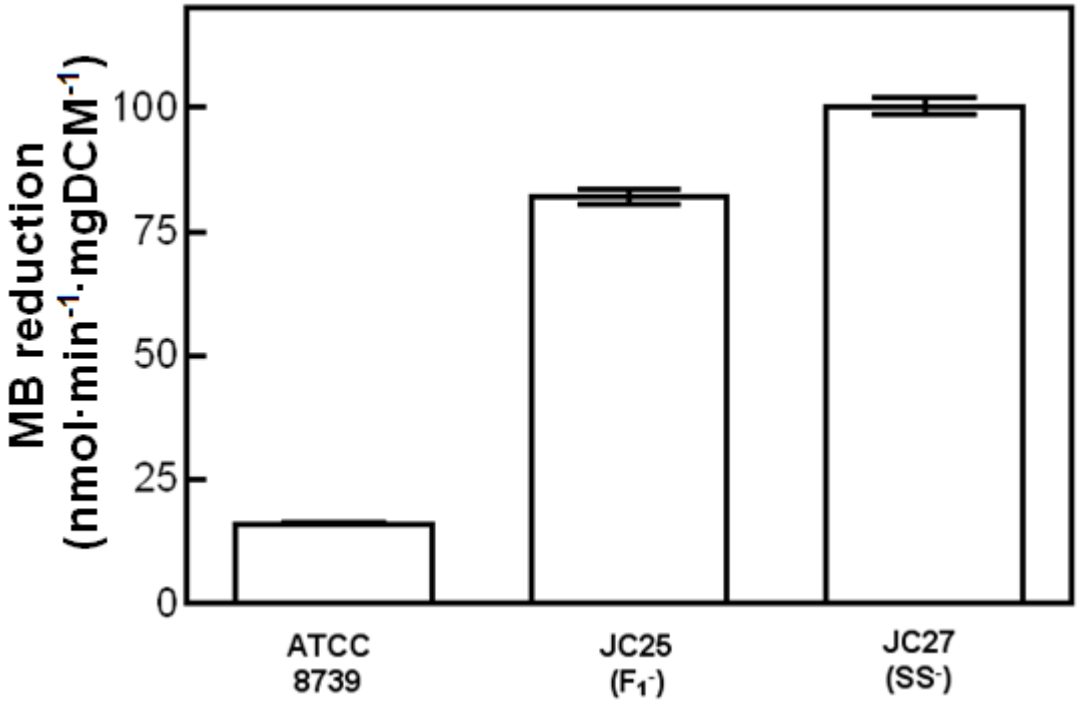

Figure 2-4. Net electron transfer from glucose as determined by methylene blue (MB) reduction by aerobically grown whole cells of *E. coli* strains indicated. Initial rates of reduction measured by decrease in A_{609}, background subtracted, calculated with MB standard curve and normalized by dry cell mass. Error bars represent standard error of the mean of quadruplicate values.

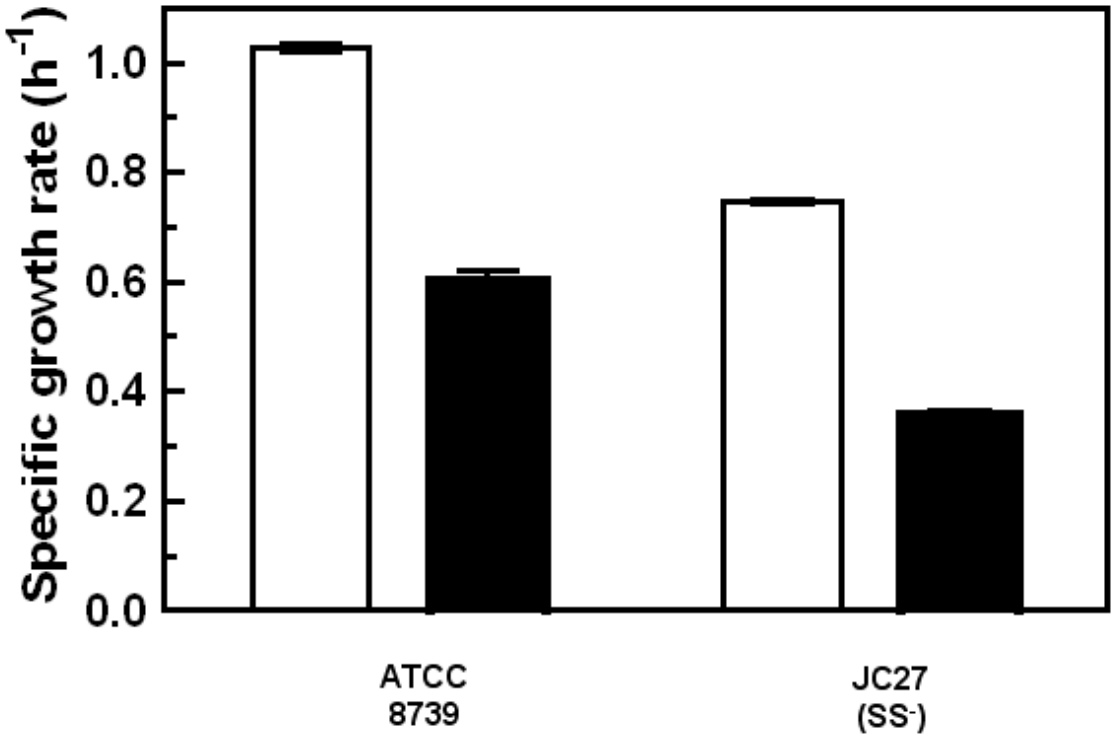

Figure 2-5. Growth rates of aerobically (open bars) and anaerobically (closed bars) grown cultures of *E. coli* strains indicated. Error bars represent standard error of the mean of triplicate values.

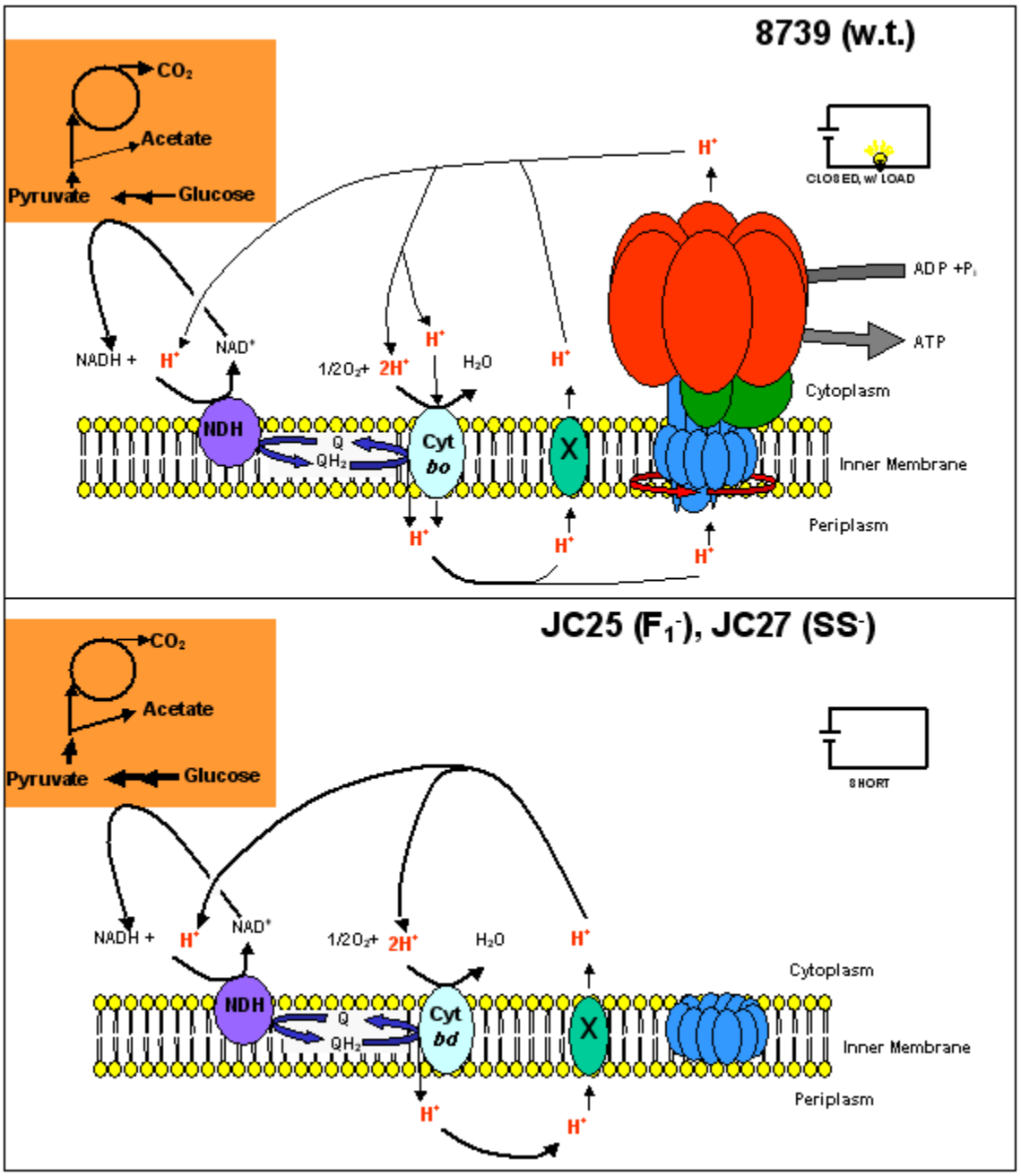

Figure 2-6. Circuit models for aerobically grown strains with glucose as carbon source. Thickness of arrows represents relative flux. NDH, NADH dehydrogenase; Cyt *bo*, Cyt *bd*, cytochrome *bo*- or *bd*-type oxidase; X, proton transporter. The large complex shown to the right side of the top panel represents the F_1F_O ATP synthase of which only the c subunit ring is present in the inner membrane of the strains represented in the bottom panel.

CHAPTER 3
DEVELOPMENT OF GENETIC TOOLS FOR STREAMLINING CHROMOSOMAL MODIFICATION OF *E. COLI*

Introduction

Development of a strain capable of efficient production of reducing equivalents at high rates required several chromosomal modifications within a single genome. Chromosomal engineering approaches previously used in our laboratory were not optimal for construction of strains with multiple modifications. We constructed tools for use in a streamlined chromosomal engineering method based upon Red recombinase-catalyzed homologous recombination and levansucrase counterselection.

Chromosomal Engineering Background

Genetic engineering through modification of chromosomal DNA has been central to many basic and applied studies. Manipulation of genomes through targeted integration or deletion has made predictable and stable genotypic alteration possible. Other tools such as random chromosomal mutagenesis and gene expression from plasmids have been used with success. However, random mutagenesis, using chemicals, transposons, or other means (such as UV radiation), is not precise and involves much screening for the desired change. Furthermore, these methods can introduce additional unintended changes which can complicate research efforts and negatively affect project goals. Plasmids can facilitate introduction of recombinant material and permit high levels of expression, but are often difficult to stably maintain over many generations.

A commonly used approach to making single gene deletions by homologous recombination in *E. coli* is a Red recombinase-catalyzed, "one-step" PCR-based method (30). Approximately 50 bp sequences, homologous to regions flanking the site for deletion, are included in the 5' end of PCR primers. These primers are used to amplify an antibiotic resistance marker and the product is used to transform the strain for deletion. The phage λ Red recombinase

genes *gam*, *bet* and *exo* are expressed from a helper plasmid with a conditional replicon in the strain that is to be modified. The Gam protein (γ) prevents degradation of the linear, dsDNA PCR product by *E. coli* nucleases (55) in the transformed cells. Exo is an exonuclease that creates 3' ssDNA overhangs which are bound by the Bet protein (β). β catalyzes the homologous recombination with the target sequence on the chromosome. Double-crossovers result in the replacement of the targeted chromosomal sequence with the PCR-amplified sequence containing the antibiotic resistance marker. The Red helper plasmid is cured from the deletion strain to prevent undesired effects from low-level expression of the Red genes in the absence of inducer. The antibiotic resistance marker can be removed later, by the activity of FLP recombinase (127) which can be expressed from another helper plasmid. FLP recombinase recognizes the FRT (FLP recognition target) sites that flank the antibiotic resistance gene and catalyzes a site-specific excision of the intervening sequence. An 82- to 85-bp scar sequence is left behind, which contains a single FRT site, along with stop codons in all reading frames.

An alternative to FLP-catalyzed antibiotic marker removal is the use of a cassette containing selective and counterselective markers. The cassette is integrated into the target by homologous recombination, as described above. A second Red recombinase-catalyzed recombination event is used to remove or replace the cassette, depending on whether seamless deletion or introduction new sequence is desired. Clones that lack the cassette are then recovered by counterselection. Counterselective markers used in this type of approach include *tetAR* (14), *tolC* (33) and *sacB* (66, 116). The *sacB* gene encodes a levansucrase, which transfers a fructosyl group from sucrose to make levan. In its native organism, *Bacillus subtilis* (and other levan producers), the levansucrase is secreted and the polymerization occurs outside the cell. In *B. subtilis* strains that are engineered to lack the ability to secrete the enzyme, the levan polymer

accumulates in the cytoplasm and leads to cell lysis. Levansucrase counterselection is effective in *E. coli*, as it cannot secrete the levansucrase.

The two-step homologous recombination strategy using selection and counterselection offers two significant advantages over the FLP-catalyzed marker removal. The first is the ability to make seamless deletions. The FRT-containing scar sequences that are left behind by FLP-catalyzed marker removal can be problematic, particularly if multiple deletions are to be made. Multiple FRT sites in the chromosome can result in rearrangement or excision events (30). Also, the FRT scar sequence can serve as a target for undesired integration of FRT-flanked marker sequences when deletions or replacements are attempted at other loci (30). Finally, for some applications, it is desirable to limit the amount of foreign sequence introduced into the chromosome in order to comply with governmental or industrial regulations.

The selection-counterselection method also permits replacement of chromosomal sequences. The popular one-step PCR-based deletion method provides a quick and simple means of making single deletions, but it is not suitable for more involved metabolic engineering projects. These projects may require multiple deletions and benefit from the ability to introduce new genes or regulatory elements into specific target sequences. Our study required multiple deletions to alleviate negative control of complete glucose oxidation and to eliminate fermentation pathways. We wanted to integrate *naoX* from *S. mutans* into the *E. coli* ATCC 8739 chromosome to increase the rate of electron transfer to an electrode via a diffusible mediator dye. Finally, we wanted to integrate *S. oneidensis* extracellular electron transfer genes to permit mediatorless electron transfer to an electrode. A streamlined method for making chromosomal gene replacements or seamless and nonpolar deletions was needed. Much time and effort is spent on the planning and construction of plasmids for specific deletions and replacements. pLOI4162

was designed to provide a versatile tool to make this process faster and easier. Use of the cassette from this plasmid, in conjunction with a two-step Red recombinase-catalyzed homologous recombination procedure allows targeted gene deletions that leave behind a minimal sequence artifact (18 bp) containing stop codons in all reading frames (Figure 3-1). Alternately, a seamless deletion can be made, by using a different second recombination step. A new sequence can be used to replace the cassette in the second step, via a simple cloning step.

While the above tools were designed to simplify new deletions and replacements, our lab had many strains with multiple FRT scar sequences in their chromosomes from prior chromosomal engineering. We were interested in removing these sequences because they were a source of chromosomal instability and further modification was unsustainable because of the effects discussed earlier. Also, some of these strains were being used in industrial processes where the amount of foreign sequence in the chromosome needed to be minimal, due to regulatory requirements. One approach that we could have used to remove these sequences would have been to delete them using the same two-step strategy described above, using the selective, counterselective cassette from pLOI4162. Another option was to construct a plasmid from which circular DNA, containing a single FRT site and lacking an origin of replication, could be made easily. This circular DNA would contain both selectable and counterselectable markers and would be used to integrate into FRT sites in the chromosome, catalyzed by the FLP recombinase (30). Then the FRT-flanked cassette could be removed in a Red-catalyzed homologous recombination step. For this purpose, pLOI4151 was constructed and used to remove scar sequences from lactate-producing strains (139).

Construction of Plasmids

Construction of pLOI4162 Containing a *cat-sacB* Cassette for Markerless Gene Deletions

To facilitate sequence replacement and sequential deletions in chromosomal DNA, plasmid pLOI4162 (Figure 3-2) was constructed with a removable *cat-sacB* cassette and the option to include an 18 bp segment of synthetic DNA with stop codons in all reading frames. This plasmid is composed of synthetic sequences and parts of plasmids pLOI2228 (79), pLOI2511 (120), and pEL04 (66, 116). Using pEL04 as a template, inside-out PCR was performed with the JMpEL04F1/R1 primers to eliminate unwanted *Sma*I and *Bam*HI sites between the *cat* and *sacB* genes. The amplified product was digested with BglII (within both primers) and self-ligated to produce pLOI4152. Plasmid pLOI4131 was constructed by ligation of the FRT-*cat*-FRT fragment (Klenow-treated *Ban*I, *Cla*I) from pLOI2228 into compatible sites of pLOI2511 (Klenow-treated NheI, ClaI). Plasmid pLOI4131 was subsequently digested with *Eco*RI and self-ligated to remove the FRT-cat-FRT fragment to produce pLOI4145, retaining single *Kas*I and *Xma*I sites. A polylinker segment (SfPBXPS) was prepared by annealing complementary oligonucleotides (SfPBXPSsense and SfPBXPScomp). After digestion with *Kas*I and *Xma*I, this segment was ligated into corresponding sites of pLOI4145 to produce pLOI4153. The modified *cat-sacB* cassette in pLOI4152 was amplified by PCR using the JM*catsacB*up3/down3 primer set. After digestion with *Bam*HI and *Xho*I, this cassette was ligated into corresponding sites of pLOI4153 to produce pLOI4146. To create an 18-bp region (5'GCCTAATTAATTAATCCC3') with stop codons in all six reading frames, pLOI4146 was digested with *Pac*I and self-ligated to produce pLOI4154 (not shown), removing the *cat-sacB* cassette. Two additional bases (T and A) were inserted between the *Sfo*I and *Pac*I sites of pLOI4154 using mutagenic primers (JM4161sense/comp) and linear plasmid amplification to produce pLOI4161 (not shown).

Finally, the *Pac*I digested fragment from pLOI4146 containing the *cat-sacB* cassette was ligated into the *Pac*I-digested site of pLOI4161 to produce pLOI4162 (GenBank accession EU531506).

Construction of pLOI4151 for Removal of FRT Sites

The *cat-sacB* cassette was PCR amplified from pEL04 (66, 116) with the JMcatsacBupNheI and JMcatsacBdownNheI primers. pLOI4151 (Figure 3-3) was constructed by ligating the *Nhe*I-digested *cat-sacB* PCR product into pLOI3421 (134).

pLOI4162-based Chromosomal Modification Procedure

The two-step recombination method for making targeted chromosomal modification using the *cat-sacB* cassette from pLOI4162 is generally described in this study (Figure 3-1) and in a previous report (51). However, as the method may be useful to those less familiar with the techniques involved, a few aspects are emphasized here. Careful design saves time later when designing PCR primers and planning construction of tools for gene deletions and replacements. The pLOI4162 method allows much flexibility in the selection of the chromosomal sequence to be deleted or replaced. Unlike the one-step PCR method (30), where practical oligonucleotide synthesis limits the length of the homologous flanking sequence used for recombination to less than 100 bp, the flanking region can be much longer. Longer homologous flanking sequence provides greater recombination efficiency and decreases the likelihood of integration into an undesired location. Flanking sequences of approximately 200 to 500 bp are generally used with this method. The product yield from the inside-out PCR step during plasmid construction may be negatively affected by designing very long flanking sequences. The pCR2.1 vector, which is used for PCR cloning the region of interest, is 3.9 kbp. Therefore flanking sequences of 1 kbp each would require PCR amplification of a 6 kbp sequence, for example. While such reactions are done routinely, using much longer flanking sequences might make plasmid construction and

recombination fragment preparation more difficult, without significantly affecting the efficiency or fidelity of recombination.

The multiple cloning sites containing the *Sma*I and *Sfo*I restriction sites used to remove the *cat-sacB* cassette from pLOI4162 contain extensive secondary structure, which may partially block restriction enzyme access. Yields from the double digest are generally around 50%. The inefficiency of the restriction digest makes it important to scale up to avoid the need for repetition. Gel purification at this step may help ligation efficiency, but is unnecessesary for downstream steps due to selection for desired transformed ligation products. Transformants containing the first step plasmid (*cat-sacB* cassette ligated into the inside-out PCR product) can be selected for with a combination of kanamycin and chloramphenicol and screened for sucrose sensitivity. After PacI digest and self-ligation (for deletion) or ligation with replacement gene, LB (no NaCl) kanamycin plates containing 6% sucrose should be used to select for transformants lacking the *cat-sacB* cassette.

Sucrose sensitivity with a single chromosomal copy of *sacB* is not strong enough to permit plate-based selection without liquid-based selection first. High copy number (pUC-based plasmid) allows plate-based sucrose selection and counterselection during plasmid construction. It is important to have a sufficient number of doublings prior to sucrose selection to allow complete chromosomal segregation. Outgrowth time depends on the growth rate of each strain, likewise time before plating from LB-sucrose liquid-based selection. Low second-step efficiency is generally due to problems in construction or due to high frequency of recombination (or lack of complexity) in target sequence region. If few of the colonies from the *cat-sacB* replacement step have the desired genotype, reanalyze target sequence region and design new primers for reconstruction of tools. Target sequence problems aside, given enough time for chromosomal

segregation and sucrose (liquid) selection, the second step *cat-sacB* replacement is highly efficient.

Applications of pLOI4162 Method

The above-described pLOI4162 method was used in all chromosomal gene deletions and replacements in our study, with the exception of the *atp* deletion strains. Additionally the method has been used for improvement of a succinate producing strain of *E. coli* (51). Several other projects in our laboratory, including those focusing on production of malate and ethanol are also using this method in their strain constructions. Recently, two papers were published describing the application of the pLOI4162 method in the modification of *Enterobacter asburiae* for the production of ethanol (13) and of optically pure D(-)-lactic acid (12) demonstrating the utility of the method in the engineering of other, related organisms. Other research groups have requested pLOI4162 since the publication of the method in the succinate production improvement paper (51). Plasmid pLOI4162 promises to be a broadly applicable tool for facilitating chromosomal modification for basic and applied research.

Applications of pLOI4151

The pLOI4162 method has been widely adopted by our lab for current and future chromosomal engineering efforts. However, prior to the introduction of pLOI4162, we used the FLP recombinase-catalyzed removal of FRT-flanked antibiotic markers (30). That method left FRT-containing "scar" artifacts in the chromosomal sequence. These sequence artifacts complicated further chromosomal engineering efforts and also created problems due to some governmental regulations and industry preferences limiting the amount of foreign DNA sequence in biocatalyst strains. The pLOI4162 method can be used to remove the sequence artifacts if the genomic context is known. However, in a few cases, due to rearrangement or other issues, this context was not known and another approach was desired. pLOI4151 was designed to provide

either a *cat-sacB* or a *sacB-aac* cassette-containing, non-replicating circle, upon removal of the origin of replication and unwanted antibiotic resistance gene. These circles are then used in a FLP-recombinase catalyzed, single-crossover homologous recombination, to integrate the cassette into the site. If the exact location in the genome is unknown, cassette-specific primers can be used to sequence the flanking regions. A library of the genomic DNA from the integration strain can be made for isolation of a plasmid containing the cassette, scar and flanking sequence. Inside-out PCR and self-ligation can be used to remove the cassette and scar sequence. The resulting plasmid can be used in a manner identical to the second step recombination of the pLOI4162 method, for removal of the cassette and scar sequence from the chromosome. The pLOI4151-based circle method was used to remove all foreign DNA sequence from a lactate producing strain of *E. coli* (139). pLOI4151 also served as selectable and counterselectable marker sequence donor for modified use in the metabolic engineering of *E. coli* for succinate and malate production (50), as well as for production of L-alanine (137) and other compounds.

Table 3-1. Plasmids and PCR primers

Plasmid/ primer	Relevant features	Reference/source
Plasmids		
pEL04	*cat-sacB*	(116)
pLOI2228	FRT-*cat*-FRT	(79)
pLOI2511	*bla*,FRT-*kan*-FRT	(119)
pLOI4131	*bla*,FRT-*cat*-FRT	(51)
pLOI4145	*bla*,FRT-*cat*-FRT	(51)
pLOI4146	*bla, cat-sacB*	(51)
pLOI4151	*bla,* FRT-*cat-sacB-aac*-FRT (Figure 3-3)	(137)
pLOI4152	*bla, cat-sacB*	(51)
pLOI4153	*bla,* SfPBXS polylinker	(51)
pLOI4154	*bla, Pac*I digested pLOI4161, self-ligation	(51)
pLOI4161	*bla, cat-sacB Pac*I cassette	(51)
pLOI4162	*bla, cat-sacB Pac*I cassette (Figure 3-2)	(51)
Primers		
JM4161sense	ACCGCATCAGGCGCCTAATTAATTAATCCC GG	(51)
JM4161comp	CCGGGATTAATTAATTAGGCGCCTGATGCG GT	(51)
JMpEL04F1	CAGCAGATCTAAGTAAATCGCGCGGGTTTG	(51)
JMpEL04R1	CAGCAGATCTAGCGGCTATTTAACGACCCT	(51)
JM*catsacB*up3	TGTGCTGCAAGGCGATTAAG	(51)
JM*catsacB*down3	TTCGATCACGGCACGATCAT	(51)
SfPBXSsense	ATGTAGGCGCCATTAATTAATGGATCCACT ATCTCGAGATTAATTAATCCCGGGACTAT	(51)
SfPBXScomp	ATAGTCCCGGGATTAATTAATCTCGAGATA GTGGATCCATTAATTAATGGCGCCTACAT	(51)

Primer sequences are 5’ to 3’

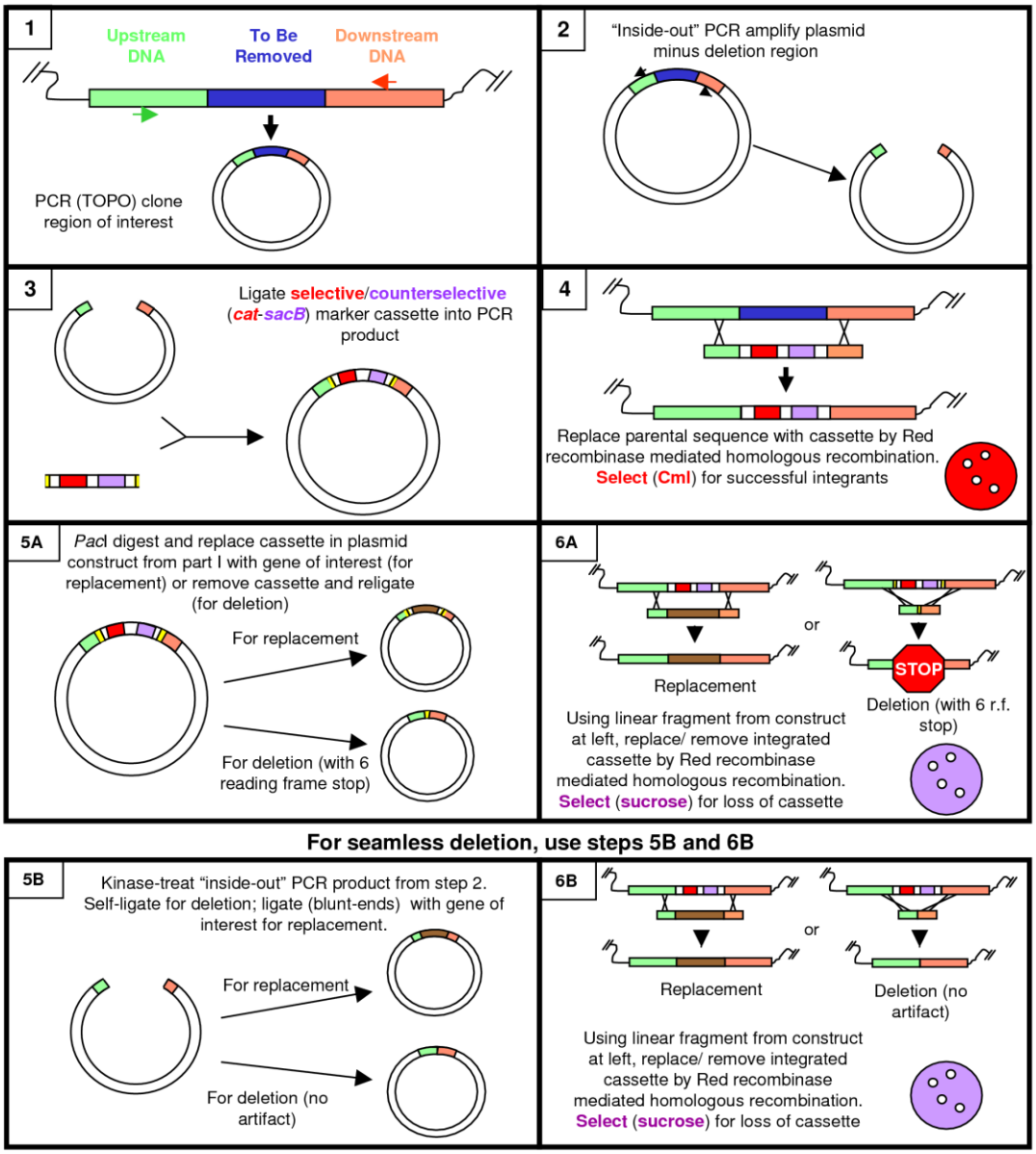

Figure 3-1. A simple method for making chromosomal deletions or replacements. Steps 1 through 4 describe the integration of the cat-sacB cassette into the region for deletion or replacement. The *cat-sacB* cassette is produced by digesting pLOI4162 with *Sma*I and *Sfo*I. The inside-out PCR uses a proofreading polymerase that leaves blunt ended products. Steps 5A and 6A describe an option for the second recombination step in which a deletion can be made, leaving a 18 bp sequence containing stop codons in all reading frames. If a gene replacement is desired, the gene of interest can be amplified by PCR with *Pvu*I recognition sequences in the primers. *Pvu*I digestion provides compatible cohesive ends for ligation into the *Pac*I-digested plasmid. Steps 5B and 6B describe another option, which produces a seamless deletion. From (51), p. 886 (Figure 1), with permission.

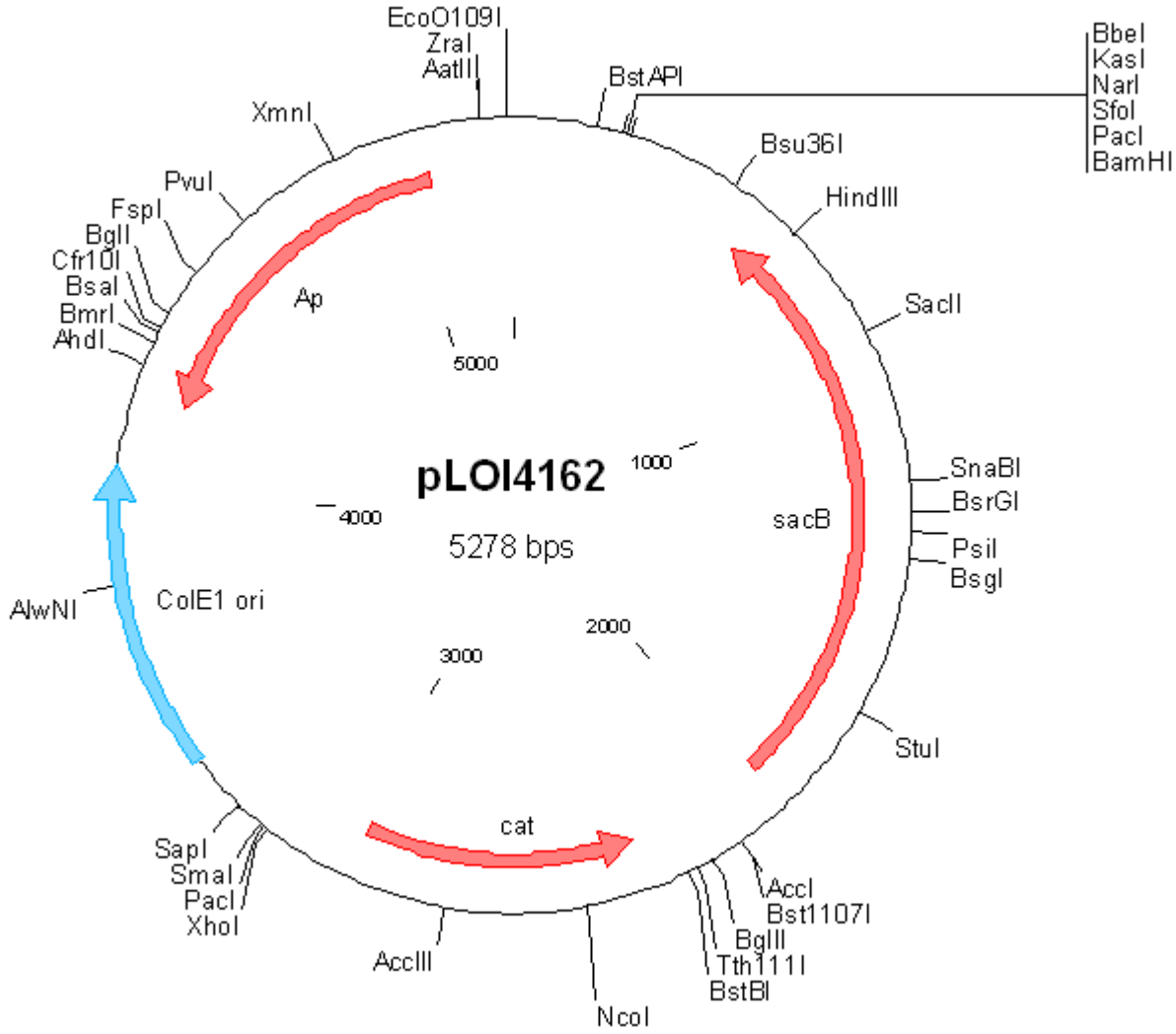

Figure 3-2. Plasmid map of pLOI4162. Ap, beta-lactamase gene; *cat*, chloramphenicol acetyltransferase gene; *sacB*, levansucrase gene. The complete sequence for this plasmid is available from GenBank (accession number EU531506).

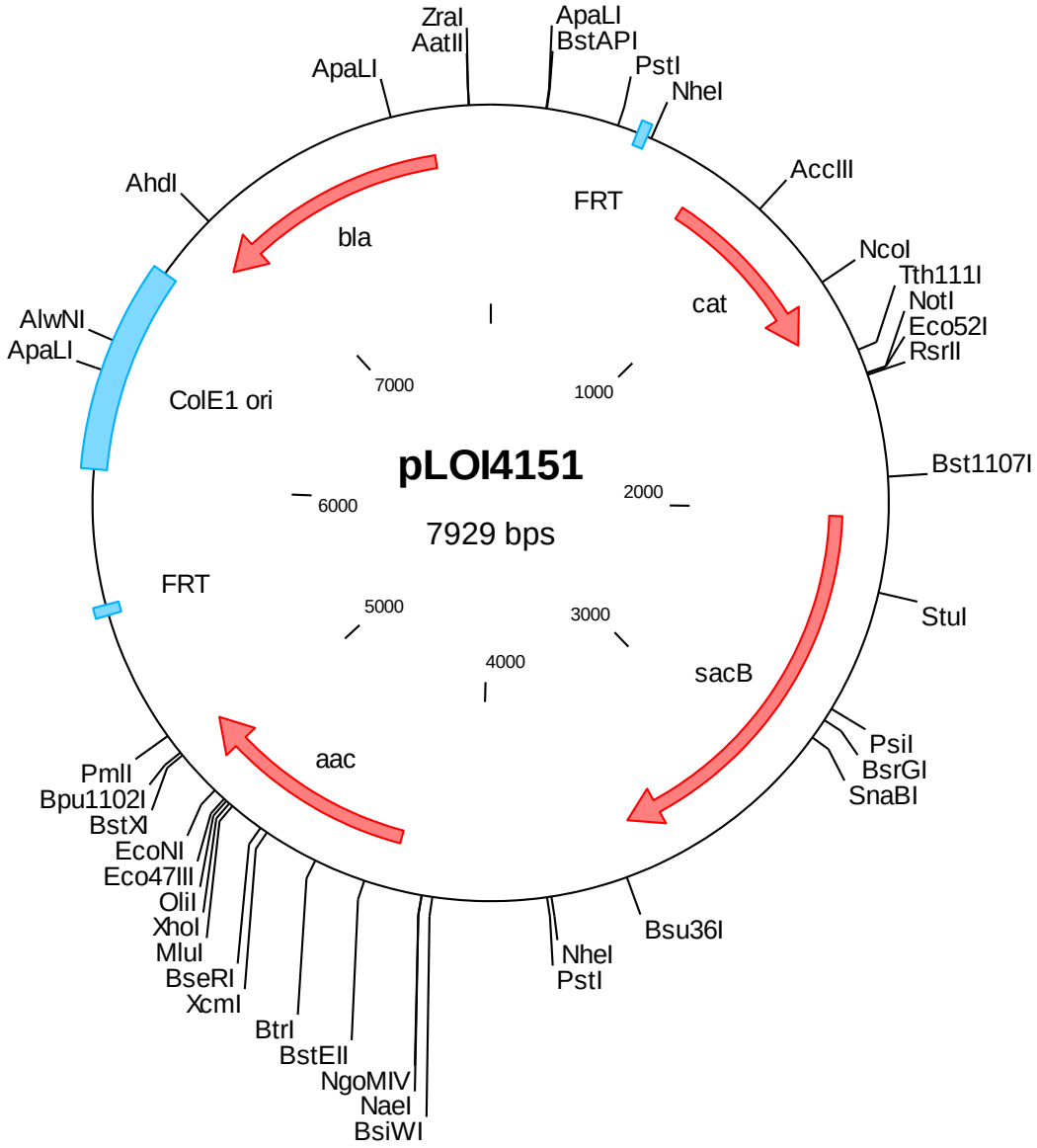

Figure 3-3. Plasmid map of pLOI4151. *bla*, beta-lactamase gene; *cat*, chloramphenicol acetyltransferase gene; *sacB*, levansucrase gene; *aac*, apramycin acetyltransferase gene.

CHAPTER 4
METABOLIC ENGINEERING OF *E. COLI* ATCC 8739 FOR INCREASED CURRENT AND COULOMBIC EFFICIENCY IN AN ELECTROCHEMICAL CELL

Introduction

Microbial fuel cell technology offers many advantages as a means of converting stored chemical energy from organic materials into electrical energy. Due to global concern about limited fossil fuel resources and about the environmental impact of current practices, there is growing interest in energy efficiency and sustainability. MFCs can be important tools for creating a more efficient and sustainable energy infrastructure. Direct, microbially catalyzed conversion of stored energy from almost any organic material into useful electrical energy provides versatility and a shorter carbon cycle. MFCs can increase efficiency through the elimination of the energy wasting intermediate steps required by most current methods of electricity production from stored chemical energy. However, widespread adoption of MFC technology is presently limited by low power output (92). Even for stationary generation of electricity from low or negative value feedstocks, such as wastewater treatment, low power output makes cost justification difficult.

Much work is being done to improve MFC design to increase power output (1, 38, 69, 100, 101). While MFC design optimization is important, a major rate-limiting factor in MFC power production is microbial catabolism of the substrate (88), coupled with the transfer of liberated electrons to the electrode. Since the discovery of mediatorless electron transfer to electrodes (59), very little work has been published on thorough study and engineering of MFC microbial biocatalyst metabolism. The bulk of the biological studies have focused on classification of the electrogenic microbial consortia enriched for in an MFC (49, 60, 61, 93, 99). MFC power increases should be possible through the engineering of microbial metabolic pathways and electron transport systems for MFCs, particularly in conjunction with MFC design optimization.

Our study endeavors to develop *E. coli* as a model for such improvements. *E. coli* was selected for its broad substrate range, ease of genetic manipulation, minimal nutrient requirements, and extensive background of physiological and genetic information.

E. coli is capable of rapid catabolism of glucose, particularly under fermentative conditions. When no external electron acceptor is present, *E. coli* derives ATP from substrate-level phosphorylation and achieves redox balance by reducing endogenous metabolic intermediates such as pyruvate in a fermentative metabolism. High glycolytic flux compensates for the lower ATP yield in the absence of oxidative phosphorylation. If electrons are harvested from reduced cofactors (such as NADH) in a microbial fuel cell (MFC), this high glycolytic flux can produce high electrical current. However, under anaerobic conditions, *E. coli* incompletely oxidizes glucose, resulting in a low electron recovery (low Coulombic efficiency) and side product formation, which can limit the long-term stability of MFC operation. For an MFC, both high rate and high Coulombic efficiency are desired.

In order to develop an improved *E. coli* strain for bioelectricity production, we have used the targeted gene deletion and replacement strategies described in the previous chapter to increase the rate and efficiency of reducing equivalent production. We focused on lowering cellular ATP/ADP and NADH/NAD^+ ratios in order to increase flux through the central metabolic pathways, while eliminating acetate overflow metabolism and pathways competing for NADH. In addition to the targeted chromosomal modification approach, aerobic batch transfers in a pyruvate mineral salts medium were used to select for increased flux through the PDH complex and through the TCA cycle.

Materials and Methods

Growth Conditions and Media

Unless otherwise specified, all working cultures of *E. coli* ATCC 8739 (51) and its derivatives were grown in a minimal MOPS (4-morpholinopropanesulphonic acid, 0.1 M, pH 7.4) buffered NBSM medium previously described (20), containing 0.05 M glucose. Baffled 250 ml flasks were used for aerobically grown batch experiments with 50 ml culture volume at 37°C and 250 rpm agitation. In aerobic pyruvate transfer experiments, 0.1 M sodium pyruvate was used in place of glucose. LB broth and LB agar plates were used during plasmid and strain construction. Glucose was added (20 g/liter) to the LB broth and plates in most cases in strains containing the *atpFH* deletion. L-arabinose was included (20 g/liter) in the medium to induce expression of the Red recombinase genes on pKD46. LB broth with NaCl omitted and containing 100 g/liter sucrose was used in selection for loss of *sacB* (encoding levansucrase). Similarly plate-based selection for removal of *sacB* used LB, no NaCl, 60 g/liter sucrose. Antibiotics were included, as necessary, during plasmid and strain construction (kanamycin, 50 mg/liter; ampicillin, 100 mg/liter; chloramphenicol, 40 mg/liter).

Genetic Methods

Construction of strains used in this study was carried out as described previously (51) and in the preceding chapter, using the *cat-sacB* cassette from plasmid pLOI4162 and two step, Red recombinase catalyzed double crossover homologous recombination for markerless deletions and integrations. Additional bacterial strains, plasmids and PCR primers, discussed in this section and not listed earlier, are listed (Table 4-1).

To eliminate pathways that could compete for NADH and limit current production, *pflB*, *adhE*, and *ldhA* were deleted from JC27 (Δ*atpFH*) to produce JC62. Briefly, each gene was amplified by PCR from ATCC 8739 genomic DNA and cloned into pCR2.1-TOPO. Each of

these plasmids was used as template for an inside-out PCR (*Pfu* polymerase) with gene-specific primers which resulted in a product consisting of linearized vector sequence, flanked by the 5' and 3' ends of the gene, with the interior of the gene sequence eliminated. The *cat-sacB* cassette from pLOI4162 was ligated into the inside-out PCR product and the ligation was transformed into TOP10F'. Desired clones were kanamycin and chloramphenicol resistant and sensitive to sucrose. This plasmid construct was linearized with an appropriate restriction enzyme, diluted 1000-fold, and amplified by PCR, using the original gene cloning primers. The product was electroporated into the parent strain, which was induced for expression of the Red recombinase genes from pKD46. Successful integrants were chloramphenicol resistant and ampicillin sensitive, after curing of pKD46 at 39°C or 40°C. The *cat-sacB* cassette-containing plasmid construct was *Pac*I digested to remove the cassette and self-ligated. The resulting plasmid was digested, diluted and PCR-amplified for use in a second homologous recombination step, to remove the *cat-sacB* from the chromosome. The replacement of the cassette resulted in an 18-bp sequence containing stop codons in all reading frames. The same procedure as used to delete *ackA* from JC62 to make JC66, to prevent flux to acetate via phosphotransacetylase and acetate kinase.

The native *lpd* (encoding dihydrolipoamide dehydrogenase) in JC101 was replaced by a copy (*lpd101*) (62) containing a single nucleotide substitution, making an acidic to basic amino acid change (E354K). ATCC 8739 genomic DNA was used as the template for PCR amplification of *lpd*. The product was cloned into pCR2.1-TOPO to produce pLOI4179. Complementary mutagenic oligonucleotides JME354Ksense and JME354Kcomp were used to introduce the *lpd101* mutation using linear plasmid amplification (51), to produce pLOI4180. Several of the resulting clones were verified by sequencing. The mutated gene was amplified by

PCR and used to replace the *cat-sacB* cassette as described above. The *lpd101* mutation in the new strain, JC80, was verified by sequencing.

Reoxidation of NADH during aerobic respiration can be rate-limiting and it is likely to be more so in an MFC, with a less positive (than oxygen) electron acceptor. The gene encoding a water-forming NADH oxidase from *Streptococcus mutans* ($naoX_{Sm}$) (80) was PCR amplified with primers containing *Pvu*I restriction sites on their 5' ends (JM*naoX*F1 and JM*naoX*R1) and cloned into pCR2.1-TOPO. The gene was integrated into two chromosomal loci, providing different levels of transcription from chromosomal promoters (or from its own promoter). A variation of the two-step homologous recombination procedure (described above) was used in the integrations. During construction of the plasmid for the second recombination step (*cat-sacB* replacement), *Pvu*I digested $naoX_{Sm}$ PCR product was ligated into the *Pac*I digested (*cat-sacB* cassette removed) vector. In this way, $naoX_{Sm}$ was integrated into *ackA* in JC62 to produce JC68 and in JC80 to produce JC85. The integrated $naoX_{Sm}$ in JC68 was oriented in the opposite orientation to *ackA*, such that the gene was not transcribed from the *ackA* promoter. JC85 had $naoX_{Sm}$ integrated into *ackA* so that it could be transcribed from the *ackA* promoter. To increase expression levels of $naoX_{Sm}$, it was also integrated into *pflB* in JC85 (under *focA-pflAB* operon promoter transcriptional control) to produce JC93.

Electrochemical Analytical Methods

Coulombic yields from glucose were measured using a three electrode, poised potential electrochemical cell (Figure 4-1). The cell was a bulk electrolysis cell (BASi, West Lafayette, IN) with a reticulated vitreous carbon working electrode, a platinum wire counter electrode in a fritted glass chamber and an Ag/AgCl reference electrode. The anode potential was poised at +100 mV vs. Ag/AgCl using eDAQ (Colorado Springs, CO) EA161 potentiostats connected to an eDAQ e-corder 821 and Chart software. The anolyte was stirred with a small magnetic stir bar

at 250 rpm and the headspace of the working electrode chamber was continuously flushed with 100 ml/min argon, to maintain anaerobic conditions.

The anolyte was composed of NBS medium (20) containing 0.1 M MOPS and 0.1 M NaCl, with 0.001 M thionin. Measurement of current began with 60 ml anolyte. Aerobically grown cells (50 ml) were harvested (5000×g, 5 min, 22°C) at stationary phase (16.5 h culture from 3 mg/liter initial cell density). The cells were washed once (30 ml anolyte, lacking thionin), centrifuged again and resuspended to a cell density of 50 mg in 15 ml anolyte. The cell suspension was added to the working electrode chamber (upon stable current baseline) and the current was monitored until all charge transfer from endogenous reserves completed and a stable baseline (no change for at least 30 min) or an arbitrarily determined 1 mA threshold level was reached. At this point, anolyte containing 0.01 M glucose was added by syringe and the resulting current was measured over time until it returned to the starting level of the first glucose pulse and the next pulse was added. In this way, multiple pulses of glucose were added and the Coulombic efficiencies determined by integrating the area under each peak above the threshold value (the current immediately before addition of glucose) and dividing by the theoretical Coulombic yield from the amount of glucose added in each pulse. All additions to the working electrode chamber were pre-sparged with at least 100 volumes of argon and were transferred anaerobically to the vessel using a stoppered flask and positive argon pressure to initiate the transfer (argon-sparged glucose transferred by 1 ml syringe).

NADH Oxidation Assay

Total cytoplasmic NADH oxidase activity was measured to determine the effect of integrations of *naoX*$_{Sm}$ into *ackA* and *pflB*. Aerobically grown cells (20 ml of a 25 ml, ~0.33 g/liter, culture in a 250 ml flask) were harvested (5000×g, 5 min, 4°C) after chilling briefly on ice. The cells were washed once with cold TM buffer (0.05 M Tris-HCl, 0.01 M MgCl, pH 7.5)

and resuspended in TM buffer (1 ml, containing 0.01 mg/liter DNase I). The cells were lysed by mechanical disruption using a Fast Prep 24 system from Molecular BioProducts (San Diego, CA).

NADH oxidase assay reactions contained NADH (0.25 mM) in TM buffer. The reaction was initiated by the addition of cell lysate (0.1 ml in a 1 ml reaction vol). NADH oxidation was followed at A_{340} at room temperature. Protein concentration of the lysates was determined using the bicinchoninic acid method (BCA Protein Assay Kit, Thermo Scientific, Rockford, IL) with bovine serum albumin as a protein standard. Specific activity (nmol min^{-1} mg $protein^{-1}$) was calculated using the molar extinction coefficient for NADH (6220 $M^{-1}cm^{-1}$).

Results

Elimination of Competition for NADH

In the presence of an electron acceptor with a sufficiently positive reduction potential, NADH should be reoxidized quickly enough to prevent the involvement of fermentative pathways during sugar metabolism in *E. coli*. The fermentative enzymes are affected by cellular redox state through regulation of their gene expression, through direct or indirect inactivation of catalytic activity, and through K_m values for NADH that are lower than the NADH dehydrogenases. Ideally, NADH reoxidation should not be rate limiting in an MFC. However, the anode potential is not as positive as oxygen, due to overpotentials, and it is subject to fluctuation if it is not kept constant with a potentiostatic system. Production of fermentation products in an MFC lowers Coulombic efficiency and their accumulation can limit long-term current stability. Therefore, it is desirable to eliminate the primary fermentation pathways through targeted gene deletion. Genes encoding alcohol dehydrogenase (*adhE*), lactate dehydrogenase (*ldhA*), and pyruvate formate-lyase (*pflB*) were deleted to produce JC62 (Figure 4-2), using the markerless gene deletion method described in a previous chapter. This method

left only an 18-bp sequence (containing stop codons in all reading frames) in each deleted region and was developed to permit multiple chromosomal modifications within a single strain, without increasing the likelihood of undesired rearrangements and without hindering the introduction of further modifications. Gene deletions were verified by PCR and by phenotype. Deletion of *adhE*, *ldhA* and *pflB* did not have a significant effect upon growth or product formation (data not shown) under aerobic conditions, nor did it significantly affect current production or Coulombic yield in poised potential electrochemical cell testing (Table 4-2).

Deletion of *ackA*

The higher rate of glycolysis in *atpFH* deletion strains leads to increased acetate production under aerobic conditions. This overflow metabolism is due to the inability of the respiratory chain to maintain redox balance. The redox imbalance limits flux through the PDH complex and through the TCA cycle. Production of acetate, via phosphotransacetylase and acetate kinase activity, yields one ATP per pyruvate and prevents the buildup of reducing equivalents that would otherwise occur through further oxidation of pyruvate via the TCA cycle. Glucose catabolism to acetate by this pathway yields four reducing equivalents, while complete oxidation of the glucose by the TCA cycle adds eight more. This overflow mechanism results in almost ten percent of glucose carbon going to acetate in aerobically grown JC27 cultures. That much incompletely oxidized side product represents a six percent reduction in Coulombic yield. The decrease in Coulombic yield due to acetate production could be even greater under MFC operating conditions.

An *ackA* deletion was made (in JC62) to decrease acetate production, resulting in JC66. This strain produced less acetate. However, the downstream rate limitation remained and pyruvate accumulated as a result of rate limitation at the PDH complex node (data not shown). Elimination of the phosphotransacetylase/acetate kinase pathway created the backup of carbon to

the pyruvate node because available catabolic pathways from pyruvate caused a redox imbalance. Oxidation of pyruvate to acetate via pyruvate oxidase yields no ATP and involves the transfer of electrons to ubiquinone. This process would decrease the amount of ubiquinone available to reoxidize NADH (catalyzed by NADH dehydrogenase) from glycolysis. Flux through the PDH complex and the TCA cycle would provide one ATP per pyruvate, but would also create a redox imbalance through production of excess reducing equivalents. Excess NADH limits flux through this pathway through the negative control of the PDH and α-KGDH complexes (62) and of other TCA cycle enzymes, particularly citrate synthase (4).

Heterologous Expression of *naoX*$_{Sm}$

The water-forming NADH oxidase from *S. mutans* catalyzes the reoxidation of NADH in the cytoplasm via a two-electron transfer to molecular oxygen (48). Heterologous expression of a gene (from *S. pneumoniae*) encoding a water-forming NADH oxidase in *E. coli* increases flux through the PDH complex and TCA cycle by helping to overcome the rate limitation of NADH reoxidation by the respiratory chain (124, 125). Initially, *naoX* from *S. mutans* was cloned into pCR2.1-TOPO and expressed in JC62 to evaluate its effect on growth and metabolism (Figure 4-3). The control strain (JC62/pCR2.1) produced a maximum of 17.7 mM pyruvate and 23.9 mM acetate from 50 mM glucose in aerobic NBSM batch culture, while JC62 transformed with pLOI4174 (*naoX*$_{Sm}$) accumulated a maximum of 3.9 mM pyruvate and 23.9 mM acetate. This result suggested that expression of *naoX*$_{Sm}$ in JC62 allowed increased flux through the PDH complex and to a lesser extent, through the TCA cycle, consistent with the previous studies (124, 125). However, much of the acetyl-CoA was still converted to acetate, indicating that citrate synthase remained as a rate-limiting step for complete glucose oxidation via the TCA cycle.

JC62 retained an intact Pta/AckA pathway. In order to be able to harvest all electrons from glucose through its complete oxidation by the TCA cycle, the carbon flow to acetate needed to

be redirected. *ackA* was replaced with $naoX_{Sm}$ by chromosomal integration to eliminate the primary route to acetate, while simultaneously enabling higher flux through the PDH complex and perhaps the TCA cycle. The resulting strain, JC68, grew slightly faster than JC66 (Δ*ackA*), presumably due to higher flux through the TCA cycle (Figure 4-4). The ATP available via succinyl-CoA synthetase of the TCA cycle could help to offset the ATP that was no longer available from acetate production in the Δ*ackA* strains. Despite the growth rate difference, both JC66 and JC68 accumulated similar concentrations of pyruvate. Without the overflow pathway to acetate, a redox imbalance was likely caused by higher flux through the TCA cycle. The NADH produced by the TCA cycle was not reoxidized fast enough, despite the presence of the water-forming NADH oxidase in JC68. A high NADH/NAD^+ ratio negatively controls PDH activity (62) and the negative redox feedback control circuit caused the pyruvate accumulation.

Different levels of $naoX_{Sm}$ expression were tested by integrating the gene in different orientations in *ackA* and by integrating an additional copy into *pflB* (gene replacement). JC68 had $naoX_{Sm}$ replacing *ackA*, but in the opposite orientation, so that it was not transcribed from the *ackA* promoter. Expression of $naoX_{Sm}$ in JC68 was presumed to be from its own promoter. The gene was replaced in the other orientation during construction of JC85, to allow its transcription from the *ackA* promoter. Next, an additional copy was used to replace *pflB*, under the control of the *focA* promoter, resulting in JC93. NADH oxidase (NOX) activity of the soluble fractions from these strains was measured to assess the relative expression of $naoX_{Sm}$ (Figure 4-5). JC68 and JC92 (JC85, Δ*pflB::cat-sacB*) soluble fractions had almost twice the NOX activity of JC62, and JC93 had approximately three-fold higher NOX activity than JC62. The NOX activity measured for the JC62 soluble fraction may have been due to other soluble dioxygenases or from other native activities. As will be described, JC85 and JC93 had additional chromosomal

modifications and their progenitors had been selectively transferred, making direct metabolic comparisons of JC92 and JC93 with JC68 difficult.

Aerobic Batch Transfers in Pyruvate for Increased TCA Cycle Flux

The pyruvate accumulation in aerobically grown JC68 cultures was indicative of negative control of PDH by an elevated NADH/NAD^+ ratio. The preferred solution to this problem would be to more rapidly reoxidize NADH, by using the water-forming NADH oxidase. The NADH oxidase activity in JC68 was not sufficient. JC68 was therefore serially transferred in NBSM pyruvate (aerobic batch cultures) to select for changes that would permit higher flux through the TCA cycle despite the high NADH/NAD^+ ratio. This selection was based upon the extra ATP available per pyruvate oxidized via the TCA cycle. Initial doubling times of the JC68 cultures grown in pyruvate were approximately 16 h (Figure 4-6A). After 20 transfers the doubling time had decreased to just over 3 h and the resulting strain was named JC100. After construction of JC72 (Δ*arcA*), doubling times increased to 7 h. Another 20 transfers (no significant change after transfer 10) brought the generation time down to that of JC100 (Figure 4-6B). The resulting strain (JC101) was tested in aerobic batch culture and found to completely oxidize glucose without the accumulation of pyruvate observed for the previous strains.

Introduction of *lpd101* for Lower Sensitivity of PDH and α-KGDH Complexes to NADH

Kim *et al*. (62) describe a mutation in *lpd* (encoding dihydrolipoamide dehydrogenase) which causes the PDH complex to be less sensitive to NADH. Since dihydrolipoamide dehydrogenase is also a part of the α-ketoglutarate dehydrogenase (α-KGDH) complex, the mutation (*lpd101*) may also allow greater flux through the TCA cycle when NADH levels are elevated. Evolved strain JC101 *lpd* was sequenced to determine whether such a mutation could explain the higher flux observed through the PDH complex. The *lpd* sequence of JC101 was identical to that of ATCC 8739.

A single nucleotide substitution (G to A) was made in ATCC 8739 *lpd* by an oligo-directed mutagenesis method, resulting in an E354K amino acid change. The mutated copy was used to replace the native copy in JC101, resulting in JC80. Aerobic JC80 batch culture growth and glucose catabolism was similar to the parent (data not shown). This was expected, because JC101 was already capable of completely oxidizing glucose aerobically, with no significant product formation. The *lpd* mutation could not provide any additional benefit under these conditions, but might under more reducing conditions (such as in an MFC).

Deletion of *arcA*

An additional approach used to circumvent negative control by NADH was to delete *arcA*. Since the phosphorylated ArcA negatively regulates expression of the genes encoding the PDH complex (as well as many TCA cycle genes) under reducing conditions, deletion of *arcA* can allow higher aerobic flux through PDH and the TCA cycle in conjunction with heterologous expression of *naoX* (125). JC72 was constructed by deleting *arcA* from JC100. JC72 accumulated a small amount of pyruvate during aerobic growth on glucose. The pyruvate accumulation was eliminated by aerobic transfers in pyruvate mineral salts medium (JC101).

Comparison of Contribution of Individual Genetic Modifications to Complete Aerobic Glucose Oxidation

Starting with JC85, individual chromosomal modifications were repaired one at a time to provide an isogenic set for determination of the relative contribution of each change to the observed phenotype. JC86 grew similarly to ATCC 8739, due to repair of the *atpFH* deletion (Figure 4-7). Repair of the *arcA* deletion (JC91) resulted in increased pyruvate accumulation during aerobic growth on glucose (Figure 4-8B). Repair of the *ackA* deletion (JC89) resulted in accumulation of acetate, as expected (Figure 4-8C). Apparently, integration of $naoX_{Sm}$ into *ackA* (JC85 vs JC84) had little effect (Figures 4-7 and 4-8), consistent with the NADH oxidase assay

results (Figure 4-5). The *lpd101* mutation (JC85 vs JC90) had no effect under the tested conditions.

Current Production and Coulombic Efficiencies Using Engineered Strains in Poised Potential Electrochemical Cell

The engineered strains were tested in a three-electrode, poised potential electrochemical cell, with glucose as the electron donor (and sole carbon source) and using thionin as a diffusible mediator. The poised potential, bulk electrolysis cell system was chosen to limit non-biological variables. A high surface area RVC electrode and excess mediator were used to further ensure that bacterial activity would be limiting. As glucose was catabolized by the bacterial cells, electrons were transferred to the anode (via the thionin) from reduced cofactors in the cells. The resulting current was measured over time (Figure 4-9A-F) and used to compare maximum current and Coulombic efficiencies of the strains (Table 4-2). Maximum current values from ATCC 8739, JC27 and JC62 were similar. C_Es were also similar (approximately 50%). Maximum current and C_E values for all tested strains with the *naoX*$_{Sm}$ integration (JC85, JC91 and JC93) were similar. Maximum current values for these strains were approximately 20% higher than wild type and C_Es were 75%.

Discussion

We have constructed a strain (JC93, Figure 4-10) that is capable of significantly higher current output and Coulombic efficiency in the conversion of the stored energy in glucose to electricity. While an *atpFH* deletion (JC27) increased the rate of glycolysis, downstream rate limitation prevented the complete oxidation of glucose. The incomplete oxidation of glucose by JC27 was evident in aerobic culture (Figure 2-3) with the production of acetate. In the electrochemical cell, the incomplete catabolism of glucose was observed as a low Coulombic yield. We attempted to overcome the downstream metabolic rate limitations through several

targeted chromosomal modifications and via aerobic transfers in a pyruvate minimal medium. We initially tested the modified strains in aerobic batch culture. We hypothesized that these conditions might be similar to an anaerobic electrochemical cell (EC) environment with a sufficiently positive reduction potential and the aerobic batch cultures were simpler for preliminary investigations. The poised potential electrochemical cell experiments were in good general agreement with the results obtained from the aerobic batch experiments. Integration of *naoX*$_{Sm}$ into *ackA* appeared to have the greatest effect upon redirecting flux through the TCA cycle and upon increasing the Coulombic yield. No significant change in current of C_E was observed upon integration of an additional copy of *naoX*$_{Sm}$. However, the additional NOX activity could be beneficial under different conditions. The increase in MFC current with NOX activity suggests that reduction of thionin via the native electron transport chain was limiting and that the cytoplasmic NADH oxidase helped to overcome that limitation. Similarly, the elimination of aerobic overflow metabolism upon introduction of the cytoplasmic NOX implicates a respiratory limitation as the primary cause of the overflow.

Interestingly, deletion of *arcA* appeared to result in higher flux through PDH and the TCA cycle under aerobic conditions (Figure 4-8B), but did not significantly affect maximum current and C_E in the electrochemical cell (Table 4-2). ArcA-P is known to repress transcription of some genes involved in anaerobic respiration while it activates transcription of genes involved in aerobic metabolism. It is possible that some of the genes involved in anaerobic respiratory metabolism are important under the tested EC conditions. It would be interesting to determine whether restoring *arcA* in JC93 provides any benefit. The metabolic engineering of JC93 was done in a way that complicated comparison of the effects of individual modifications. In particular, the aerobic pyruvate transfers that were done in between targeted modifications made

the genetic backgrounds of subsequent strains uncertain. The decreases in generation times resulting from the transfers were likely due to subtle flux redistributions and readaptation to mineral salts medium culture conditions after chromosomal modifications were made (in rich media). In order to make strain comparisons, it was necessary to restore individual modifications in JC85. It may be useful to return to JC62 and integrate *naoX*$_{Sm}$ into *ackA* and into *pflB* (or another site that would provide a higher level of expression). Transfers could be made (to select for higher C_E, if necessary) after the changes were made in the cleaner genetic background.

The results of our study suggest that oxygen is not necessary for the complete oxidation of glucose, only sufficiently oxidizing conditions are required. It also provides further evidence that the respiratory chain limits PDH complex and TCA cycle flux and leads to overflow metabolism when the glycolytic rate is increased (here due to Δ*atpFH*). The higher rate of NADH oxidation (by oxygen or by thionin) catalyzed by the cytoplasmic NOX from *S. mutans* alleviates negative control of downstream catabolic steps in JC93 and allows a higher Coulombic yield at a high metabolic rate. These attributes make JC93 an attractive candidate for application in a mediated MFC or in a mediatorless MFC after introducing heterologous genes for extracellular electron transfer.

Table 4-1. Strains, plasmids, and PCR primers

Strain/plasmid/primer	Relevant features	Reference/source
E. coli		
JC62	JC27, Δ*pflB,* Δ*adhE,* Δ*ldhA*	This study
JC66	JC62, Δ*ackA*	This study
JC68	JC62, Δ*ackA*::*naoX*$_{Sm}$ (opposite orientation)	This study
JC72	JC100, Δ*arcA*	This study
JC80	JC101, *lpd101*	This study
JC84	JC85, Δ*ackA*::*cat-sacB*	This study
JC85	JC80, Δ*ackA*::*naoX*$_{Sm}$	This study
JC86	JC85, *atpFH*$^{+}$	This study
JC89	JC85, *ackA*$^{+}$	This study
JC90	JC85, *lpd*$_{wt}$$^{+}$	This study
JC91	JC85, *arcA*$^{+}$	This study
JC92	JC85, Δ*pflB*::*cat-sacB*	This study
JC93	JC85, Δ*pflB*::*naoX*$_{Sm}$	This study
JC100	JC68, 20 transfers +O_2, NBSM pyruvate	This study
JC101	JC72, 20 transfers +O_2, NBSM pyruvate	This study
Plasmids		
pLOI4147	*adhE* in pCR2.1	This study
pLOI4148	*adhE*::*cat-sacB* (from pLOI4162)	This study
pLOI4149	*adhE*::6RFstop	This study
pLOI4158	*ackA* in pCR2.1	This study
pLOI4159	*ackA*::*cat-sacB* (from pLOI4162)	This study
pLOI4160	*ackA*::6RFstop	This study
pLOI4163	*pflB* in pCR2.1	This study
pLOI4164	*ldhA* in pCR2.1	This study
pLOI4165	*ldhA*::*cat-sacB* (from pLOI4162)	This study
pLOI4166	*ldhA*::6RFstop	This study
pLOI4171	*pflB*::*cat-sacB* (from pLOI4162)	This study
pLOI4172	*pflB*::6RFstop	This study
pLOI4175	*ackA*::*naoX*$_{Sm}$	This study
pLOI4176	*arcA* in pCR2.1	This study
pLOI4177	*arcA*::*cat-sacB* (from pLOI4162)	This study
pLOI4178	*arcA*::6RFstop	This study
pLOI4179	*lpdA* in pCR2.1	This study
pLOI4180	*lpd101*	This study

Table 4-1. Continued

Plasmid/primer	Relevant features	Reference /source
pLOI4181	*lpdA*::*cat-sacB* (from pLOI4162)	This study
pLOI4182	$naoX_{Sm}$ in pCR2.1	This study
pLOI4184	*ackA*::$naoX_{Sm}$	This study
pLOI4185	*ackA*::$naoX_{Sm}$ (opp. orient.)	This study
pLOI4190	*pflB*::$naoX_{Sm}$	This study
Primers		
JM*adhE*up	TCGCTGAACTTAACGCACTC	This study
JM*adhE*down	ACGACCGTAGTAGGTATCCA	This study
JM*adhE*iodown2	GACCGTACTGCTGCTAAGAT	This study
JM*adhE*ioup2	GTGTCGTCTTCAGACAGAAC	This study
JM*ackA*F1	GCCTGAAGGCCTAAGTAGTA	This study
JM*ackA*R1	GCACGATAGTCGTAGTCTGA	This study
JM*ackA*down1	GCCGCAATGGTTCGTGAACT	This study
JM*ackA*up1	GTTGAGCGCTTCGCTGTGAG	This study
JM*pflB*F1	CCGGTTACGATCGGCAACAT	This study
JM*pflB*R1	TCGAAGGCTACGTCGAGTCT	This study
JM*pflB*down1	ATGCACGGTCGTGACCAGAA	This study
JM*pflB*up1	GGAAGCAACAGCGGTGTCAA	This study
JM*ldhA*F1	AAGGTTGCGCCTACACTAAG	This study
JM*ldhA*R1	GCGATGATGCTGTAGCTGTT	This study
JM*ldhA*down1	CGCGTCAAGGTCGACGTTAT	This study
JM*ldhA*up1	TCTCAGGCAGCAATTGAAGC	This study
JM*arcA*F1	GCTCAACTCTGCCGATAGC	This study
JM*arcA*R1	CAACTTATTACGCGGTGCGA	This study
JM*arcA*down1	TATCGCTTCTGCGGTGATCT	This study
JM*arcA*up1	CGTGTTACCAACTCGTCTTC	This study
lpdA-A	first 18 bases of *lpdA* ORF	Sigma
lpdA-C	last 18 bases of *lpdA* ORF	Sigma
JME354Ksense	CGTCCATCGCCTATACCAAACCAGAAGTTGCATGG	This study
JME354Kcomp	CCATGCAACTTCTGGTTTGGTATAGGCGATGGACG	This study
JM*lpdA*down1	TTCTGGCCGTGCTATCGCTT	This study
JM*lpdA*up1	AGCAGGCGTTCTGGTACTTC	This study
JM*naoX*F1	CACGATCGGCTAGCAATCAGGAGCTTAT	This study
JM*naoX*R1	CACGATCGGCTGTGGTTCTCTTAGAAGT	This study

Primer sequences are 5’ to 3’

Table 4-2. Coulombic efficiencies and maximum current from engineered strains in glucose-fed bulk electrolysis cell (BEC) testing

Strain	Coulombic efficiency (%)	Maximum current (mA)
ATCC 8739	48.6 ± 2.8	3.90 ± 0.23
JC27 (Δ*atpFH*)	55.9 ± 10.1	3.96 ± 0.67
JC62 (JC27, Δ*ldhA*, Δ*adhE*, Δ*pflB*)	53.0 ± 4.3	3.65 ± 0.19
JC91 (JC62, Δ*ackA*::$naoX_{Sm}$)	81.5 ± 16.2	4.48 ± 0.26
JC85 (JC91, Δ*arcA*)	74.7 ± 9.7	4.71 ± 0.34
JC93 (JC85, Δ*pflB*::$naoX_{Sm}$)	76.0 ± 6.6	4.64 ± 0.26

All values are reported as mean ± SD, n = 3

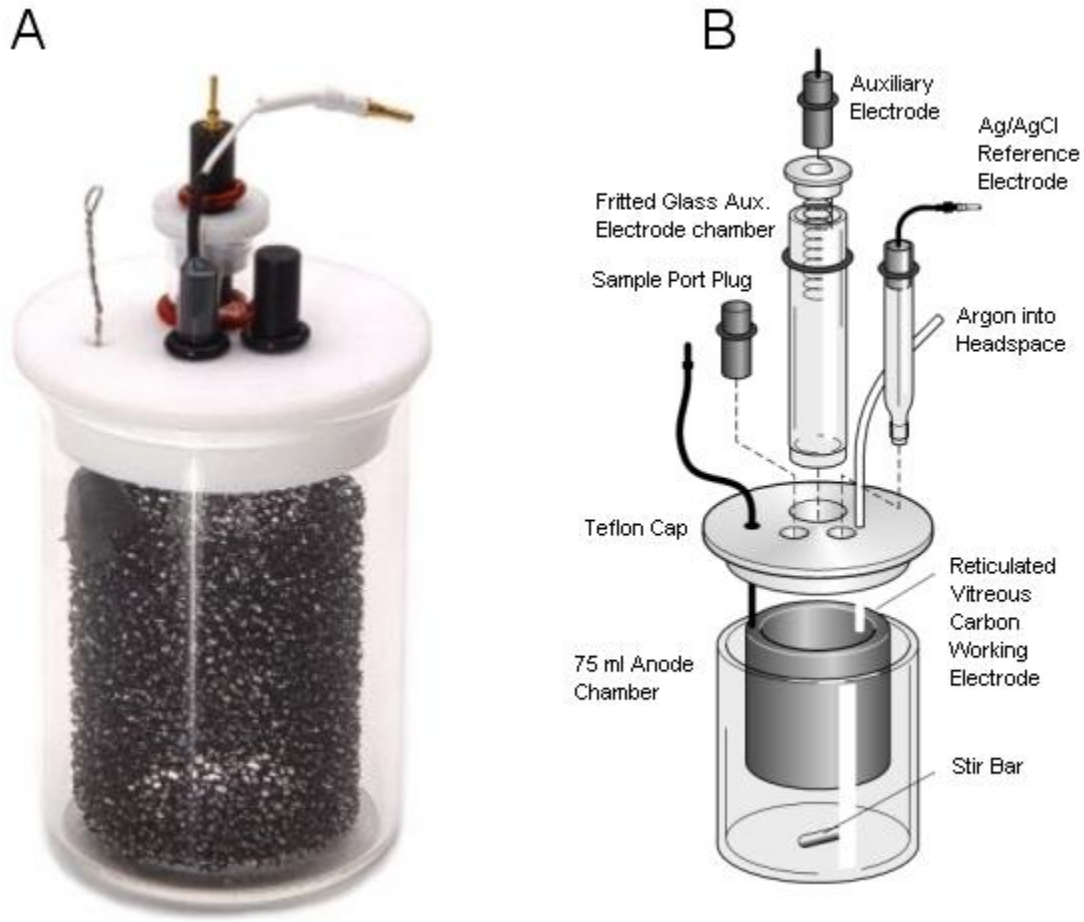

Figure 4-1. Photograph (A) and expanded schematic (B) of the bulk electrolysis cell used in this study for electrochemical measurements. Adapted from BASi product literature (Bioanalytical Systems, Inc., West Lafayette, IN).

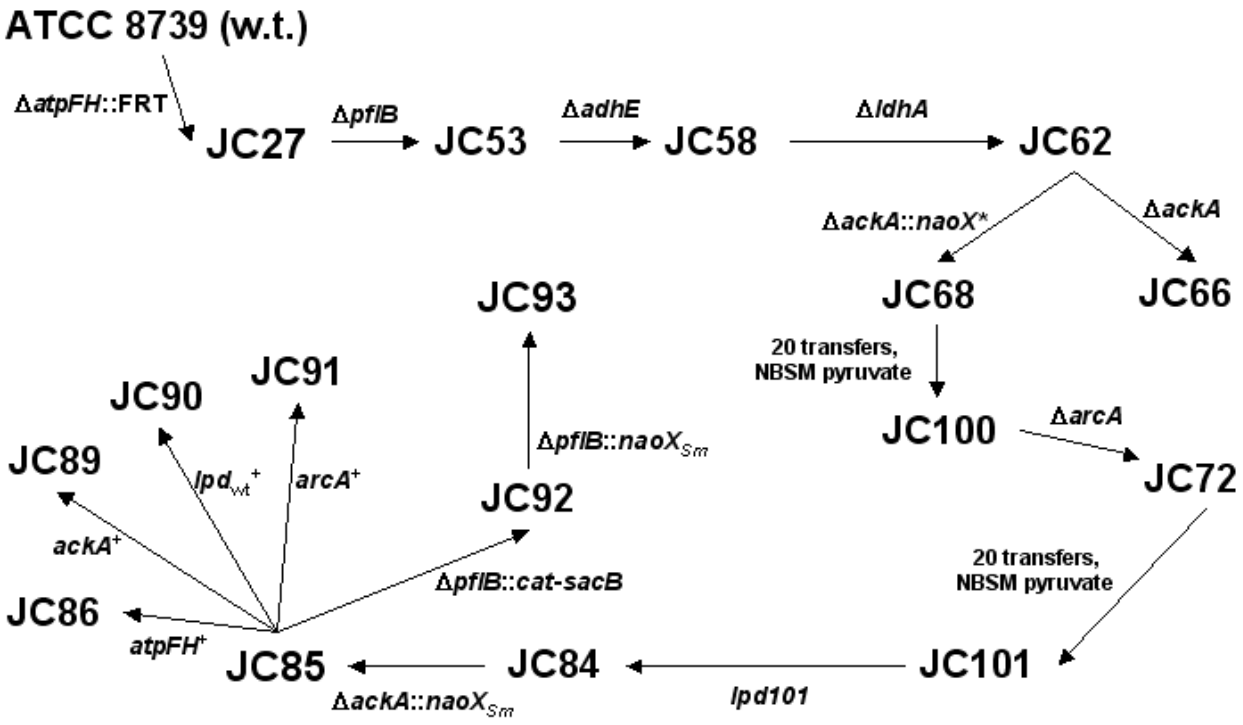

Figure 4-2. Summary of strain construction. Δ*ackA*::*naoX**, $naoX_{Sm}$ not transcribed from *ackA* promoter.

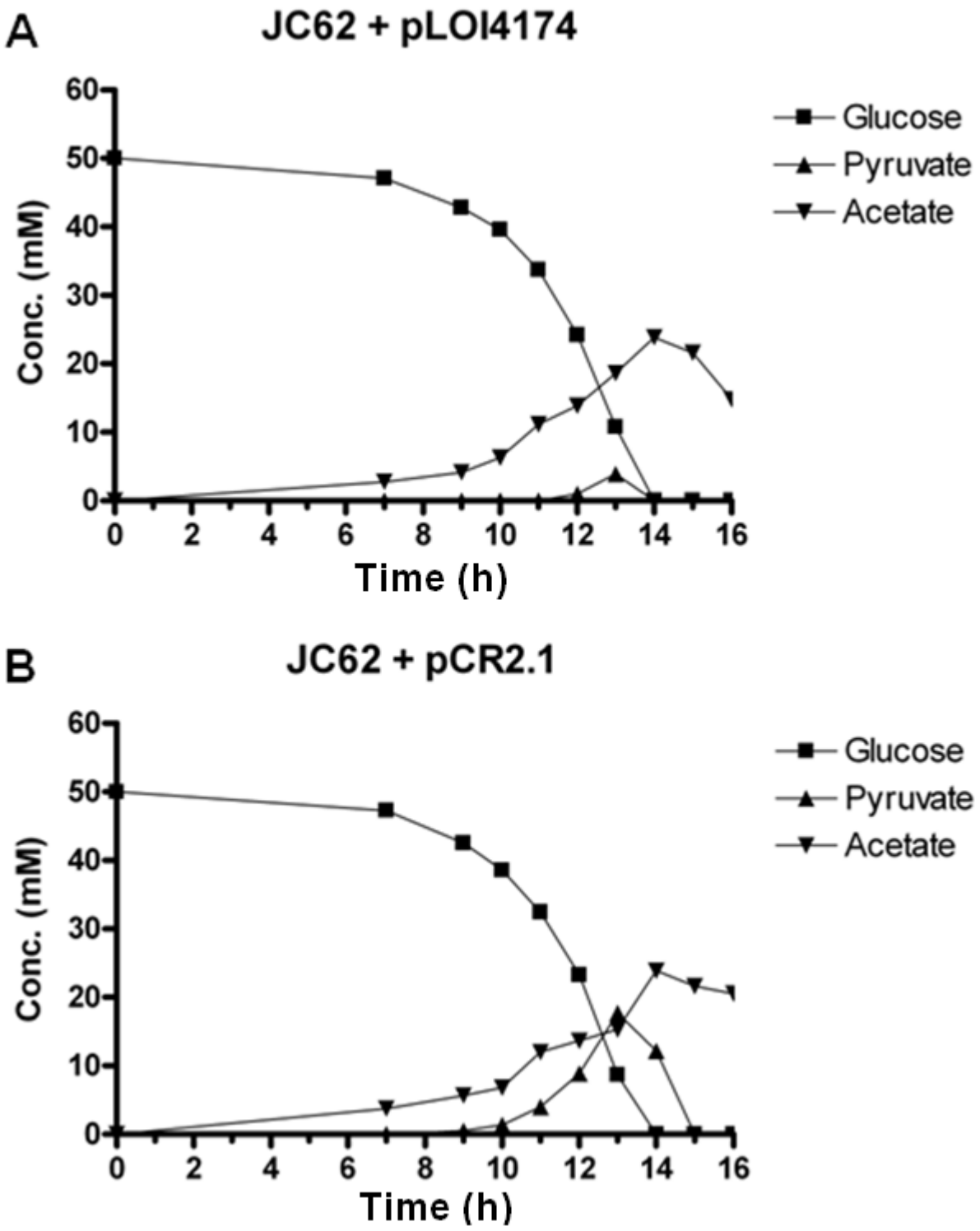

Figure 4-3. Decreased pyruvate accumulation with overexpression of *naoX* from *Streptococcus mutans* in JC62 (Δ*atpFH*, Δ*ldhA*, Δ*adhE*, Δ*pflB*) (A) vs. JC62 with empty vector (B).

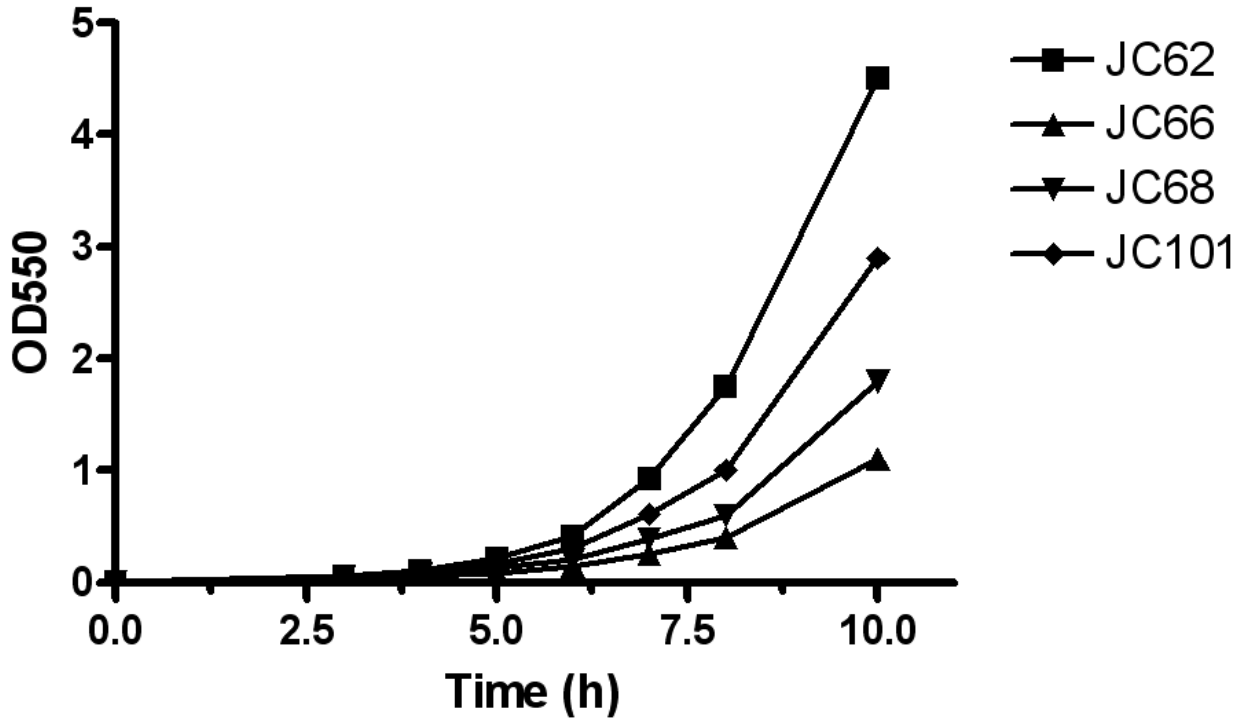

Figure 4-4. Partial restoration, through $naoX_{Sm}$ integration (JC68) and pyruvate transfers (JC101), of JC62 (Δ*atpFH*, Δ*ldhA*, Δ*adhE*, Δ*pflB*) growth rate after deletion of *ackA* (JC66).

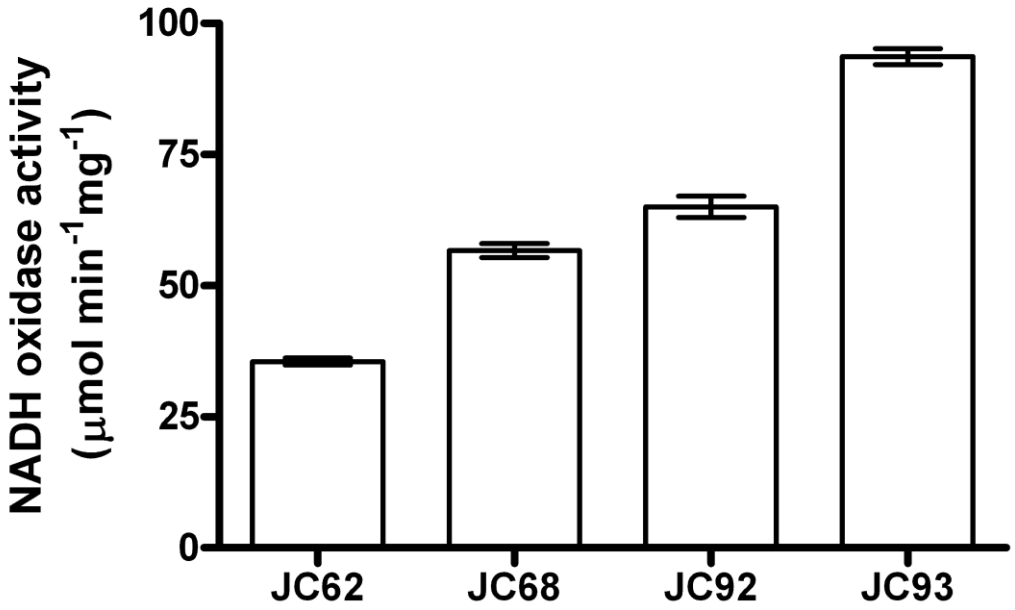

Figure 4-5. Cytoplasmic NADH oxidase activity from aerobically grown strains with different *naoX*$_{Sm}$ integrations. JC62 (Δ*atpFH*, Δ*ldhA*, Δ*adhE*, Δ*pflB*), JC68 (JC62, Δ*ackA*::*naoX*$_{Sm}$, transcription from native *naoX*$_{Sm}$ promoter), JC92 (Δ*ackA*::*naoX*$_{Sm}$, *naoX*$_{Sm}$ transcription from *ackA* promoter), JC93 (JC92, Δ*pflB*::*naoX*$_{Sm}$, *naoX*$_{Sm}$ transcription from *focA* promoter.

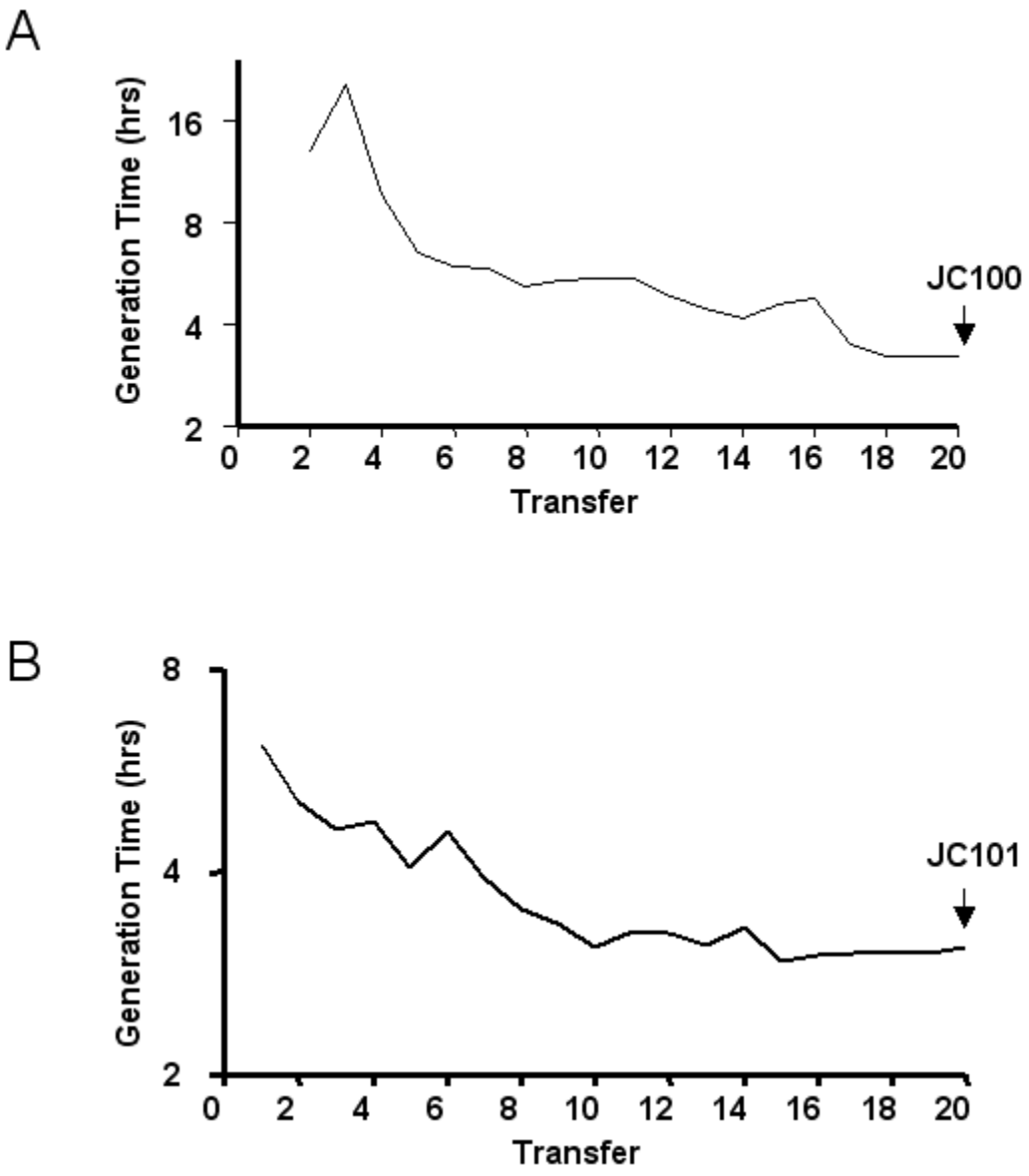

Figure 4-6. Aerobic batch culture transfers of JC68 (ΔatpFH, ΔldhA, ΔadhE, ΔpflB, ΔackA::naoXSm, transcription from native naoXSm promoter) (A) and JC72 (JC100, ΔarcA)(B) in pyruvate mineral salts medium for shorter generation times. Final transferred strain designation indicated with an arrow.

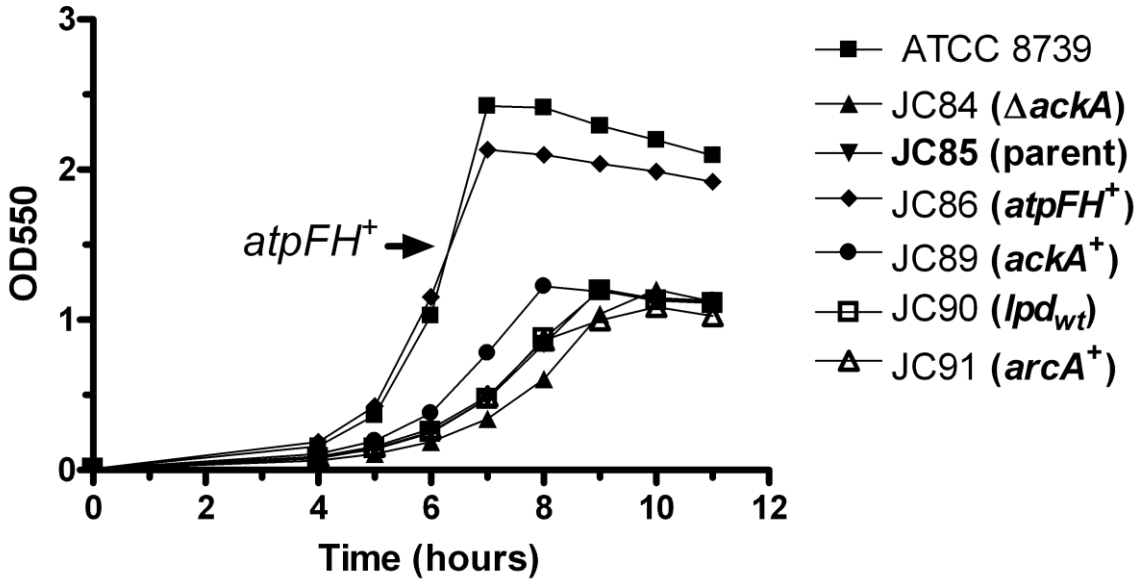

Figure 4-7. Growth curves of aerobic glucose mineral salts medium cultures of isogenic set of strains with restoration of each chromosomal modification present in JC85. ATCC 8739 growth is included as a reference.

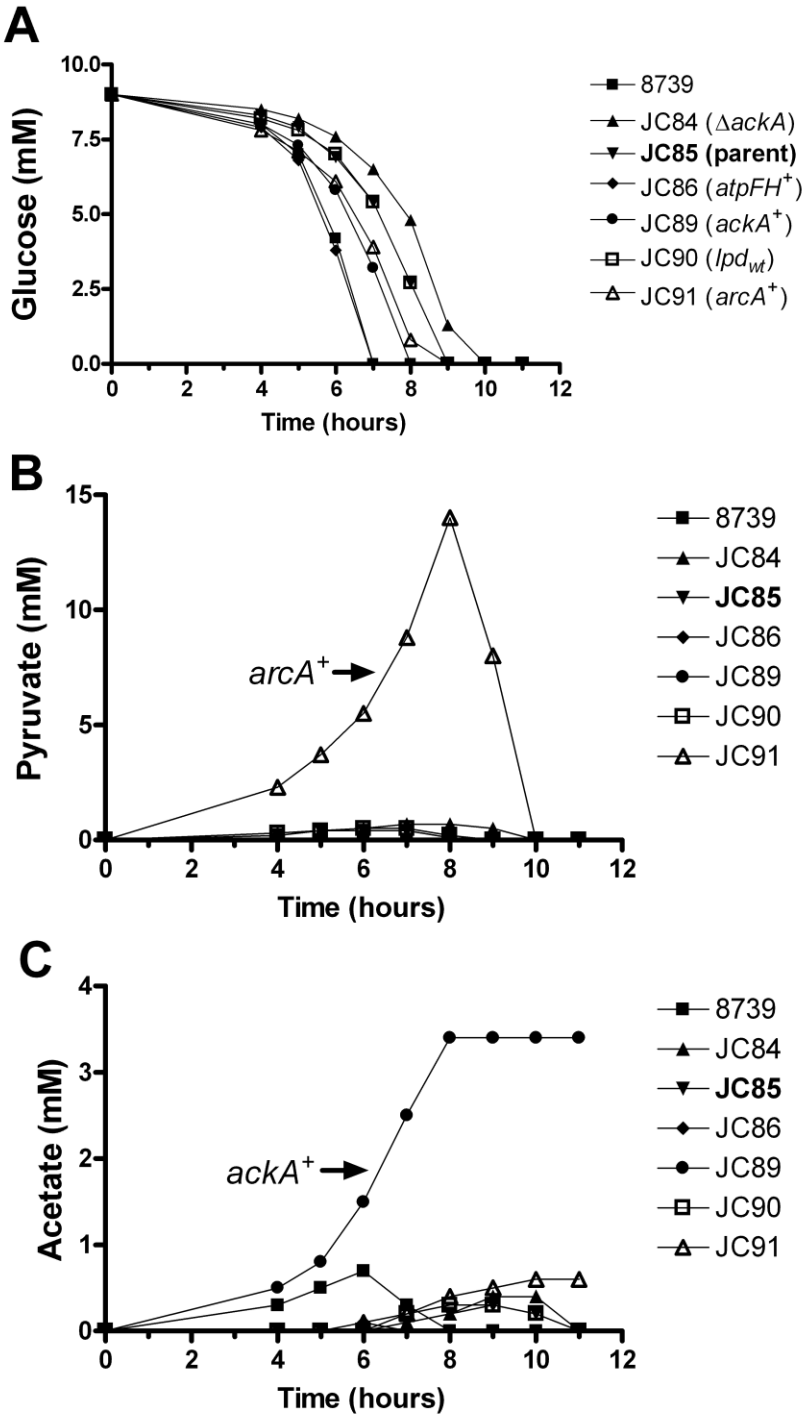

Figure 4-8. Glucose utilization and product formation of aerobic cultures (glucose mineral salts medium) of isogenic set of strains with restoration of each chromosomal modification present in JC85.

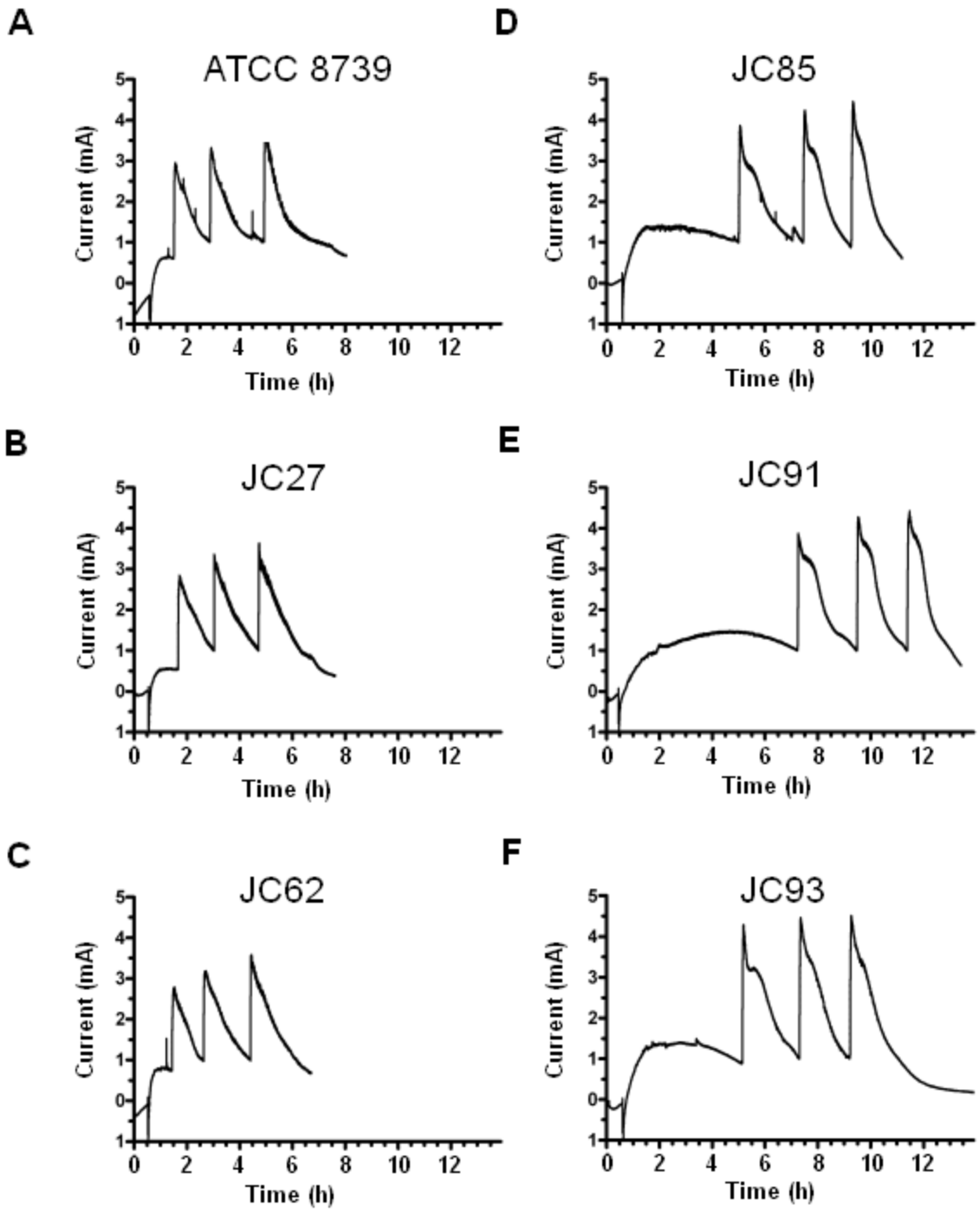

Figure 4-9. Current production over time with glucose-fed (5 μmol glucose per peak) cells in bulk electrolysis cell (poised potential at +100mV vs Ag/AgCl).

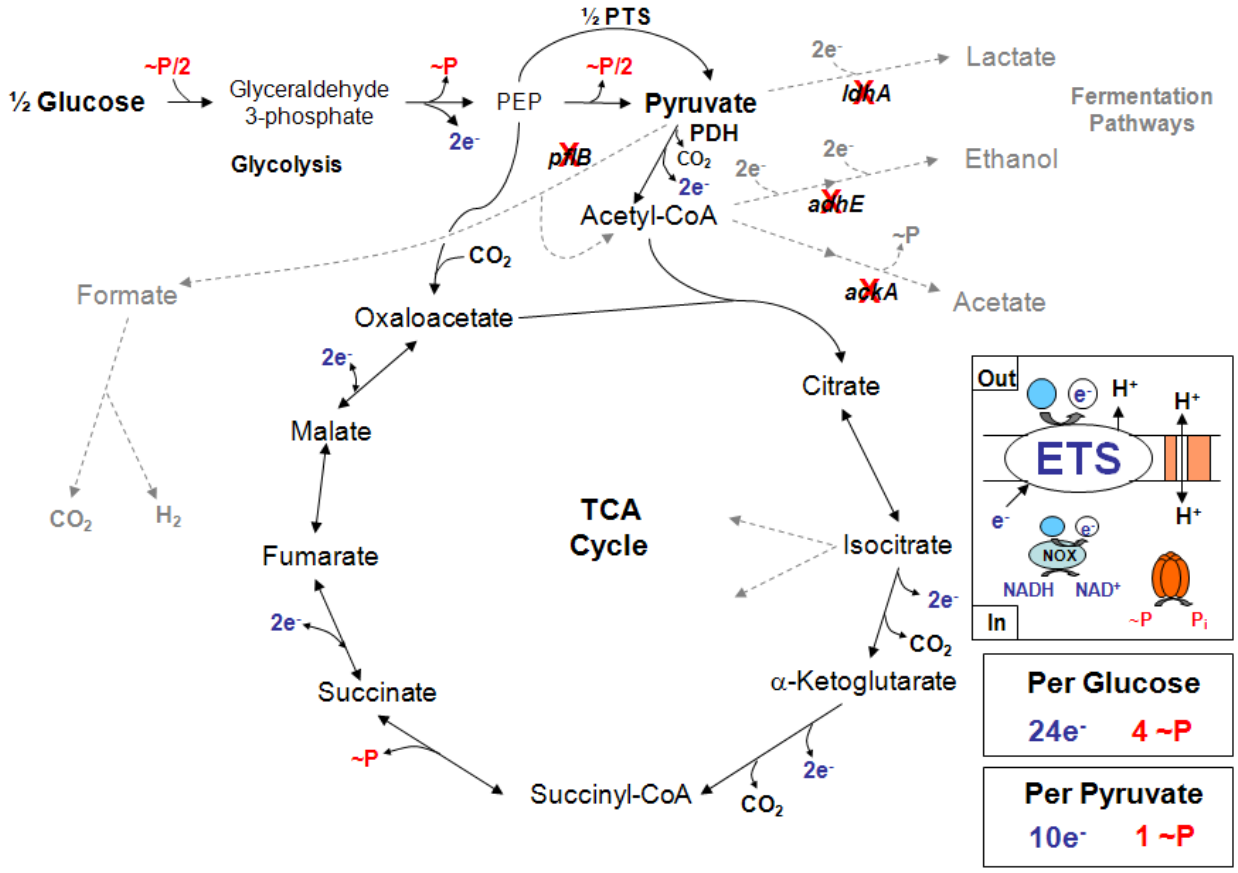

Figure 4-10. Simplified metabolic overview of JC93. Uncoupled electron transfer to exogenously supplied redox dye (blue and white circles) via the native electron transport system (ETS) and NADH oxidase from *S. mutans* and proton leakage across cytoplasmic membrane shown in inset panel. Electron (e^-) and ATP (~P) maximum theoretical net yields from substrates are given for JC93.

CHAPTER 5
HETEROLOGOUS EXPRESSION OF GENES ENCODING EXTRACYTOPLASMIC CYTOCHROMES FROM DISSIMILATORY METAL REDUCING BACTERIA IN *E. COLI* FOR EXTRACELLULAR ELECTRON TRANSFER

Introduction

MFC operation using *E. coli* as the biocatalyst requires the addition of exogenous, soluble electron carriers. The *E. coli* outer membrane lacks the terminal reductase cytochromes of the DMRB and prevents direct contact between insoluble exracellular electron acceptors and the electron transport chain. *E. coli* does not produce its own soluble electron carriers as do *Shewanella* (78, 128) and *Pseudomonas* (47, 98) species, for example. Due to these limitations, mediatorless *E. coli* MFCs do not produce significant electrical current. There have been a few reports of evolved populations of *E. coli* in MFCs which were capable of mediatorless electrode reduction (129, 136), but no independent confirmation has been reported. One study found quinones in the anolyte and concluded that selection for extracellular electron transfer had led to production and secretion of small molecule electron shuttles (97). However, it is also possible that the low levels of these compounds were present because of cell lysis. More evidence is needed to confirm extracellular electron transfer by evolved strains of *E. coli*.

Another approach to enabling mediatorless electron transfer by *E. coli* is the heterologous expression of electron carrier-encoding genes from DMRB. *S. oneidensis* extends its electron transport chain to the extracellular environment via several multiheme-containing cytochromes. The periplasmic decaheme cytochrome MtrA from *S. oneidensis* is capable of accepting electrons from the native NapC (a cytoplasmic membrane-located *c*-type cytochrome involved in periplasmic nitrate reduction) in *E. coli* and reducing soluble ferric compounds (94). A separate study showed that *S. oneidensis* outer membrane terminal reductase OmcA can localize to the outer membrane of *E. coli* B and can be oxidized by insoluble ferric oxide (34). Proper

localization of OmcA was absent in a K12 strain of *E. coli*. *E. coli* K12 strains do not express the necessary *gsp* genes encoding the components of the type II secretion system (T2SS) under any tested conditions (39). The *gsp* genes in *E. coli* K12 strains (and in ATCC 8739) are organized into two divergently transcribed operons (Figure 5-1). The histone-like nucleoid structuring protein (H-NS) reportedly binds to the region between the operons and represses their transcription (39).

The T2SS of *E. coli* is responsible for secretion of some exotoxins (114) and chitinase (39). It is similar to the Pul (pullulunase secretion) system of *Klebsiella* strains (31), the Out (pectate lyase secretion) system of *Erwinia chrysanthemi* (45) and the Gsp system of *S. oneidensis* (responsible for secretion of outer membrane cytochromes) (107). While T2SS systems from various bacteria share organizational and functional characteristics, most are specific for their substrates. Surprisingly, *E. coli* Type II secretion is sufficient and necessary for functional localization of the heterologously produced OmcA (34). Reconstitution of a functional *S. oneidensis* MR-1 extracellular electron transport system in *E. coli* would establish the minimal set of genes needed for reduction of insoluble acceptors. We attempted to achieve this goal and to enable mediatorless electrode reduction through genetic engineering of JC85 (Figure 5-2).

Materials and Methods

Growth Conditions and Media

E. coli cultures were grown as described elsewhere in this study, unless otherwise specified. Antibiotics were included in growth medium, where appropriate, to maintain plasmids. *S. oneidensis* MR-1 was acquired from ATCC (ATCC 700550) and grown aerobically at 30°C, in LB broth, for genomic DNA extraction using the Qiagen DNeasy procedure.

Integration of Heterologous Genes and Replacement of *gsp* Promoters

A combinatorial approach was used in the chromosomal integration of *omcA* and *mtrCAB* from *S. oneidensis* MR-1 into *adhE* and *pflB* of JC85. *S. oneidensis* MR1 genomic DNA was used as a template for PCR amplification of the region containing *omcA* and *mtrCAB* with the primer set JM*omcA*F2/JM*mtrB*R2 (all strains, plasmids and primers introduced in this chapter are listed in Table 5-1). The product was used for nested PCR to amplify the entire region (with primer set JM*omcA*F1/JM*mtrB*R1), *omcA* (JM*omcA*F1/R1), and *mtrCAB* (JM*mtrC*F1/*mtrB*R1). These primers contained *Pvu*I restriction sites and *Pvu*I digests left ends that were compatible with *Pac*I digested (*cat-sacB* cassette removed) pLOI4171 and pLOI4148. Ligation of each *Pvu*I digested product into each *Pac*I digested plasmid resulted in pLOI4192 and pLOI5009 through pLOI5013. These plasmids were linearized with an appropriate restriction enzyme, diluted and PCR-amplified for use as integration fragments to replace the *cat-sacB* cassette in the second step of the two-step chromosomal sequence replacement strategy described previously (51). The entire *omcAmtrCAB*$_{So}$ region was integrated into *pflB* and *adhE* (JC94 and JC123, respectively). In another strain, *omcA*$_{So}$ was integrated into *pflB* and *mtrCAB*$_{So}$ into *adhE* (JC121). For construction of JC122, *omcA*$_{So}$ was integrated into *adhE* and *mtrCAB*$_{So}$ into *pflB*.

The *gspA and gspC* promoters in strains JC94, JC121, JC122 and JC123 were replaced with constitutive promoters. The entire intergenic region between *gspA* and *gspC* (containing the divergent promoters P_{gspA} and P_{gspC} and the H-NS binding region) was replaced (in the same manner as the replacements of *adhE* and *pflB*) by a construct containing divergent constitutive promoters (P_{bla} and P_{cat}). Inside-out PCR was used (JM41XX*cat*modF2/R1 primer set) to amplify pLOI5000, omitting P_{cat}. The primers contained *Nhe*I sites and the product was self-ligated after digest to produce pLOI5001. pLOI5000 was digested with *Nde*I and *Nhe*I, Klenow fragment-treated and self-ligated to produce pLOI5003. Plasmid pLOI5003 was amplified by

PCR (JM41X5promF1/R1 primers), digested with *Nhe*I/*Cla*I and ligated into compatible ends of PCR- amplified (JM41X3*bla*modprodF1/R1 primers) pLOI5001. The resulting plasmid (pLOI5002) contained *bla* and *cat* genes, divergently transcribed, with a minimal sequence between them.

The 5' ends of *gspA* and *gspC* and the intergenic region between them were amplified by PCR (JMgspCAF2/R2 primers) from ATCC 8739 genomic DNA and cloned into pCR2.1-TOPO (resulting in pLOI5006). Appropriate constructs were made (in the manner described above and using primers JM*gspA*up1/JM*gspC*up2 for the inside-out PCR) for the two-step replacement of the *gspA*/*gspC* intergenic region with the P_{bla}/P_{cat} sequence.

SDS-PAGE and Heme Staining

Cultures for analysis by SDS-PAGE with heme staining were grown (250 ml flasks, 30 ml LB broth, 30°C, 120 rpm) to stationary phase (48 h, 0.5 gDCM/liter), harvested (25 ml, 8,000×g, 4°C) and stored at -20°C. Cells were disrupted by two passages through a French pressure cell (14,000 psi). Unbroken cells were removed (5,000×g, 4°C) and a crude membrane fraction was prepared from 1.5 ml supernatant (16,900×g, microcentrifuge, 4°C). Crude membrane fraction samples were incubated for 1h at room temperature in SDS sample buffer (46) and resolved on a 4 to 15% gradient polyacrylamide gel with Tris-glycine running buffer (65) for 35 min at 200 V. The heme staining procedure was modified from the method of Francis and Becker (40). Gels were washed with 12.5 % trichloroacetic acid for 30 min with rocking, followed by a 30 min rinse with deionized water. The gel was developed using a peroxidase staining method. The gel was developed in (final concentrations): 10% acetic acid, 1 g/liter *o*-dianisidine, and 0.06% hydrogen peroxide in 0.05 M citrate buffer, pH 4.4.

Electrochemical Analytical Methods

Recording of current output over time with the engineered strains was done with the poised potential BEC system described in the previous chapter, with the following modifications. Riboflavin (10 µM) and homogentisic acid (HGA, 0.1mg/ml) were included in the anolyte (first trial) to facilitate electron transfer. A second trial used each compound at half concentration. Glucose (10 µmol) was added to the anolyte (without cells) upon reaching a stable baseline and bacterial cells (grown to late stationary phase at 100rpm, 0.67g/liter, final in BEC) were added approximately 1 h after glucose addition.

Results and Discussion

Chromosomal Integration of *omcA*$_{So}$ and *mtrCAB*$_{So}$ and Replacement of *gsp* Promoters in JC85

The *omcA* and *mtrCAB* genes from *S. oneidensis* MR-1 were integrated into the chromosome of JC85 by targeted gene replacement to construct a functional extracellular electron transfer system. JC85 was chosen as the parent strain because while the presence of the cytoplasmic water-forming NADH oxidase (from *S. mutans*) might be beneficial (for oxygen scavenging), higher-level expression (JC93) would be unnecessary in the mediatorless system. A combinatorial approach was used for integration into the native *adhE* or *pflB* to increase the probability of finding the optimal expression pattern of the heterologous genes. JC94 and JC123 had the entire gene cluster (*omcAmtrCAB*) integrated into *pflB* or *adhE* (respectively). Since *omcA* and *mtrCAB* are transcribed separately in *S. oneidensis* MR-1 (10), o*mcA* transcription was from the *pflB* or *adhE* promoters, while the *mtrCAB* was transcribed from its own promoter. For JC121 and JC122, *omcA* and *mtrCAB* were integrated into the sites separately. Integrations were confirmed by PCR and by DNA sequence analysis. The chromosomal sequence between the *gsp* operons (of JC94, JC121, JC122 and JC123) was replaced with constitutive promoters (P_{bla} and

P_{cat}). Replacement of the *gsp* promoters resulted in strains JC128 through JC131. Cell pellets from strains with integration of the heterologous genes were observed to be a darker orange color than the parental strain, characteristic of cytochrome *c* production (34).

Preliminary SDS-PAGE (with heme-staining) results suggested that the integrated cytochrome genes from *S. oneidensis* MR-1 were expressed in the tested strains (Figure 5-3). *E. coli* requires expression of cytochrome *c* maturation genes (*ccmABCDEFGH*) to make functional *c*-type cytochromes (117) such as the native NapC (or MtrA, MtrC and OmcA from *S. oneidensis* MR-1). The *ccm* genes are normally only expressed under nitrate-respiring conditions, so strains were transformed with pEC86 (constitutive expression of *ccm* genes) for testing. There appeared to be high molecular weight staining for the integration strains (lanes 1-4) that corresponded with the heme-staining seen for *S. oneidensis* MR-1 (lane 5). The poorly resolved high molecular weight staining was from outer membrane cytochromes OmcA and MtrC (75 kDa) (106). No 35 kDa band for MtrA (periplasmic decaheme cytochrome *c*) (94) was visible in any of the *E coli* samples. No heme staining at all was seen for the parent strain sample (lane 6). The heme staining high molecular weight bands from the integration strain samples were faint and the results were not consistently reproducible. Expression levels may have been suboptimal due to copy number or induction conditions. Other studies reporting heterologous expression of the *S. oneidensis* MR-1 cytochrome *c* genes used similar induction conditions (aerobic cultures grown at 30°C to late stationary growth phase), but the genes were overexpressed from plasmids (34). Further study using higher expression levels and anaerobic respiratory growth conditions may be beneficial.

Production of Current by JC131

The EC testing (with addition of riboflavin and homogentisic acid) results were also inconclusive. Based upon the preliminary heme staining observations, JC131 (transformed with

pEC86) was selected for comparison of current production with JC85/pEC86. In the first trial, JC131/pEC86 produced 50% higher average current from glucose versus the parent, but the average current produced by each was low (40 µA vs. 10 µA, respectively, baseline corrected). The C_E values were extremely low, less than 7% and 2% (respectively). The average current produced by JC131/pEC86 in a second trial (5µM thionin, 0.05 mg/ml HGA) was 76µA (baseline corrected) vs. 66 µA for JC85/pEC86. C_Es were 3.7% and 3.5% (respectively).

At the end of the experiments the JC85/pEC86-containing anolyte (Figure 5-4B) was observed to be darker (brown) in color than the anolyte containing JC131/pEC86 (Figure 5-4A). Oxidized homogentisic acid polymerizes to form pyomelanin, a brown pigment (25). The lighter pigmentation observed in the JC131/pEC86 MFC anolyte indicated that the homogentisic acid was being kept in a more reduced state (less pyomelanin formed), possibly by extracellular electron transfer from JC131. Overall, the results show that electron transfer from the cells was inefficient and that it was limiting MFC current production. Further investigation and optimization of expression are necessary. It is also possible that the *gsp* genes were not properly expressed, leading to problems with secretion of the outer membrane cytochromes.

Table 5-1. Strains, plasmids, and PCR primers

Strain/plasmid/primer	Relevant features	Reference/source
Escherichia coli		
JC94	JC85, Δ*pflB*::*omcAmtrCAB*$_{So}$	This study
JC95	JC85, Δ*pflB*::*omcA*$_{So}$	This study
JC96	JC85, Δ*pflB*::*mtrCAB*$_{So}$	This study
JC99	JC85, Δ*adhE*::*cat-sacB*	This study
JC121	JC95, Δ*adhE*::*mtrCAB*$_{So}$	This study
JC122	JC96, Δ*adhE*::*omcA*$_{So}$	This study
JC123	JC85, Δ*adhE*::*omcAmtrCAB*$_{So}$	This study
JC128	JC94, Δ(P_{gspC}/ P_{gspA})::P_{bla}/ P_{cat}	This study
JC129	JC123, Δ(P_{gspC}/ P_{gspA})::P_{bla}/ P_{cat}	This study
JC130	JC121, Δ(P_{gspC}/ P_{gspA})::P_{bla}/ P_{cat}	This study
JC131	JC122, Δ(P_{gspC}/ P_{gspA})::P_{bla}/ P_{cat}	This study
Shewanella oneidensis MR1		ATCC (700550)
Plasmids		
pEC86	*cat*, *ccm*	(6)
pLOI4192	*bla*, *kan*, *pflB*::*omcAmtrCAB*$_{So}$	This study
pLOI5000	*bla*, *cat*, self-ligation of (Klenow-treated) pLOI4151, *Sap*I/*Not*I frag. removed	This study
pLOI5001	*bla*, *cat* (Δ P_{cat})	This study
pLOI5002	*bla*, *cat* (divergent P_{bla}/ P_{cat})	This study
pLOI5003	*bla* (Δ P_{bla}), *cat*	This study
pLOI5006	*bla*, *kan*, P_{gspC}/ P_{gspA} in pCR2.1	This study
pLOI5007	Δ(P_{gspC}/ P_{gspA})::*cat-sacB*	This study
pLOI5008	Δ(P_{gspC}/ P_{gspA})::P_{bla}/ P_{cat} (divergent)	This study
pLOI5009	*bla*, *kan*, *pflB*::*omcA*$_{So}$	This study
pLOI5010	*bla*, *kan*, *adhE*::*omcA*$_{So}$	This study
pLOI5011	*bla*, *kan*, *pflB*::*mtrCAB*$_{So}$	This study
pLOI5012	*bla*, *kan*, *adhE*::*mtrCAB*$_{So}$	This study
pLOI5013	*bla*, *kan*, *adhE*::*omcAmtrCAB*$_{So}$	This study
Primers		
JM41XX*cat*modF2	CGCTGCTAGCAAGGAAGACCTGCGATG GAGAAAAAAATCACTGG	This study
JM41XX*cat*modR1	CGCTGCTAGCTTAGACGTCAGGTGGCAC TT	This study
JM41X5promF1	CGCTGCTAGCGTCTCATGAGCGGATACA	This study
JM41X5promR1	CGCTATCGATGCTTCCTTAGCTCCTGAA	This study

Table 5-1. Continued

Primer	Relevant features	Reference/source
JM41X3*bla*modF1	CGCCATCGATAAGGAAGGCTCTTCATGAGTATTCAACATTTCCG	This study
JM41X3*bla*modR1	CGCTATCGATCTAAGCTAGCAAGGAAGAC	This study
JM*gsp*CAF2	CTGCCACGGGATTTGCATCT	This study
JM*gsp*CAR2	TATGCGGCGGTGATTCAGGT	This study
JM*gsp*Aup1	CGCCATCGATAAGGAAGTTCTATGTCTACGAGAAGAG	This study
JM*gsp*Cup2	CGCTGCTAGCTCCTTCCTTACATCGTGCCCACACTACGTTTCC	This study
JM41X5promF*Pvu*I	CGCTCGATCGGTCTCATGAGCGGATACA	This study
JM41X5promR*Pvu*I	CGCTCGATCGGCTTCCTTAGCTCCTGAA	This study
JM*omcA*F2	ACCTCTCGCGCTTAACAATG	This study
JM*mtrB*R2	TATCAAGGCGCTCAGTGGTA	This study
JM*omcA*F1	CACGATCGAGGCCTGCAACTGCCAAT	This study
JM*omcA*R1	CGTTCGATCGCGACTTAGTTACCGTGTGCTTCCA	This study
JM*mtrC*F1	CGTTCGATCGCCCTTGTGGTTTAACTACC	This study

Primer sequences are 5’ to 3’

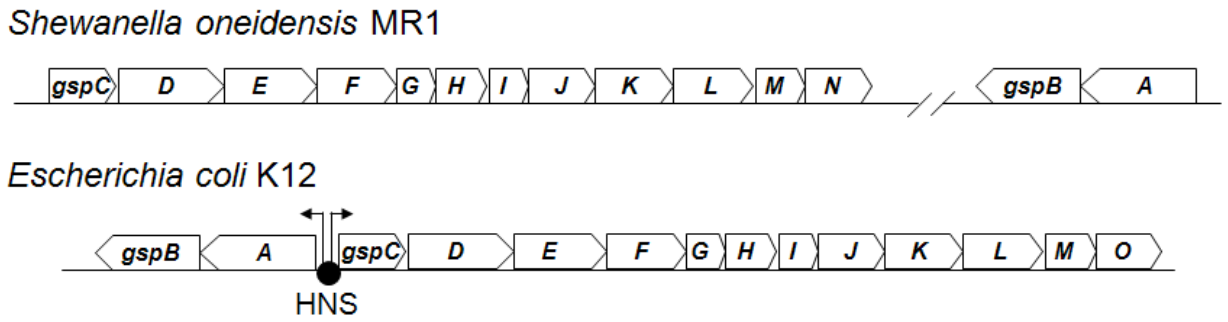

Figure 5-1. Arrangement of *gsp* (general secretory pathway, T2SS) genes in representative strains. H-NS (histone-like nucleoid structuring protein) is shown binding to the operator region between *gspA* and *gspC* of *E. coli* K12, blocking transcription from divergent promoters

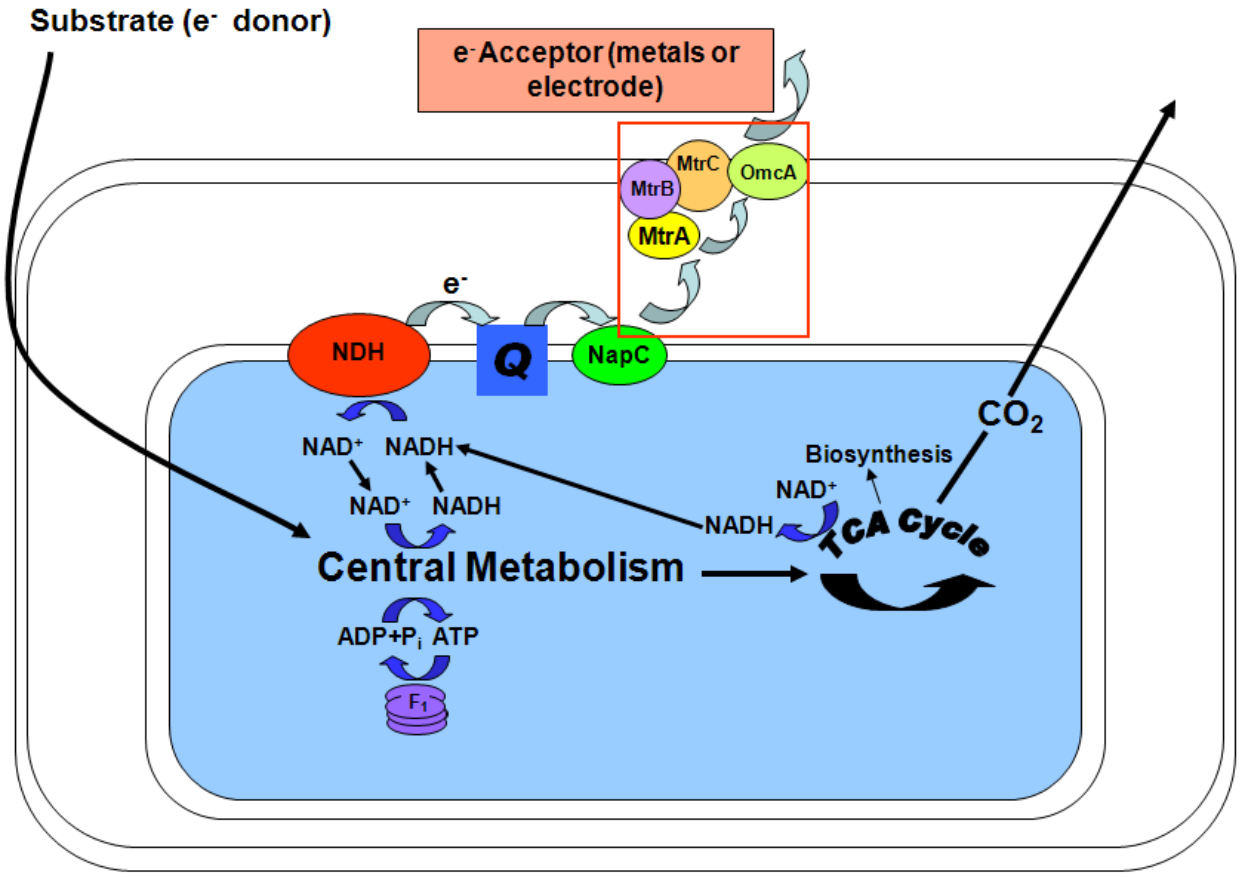

Figure 5-2. A model for extracellular electron transfer by an engineered *E. coli* strain producing periplasmic (MtrA) and outer membrane cytochromes (MtrC, OmcA) from *Shewanella oneidensis* MR-1

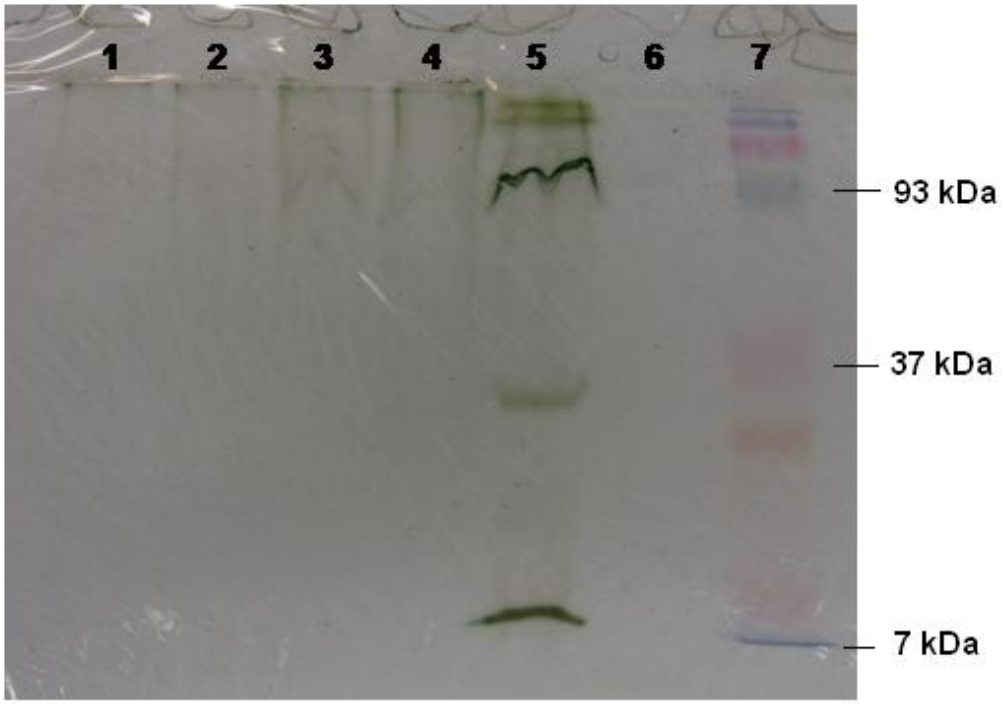

Figure 5-3. Heme-stained crude membrane fractions (after SDS-PAGE) of JC128/pEC86, lane 1; JC129/pEC86, lane 2; JC130/pEC86, lane 3; JC131/pEC86, lane 4; *S. oneidensis* MR-1, lane 5; JC85/pEC86, lane 6; MW markers (BioRad Kaleidoscope protein standards), lane7

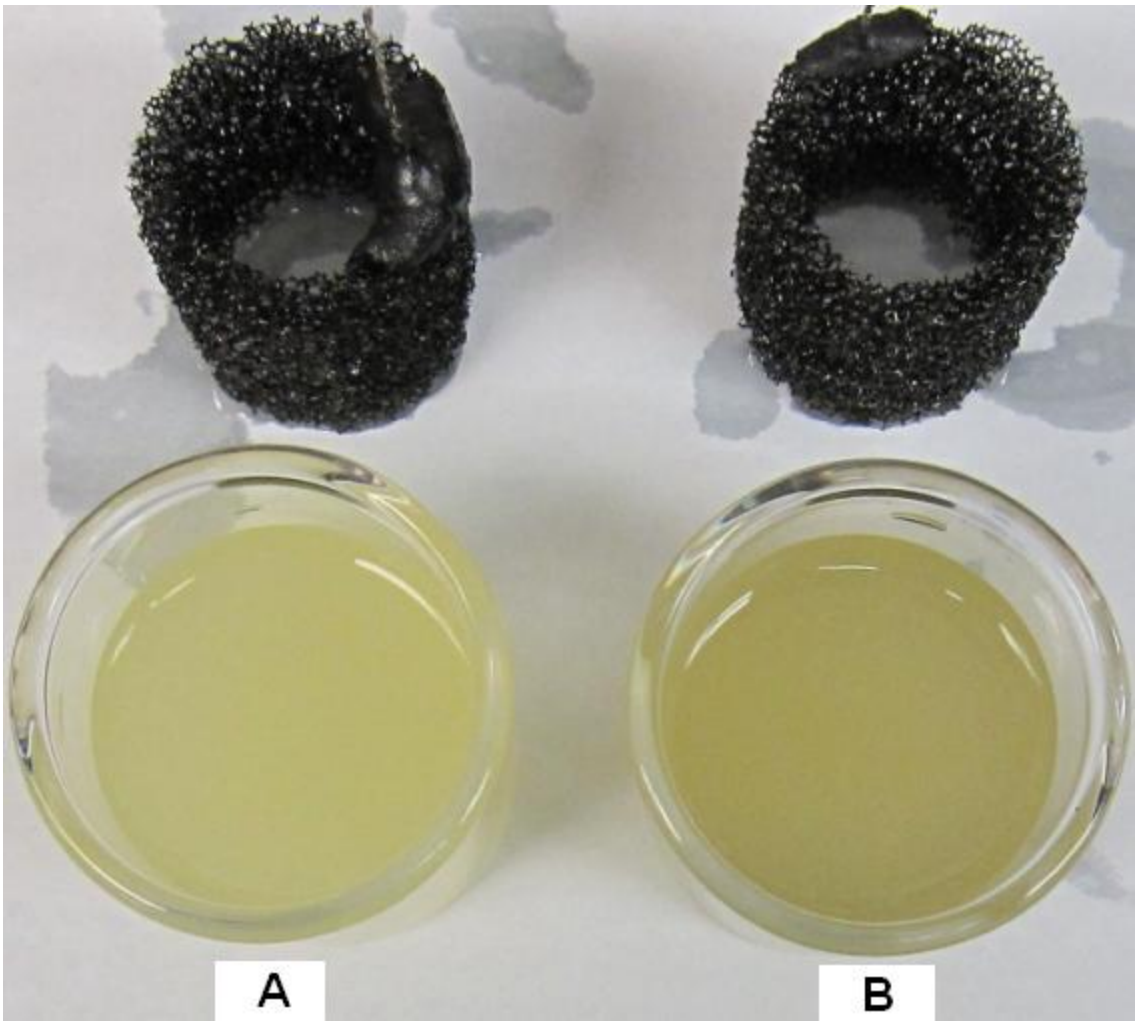

Figure 5-4. Electrochemical cell (EC) anolytes (post-run) from the first trial with JC131/pEC86 (A) and JC85/pEC86 (B). Anolytes contained riboflavin (5µM) and homogentisic acid (1 mg/ml). ECs were disassembled and electrodes (top) were removed from the anode chamber in the photo

CHAPTER 6
OPTIMIZATION OF ELECTRON TRANSFER TO THE ANODE IN A MICROBIAL FUEL CELL USING SINGLE WALL CARBON NANOTUBES AND MIXED LENGTH CARBON FIBERS

Introduction

Microbial fuel cells are devices that transform stored chemical energy in organic materials into electrical energy for useful work. The MFC uses microbial whole cell biotransformation, versus the immobilized enzyme biocatalysis used in other types of biological fuel cells. Using whole cells has advantages, particularly low cost of materials and the potential for indefinite stability and regeneration of biocatalyst. This approach also brings challenges, primarily the lower power densities achieved versus enzymatic and non-biological fuel cells. The important roles of microbial metabolic rates and transfer of electrons across biological membranes in MFC power output was addressed in previous chapters. We anticipated that once the biological current production and efficiency of electron transfer to the exterior of the bacterium were optimized, it would be important to minimize overpotential losses. Single-walled carbon nanotubes (SWNT) (35) and mixed-length bulk carbon fibers (111) were therefore tested in the anode compartment of a dual-chambered MFC, using *E. coli* W3110 as the whole cell biocatalyst and methylene blue as the diffusible electron-carrying mediator. These micro and nanoscale carbon structures were included in a suspended, conductive network in order to decrease overpotentials due to mediator diffusion and anode reduction limitations. Minimization of losses downstream of bacterial electron transfer through anode optimization would complement the genetic engineering efforts.

SWNTs are cylindrical structures whose walls consist of a graphitic sheet of carbon atoms (one atom thick). SWNT diameters can be as small as 0.5 nm, while their length depends upon the method of synthesis, but provide high aspect ratios and surface areas. This geometry, along with their high electrical conductivity, make SWNTs ideal for increasing MFC anode surface

area and decreasing diffusional distance of the mediator. The SWNT suspension density could be optimized to maximize conductivity without limiting bacterial loading. It is also possible that the hydrophobic SWNTs could infiltrate the *E. coli* membranes and allow direct electron transfer to the anode.

Micro-scale carbon fibers can also be used to limit concentration overpotentials. While nanotubes have higher aspect ratios, surface area densities, and conductivities (in some cases), their synthesis and purification are still more difficult and expensive than the larger carbon fibers. It is important for MFCs to be constructed with inexpensive materials and to be scalable, which would be difficult (at this time) with SWNTs. Bulk carbon fibers may help to optimize electron transfer to the electrode, are less expensive than SWNTs and are available in large quantities.

Single-walled carbon nanotubes or mixed length carbon fibers were suspended in the anode compartment of a two-chambered MFC for the purpose of increasing stable current production. The MFC employed *E. coli* W3110 as the microbial biocatalyst in the anode compartment and methylene blue as the redox mediator. Current produced from glucose catabolism was measured over time and the performance of the SWNT MFCs compared with the control MFCs, containing only a graphite felt electrode. The effect of SWNT or CF inclusion on the magnitude and stability of electrical current production under different MFC operating conditions was evaluated.

Materials and Methods

Materials, Instrumentation and MFC Assembly

The basic MFC assembly (NCBE, The University of Reading, UK) consisted of Perspex (acrylic) chambers, neoprene gaskets, carbon fiber electrodes (cut to 2.4 cm × 3.3 cm) and a cation-exchange membrane. Assembly of these components was performed as outlined by the

supplier and as described by Bennetto (11). In addition, platinum wire (from Mini-Subcell GT electrophoresis apparatus electrodes, BioRad, Hercules, CA) was used to connect the carbon fiber electrodes to the external circuit, consisting of a 1000 ohm resistor and an ammeter (46-Range Digital Multimeter with PC interface and data-logging MeterView 1.0 software, RadioShack, Fort Worth, TX), in series. Argon was bubbled into the anode compartment using 1 mm outer diameter, 0.2 mm inner diameter PTFE tubing passing through the same aperture as the platinum wire of the anode, down to the bottom of the chamber. This aperture was sealed to divert exiting gases to the feeding/venting tube, located in the other aperture of the chamber. The argon flow rate was maintained at approximately 3.5 ml/min, as measured at the venting tube using a J&W Scientific (Folsom, CA) ADM 2000 flow meter. The cathode chamber was modified in the same manner as the anode chamber; however, no gas was delivered to the cathode chamber and the electrode aperture was not sealed. The catholyte (9 ml total volume added per MFC after assembly) consisted of 50 mM potassium ferricyanide in 100 mM sodium phosphate buffer, pH 7.0. A cloth layer (75% rayon, 25% polyester, EasyWipe, Magla Products L.L.C., Morristown, New Jersey) was used to separate the electrodes from the cation-exchange membrane in each chamber. Both assembled MFCs were attached to a weight, placed in a one gallon plastic freezer bag and immersed (to the top of the MFCs) in a 37^{o} C water bath.

Media and Growth of Cultures

E. coli W3110 (ATCC 27325) cultures were inoculated from a single colony on a NBSM (with 20 g/liter glucose) agar plate into 50 ml NBSM glucose medium (medium contained 30 g/liter glucose unless otherwise noted) in a 250 ml baffled Erlenmeyer flask. Cultures were grown aerobically (37°C, 250 rpm) and 10.9 ml was harvested (5000×g, 5 min, 22°C) at a density of approximately 36.3 mgDCM/liter) and resuspended in 0.5 ml NBSM glucose medium.

SWNT MFC Anolyte Preparation and Inoculation

The SWNT suspension (0.06 mg/ml) to be used in the MFC was washed in an equal volume of NBSM glucose medium to minimize carryover of detergent used in its preparation as well as to limit the dilution of the medium. The tube was inverted to mix and was spun down in a clinical centrifuge for 2 min. This caused aggregation of the SWNTs and they were transferred in a minimal volume (2 ml) to a fresh tube. To this tube was added an additional 4 ml of medium. 2 ml of the SWNT wash was transferred to a fresh tube and 4 ml medium was added to it for use in the no-SWNT control MFC. The resuspended cells were added to each of these tubes and briefly sparged with argon, using a 25 $^{5}/_{8}$ gauge needle on a 1 ml syringe with plunger removed and an argon-filled balloon on the other end. The suspensions were then transferred to the anode chamber of their respective MFCs by means of a 10 ml syringe equipped with an 18 gauge cannula. The final cell density in the anolytes was approximately 60 mgDCM/liter. Methylene blue (480 μl of a 10 mM stock) was added to each anolyte by syringe.

CF MFC Preparation

The procedure for preparation of CF MFCs was as described for the SWNT MFCs, but a mixed-length carbon fiber suspension was used in place of the nanotubes. During the first trial it was found that the mixed carbon fibers could not be transferred by syringe. This necessitated the feeding of the aggregated fibers through the feeding/vent tube in the anode chamber, after the addition of the cell suspension and prior to addition of mediator. The CF transfer was done by pushing the fibers through the tube with toothpicks.

For the second trial, the carbon fiber suspension was transferred as several aggregates (from which most of the liquid had been removed) to the anode compartment during assembly. *E. coli* W3110 cells were resuspended (60 mgDCM/liter in 6.5 ml total volume NBSM glucose

medium) for each MFC (CF MFC and control MFC) and cell suspensions were transferred to the MFC anode chambers, followed by addition of methylene blue.

Results

SWNT MFC Current Production

After addition of cells and mediator (and after a brief current spike in which the no-SWNT MFC surpassed that of the SWNT MFC), the SWNT MFC sustained a higher current (Figure 6-1). After approximately 7 h, the SWNT MFC current dropped to the same level as the control MFC (~ 0.1 mA). Argon flow was stopped 19 h into the run to determine the current produced by each MFC in the absence of anolyte mixing (Figure 6-2). The SWNT MFC produced a current that was over 2.5-fold greater than that of the no-SWNT control MFC. The current levels were stable for 1.5 h, at which point the SWNT MFC's current dropped to just under 2 times that of the control. Brief mixing with argon, performed 2 h after this observed drop, greatly increased the SWNT MFC current and resulted in a stable 3-fold higher current for an additional 1.5 h.

A second experiment was performed in which argon mixing was halted soon after inoculation of the MFCs and addition of mediator. The same MFC setup procedure was followed as in the initial experiment. However, the inoculated anolyte cell density was slightly higher (~ 66 mgDCM/liter). The SWNT MFC current was about 50% higher than that of the control MFC (Figure 6-3).

CF MFC Current Production

Upon addition of all components, the CF MFC was observed to produce a current that was nearly twice that of the control MFC (Figure 6-4). Initial current was only slightly higher from the CF MFC. However, over a 12 h period the CF MFC produced a stable current that averaged at least 40% higher than that of the control MFC (Figure 6-5).

Discussion

Minimizing concentration overpotentials (and ohmic losses) and increasing active electrode surface area are critical factors for increasing MFC power output. These improvements are of particular importance as the limitations of bacterial metabolic rate and efficiency of extracellular electron transport are alleviated. The results of the SWNT and CF MFC testing showed that the CFs and SWNTs also provided higher stable current production without continuous mixing. These results suggest that the dynamic anode matrix composed of bacterial cells and SWNTs (or CFs) was able to form a stable, active and conductive matrix after mixing was stopped. In contrast, the MFCs without the SWNT or CF addition experienced significant decreases in current production after stirring was stopped. In those MFCs, planktonic cells sank to the bottom of the vessel and were not as readily accessible to the mediator. Thus, concentration overpotentials were likely greater in the control MFCs. Further MFC design improvements that incorporate the type of high surface area, robust electrode design discussed here will help to increase MFC power output and reliability in mediatorless and mediated systems.

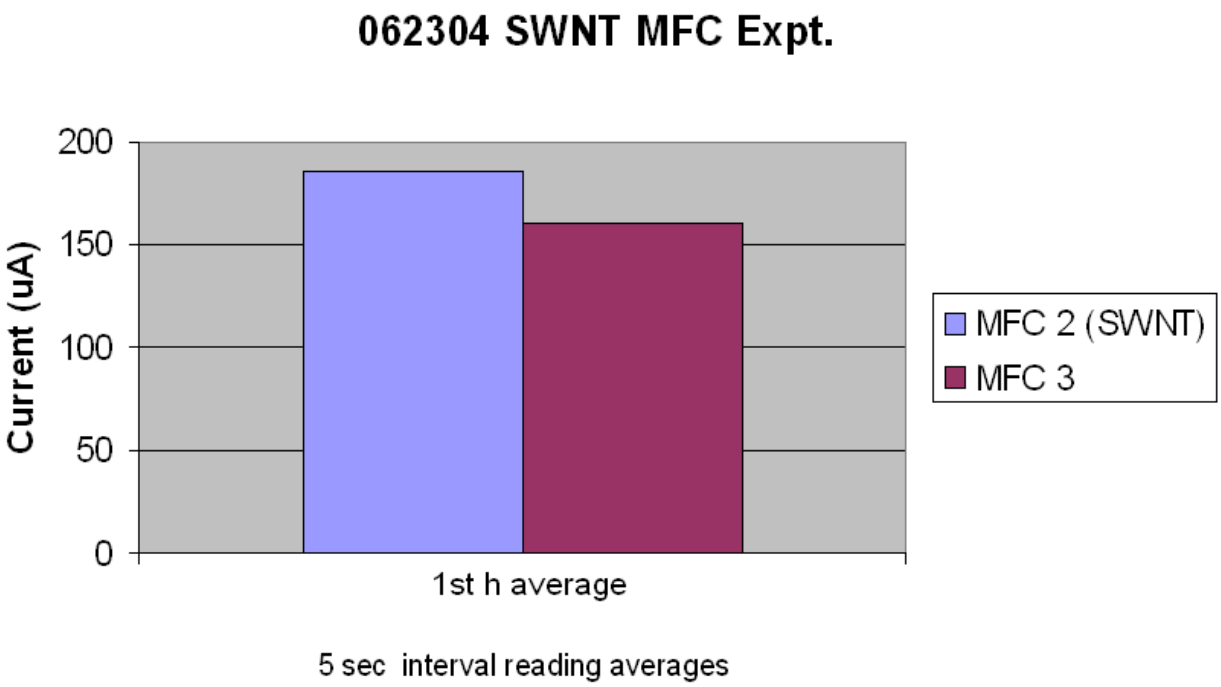

Figure 6-1. Initial hour (mixing) average current with and without addition of single-walled carbon nanotubes (SWNT).

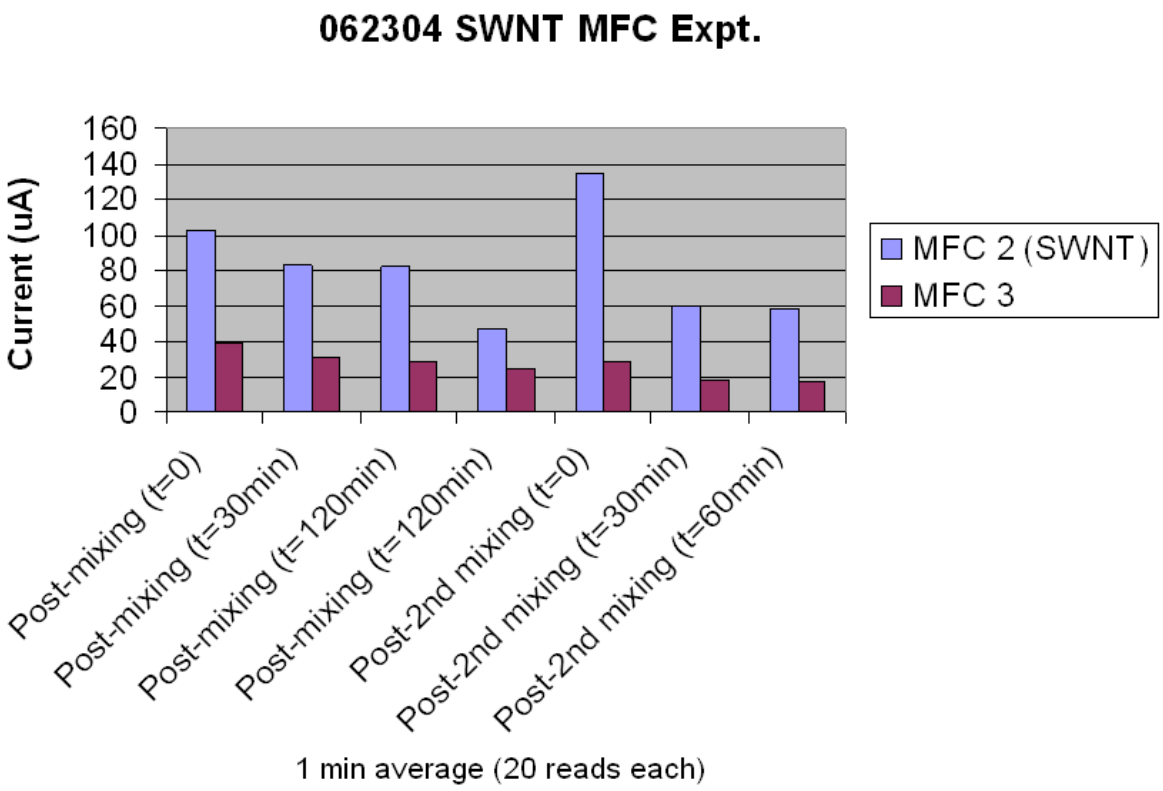

Figure 6-2. Average current with and without addition of single-walled carbon nanotubes (SWNT).

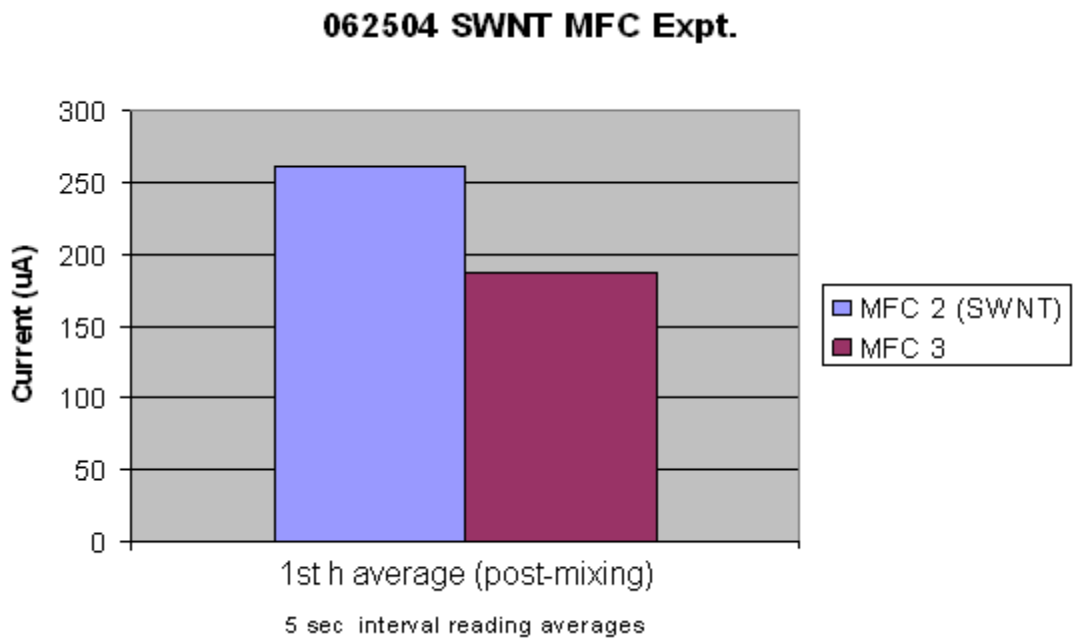

Figure 6-3. Initial hour (post-mixing) average current with and without addition of single-walled carbon nanotubes (SWNT).

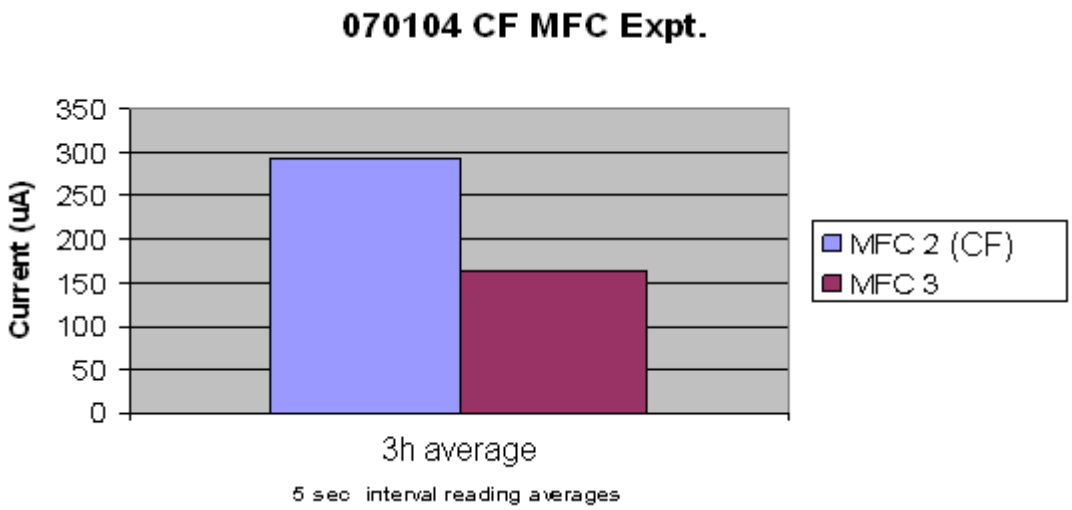

Figure 6-4. Average current with and without addition of micro-scale carbon fibers (CF).

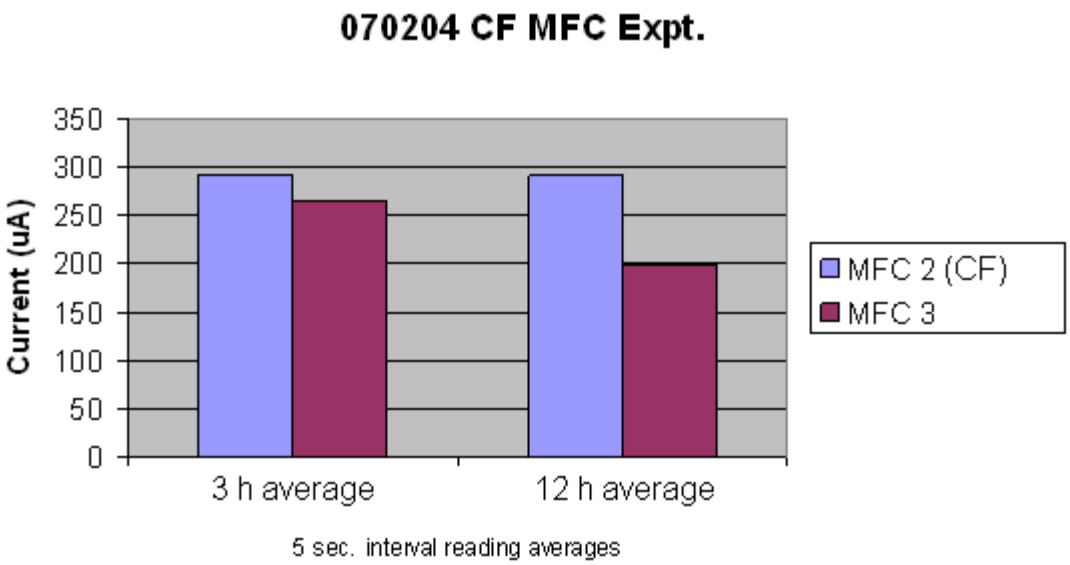

Figure 6-5. Second trial average current with and without addition of micro-scale carbon fibers (CF).

CHAPTER 7
CONCLUSIONS AND FUTURE DIRECTIONS

A sustainable energy infrastructure depends upon increased efficiency and use of renewable sources. Microbial fuel cells can contribute by adding value to byproducts (currently considered waste streams) from various agricultural, industrial and municipal processes. At present, wastewater treatment strategies are energetically and economically costly. MFCs can be used to remove most of the organic material from the wastewater, while providing electricity to run the facility. Wastewater treatment is one prominent example of how MFCs can increase energy efficiency and decrease costs. The processes at breweries, food processing plants, green waste disposal and biofuel processing plants could also be complemented by MFC-based energy recovery from wastes. Solar, wind, geothermal and hydroelectric energy are important components of a comprehensive renewable energy strategy, but all have specific siting requirements and some can only provide intermittent power. MFCs can be run continuously and located virtually anywhere, without requiring sunlight, wind, drilling, or large bodies of water. Depending upon the organisms used, they can be operated at a wide range of temperatures, with many types of fuels.

Despite all of these compelling positive attributes, MFC technology is still in its early stages and is not ready for widespread adoption as part of our energy infrastructure. MFC designs need to be tested at larger scale, cost of materials must be minimized, and power densities need to be increased. Further study is needed of the biological factors that influence MFC power output. Metabolic engineering of microorganisms for use in MFCs can help make generation of electricity with MFCs more practical.

Our study focused on improvement of *E. coli* ATCC 8739 as a biocatalyst for production of electricity in an MFC. We used a cofactor engineering approach to increase the rate and yield

of production of electrons from glucose. Elimination of oxidative phosphorylation lowered the ATP/ADP ratio and led to a 44% increase in the rate of glycolysis. However, transfer of electrons from NADH to oxygen or to the anode (via thionin) was enzyme-limited (by dehydrogenases of the ETS). This caused overflow metabolism (acetate production) and limited the electric current and C_E in the poised potential MFC system. Heterologous expression of $naoX_{Sm}$ provided an alternate electron route from NADH to the terminal electron acceptor. This removed the electron transfer rate limitation and lowered the NADH/NAD^+ ratio, resulting in a 19% increase in current (JC93 versus wild type) and an increase in C_E from 49% to 76%.

Future directions for this research include testing the engineered strains in design-optimized MFCs, further study of expression of extracellular ETS genes, and the metabolic engineering of other MFC biocatalysts (such as DMRB). A poised-potential electrochemical cell allowed us to study processes upstream of the anode without the influence of internal resistance or cathodic overpotentials. It is important to test the engineered strains under non-idealized MFC conditions to see if high rates and yields can be achieved.

Some limitation of current may have occurred in the poised-potential system due to mass transfer limitations. At high current low pH may have affected the electrochemical activity of the bacteria. Reoxidation of thionin may also have become limiting. Coulombic efficiency may have been limited at high current due to diffusion of oxygen (and H_2O_2) into the anolyte from the cathode. Testing the improved strains in an optimized MFC design may help to eliminate concentration overpotentials. In our study, we have shown that supplementation of the anode with mixed length carbon fibers and SWNTs can result in increased current. Optimization of expression of the *omcA-mtrCAB*$_{So}$ genes in the engineered strains may minimize activation overpotentials and enable mediatorless MFC operation with high power densities. Following the

S. oneidensis model, overproduction of flavin electron shuttles may also be beneficial. We investigated the incorporation of an extracellular ETS into an improved *E. coli* MFC biocatalyst. However, our genetic engineering strategy could also be applied to optimization of the metabolism of an exoelectrogen for increased MFC power density and broader fuel range.

REFERENCES

1. **Aelterman, P., K. Rabaey, H. T. Pham, N. Boon, and W. Verstraete.** 2006. Continuous electricity generation at high voltages and currents using stacked microbial fuel cells. Environmental Science & Technology **40:**3388-3394.

2. **Ahmad, M., and V. K. Jindal.** 2006. An automatic procedure for rapid online estimation of raw milk quality. LWT-Food Science and Technology **39:**432-436.

3. **Allen, R. M., and H. P. Bennetto.** 1993. Microbial fuel cells - Electricity production from carbohydrates. Applied Biochemistry and Biotechnology **39:**27-40.

4. **Anderson, D. H., L. J. Donald, M. V. Jacob, and H. W. Duckworth.** 1991. A mutant of *Escherichia coli* citrate synthase that affects the allosteric equilibrium. Biochemistry and Cell Biology-Biochimie Et Biologie Cellulaire **69:**232-238.

5. **Aoki, R., M. Wada, N. Takesue, K. Tanaka, and A. Yokota.** 2005. Enhanced glutamic acid production by a H^+ ATPase-defective mutant of *Corynebacterium glutamicum*. Bioscience Biotechnology and Biochemistry **69:**1466-1472.

6. **Arslan, E., H. Schulz, R. Zufferey, P. Kunzler, and L. Thony-Meyer.** 1998. Overproduction of the *Bradyrhizobium japonicum c*-type cytochrome subunits of the cbb(3) oxidase in *Escherichia coli*. Biochemical and Biophysical Research Communications **251:**744-747.

7. **Babul, J., and V. Guixe.** 1983. Fructose bisphosphatase from *Escherichia coli.* Purification and characterization. Archives of Biochemistry and Biophysics **225:**944-949.

8. **Bapat, P., S. K. Nandy, P. Wangikar, and K. V. Venkatesh.** 2006. Quantification of metabolically active biomass using Methylene Blue dye Reduction Test (MBRT): Measurement of CFU in about 200 s. Journal of Microbiological Methods **65:**107-116.

9. **Behera, M., P. S. Jana, and M. M. Ghangrekar.** 2010. Performance evaluation of low cost microbial fuel cell fabricated using earthen pot with biotic and abiotic cathode. Bioresource Technology **101:**1183-1189.

10. **Beliaev, A. S., D. A. Saffarini, J. L. McLaughlin, and D. Hunnicutt.** 2001. MtrC, an outer membrane decahaem *c* cytochrome required for metal reduction in *Shewanella putrefaciens* MR-1. Molecular Microbiology **39:**722-730.

11. **Bennetto, H. P.** 1990. Electricity generation by microorganisms. Biotechnology Education **1:**163-168.

12. **Bi, C., X. Zhang, J. D. Rice, L. O. Ingram, and J. F. Preston.** 2009. Genetic engineering of *Enterobacter asburiae* strain JDR-1 for efficient D(-) lactic acid production from hemicellulose hydrolysate. Biotechnology Letters **31:**1551-1557.

13. **Bi, C. H., X. L. Zhang, L. O. Ingram, and J. F. Preston.** 2009. Genetic engineering of *Enterobacter asburiae* strain JDR-1 for efficient production of ethanol from hemicellulose hydrolysates. Applied and Environmental Microbiology **75:**5743-5749.

14. **Bochner, B. R., H. C. Huang, G. L. Schieven, and B. N. Ames.** 1980. Positive selection for loss of tetracycline resistance. Journal of Bacteriology **143:**926-933.

15. **Bowman, J. P., S. A. McCammon, D. S. Nichols, J. H. Skerratt, S. M. Rea, P. D. Nichols, and T. A. McMeekin.** 1997. She*wanella gelidimarina* sp. nov. and *Shewanella frigidimarina* sp. nov., novel Antarctic species with the ability to produce eicosapentaenoic acid (20:5 omega 3) and grow anaerobically by dissimilatory Fe(III) reduction. International Journal of Systematic Bacteriology **47:**1040-1047.

16. **Boyer, P. D.** 1993. The binding change mechanism for ATP synthase-Some probabilities and possibilities. Biochimica et Biophysica Acta **1140:**215-250.

17. **Calhoun, M. W., K. L. Oden, R. B. Gennis, M. J. T. Demattos, and O. M. Neijssel.** 1993. Energetic efficiency of *Escherichia coli* - Effects of mutations in components of the aerobic respiratory chain. Journal of Bacteriology **175:**3020-3025.

18. **Campbell, J. E., D. B. Lobell, and C. B. Field.** 2009. Greater transportation energy and GHG offsets from bioelectricity than ethanol. Science **324:**1055-1057.

19. **Causey, T. B., K. T. Shanmugam, L. P. Yomano, and L. O. Ingram.** 2004. Engineering *Escherichia coli* for efficient conversion of glucose to pyruvate. Proceedings of the National Academy of Sciences of the United States of America **101:**2235-2240.

20. **Causey, T. B., S. Zhou, K. T. Shanmugam, and L. O. Ingram.** 2003. Engineering the metabolism of *Escherichia coli* W3110 for the conversion of sugar to redox-neutral and oxidized products: Homoacetate production. Proceedings of the National Academy of Sciences of the United States of America **100:**825-832.

21. **Chang, I. S., H. Moon, O. Bretschger, J. K. Jang, H. I. Park, K. H. Nealson, and B. H. Kim.** 2006. Electrochemically active bacteria (EAB) and mediator-less microbial fuel cells. Journal of Microbiology and Biotechnology **16:**163-177.

22. **Chaudhuri, S. K., and D. R. Lovley.** 2003. Electricity generation by direct oxidation of glucose in mediatorless microbial fuel cells. Nature Biotechnology **21:**1229-1232.

23. **Cheng, S. A., and B. E. Logan.** 2007. Ammonia treatment of carbon cloth anodes to enhance power generation of microbial fuel cells. Electrochemistry Communications **9:**492-496.

24. **Clauwaert, P., P. Aelterman, T. H. Pham, L. De Schamphelaire, M. Carballa, K. Rabaey, and W. Verstraete.** 2008. Minimizing losses in bio-electrochemical systems: the road to applications. Applied Microbiology and Biotechnology **79:**901-913.

25. **Coon, S. L., S. Kotob, B. B. Jarvis, S. J. Wang, W. C. Fuqua, and R. M. Weiner.** 1994. Homogentisic acid is the product of MelA, which mediates melanogenesis in the marine bacterium *Shewanella colwelliana* D. Applied and Environmental Microbiology **60:**3006-3010.

26. **Coursolle, D., D. B. Baron, D. R. Bond, and J. A. Gralnick.** 2009. The Mtr respiratory pathway is essential for reducing flavins and electrodes in *Shewanella oneidensis*. Journal of Bacteriology (Online ahead of print).

27. **Cozzone, A. J., and M. El-Mansi.** 2005. Control of isocitrate dehydrogenase catalytic activity by protein phosphorylation in *Escherichia coli*. Journal of Molecular Microbiology and Biotechnology **9:**132-146.

28. **Cunningham, L., D. Georgellis, J. Green, and J. R. Guest.** 1998. Co-regulation of lipoamide dehydrogenase and 2-oxoglutarate dehydrogenase synthesis in *Escherichia coli*: characterisation of an ArcA binding site in the *lpd* promoter. FEMS Microbiology Letters **169:**403-408.

29. **D'Alessandro, M., P. Turina, and B. A. Melandri.** 2008. Intrinsic uncoupling in the ATP synthase of *Escherichia coli*. Biochimica Et Biophysica Acta-Bioenergetics **1777:**1518-1527.

30. **Datsenko, K. A., and B. L. Wanner.** 2000. One-step inactivation of chromosomal genes in *Escherichia coli* K12 using PCR products. Proceedings of the National Academy of Sciences of the United States of America **97:**6640-6645.

31. **Denfert, C., A. Ryter, and A. P. Pugsley.** 1987. Cloning and expression in *Escherichia coli* of the *Klebsiella pneumoniae* genes for production, surface localization and secretion of the lipoprotein pullulanase. EMBO Journal **6:**3531-3538.

32. **Devillebonne, D., and J. R. Garel.** 1992. A conformational transition involved in antagonistic substrate binding to the allosteric phosphofructokinase from *Escherichia coli*. Biochemistry **31:**1695-1700.

33. **DeVito, J. A.** 2008. Recombineering with *tolC* as a selectable/counter-selectable marker: remodeling the rRNA Operons of *Escherichia coli*. Nucleic Acids Research **36:**e4.

34. **Donald, J. W., M. G. Hicks, D. J. Richardson, and T. Palmer.** 2008. The *c*-type cytochrome OmcA localizes to the outer membrane upon heterologous expression in *Escherichia coli*. Journal of Bacteriology **190:**5127-5131.

35. **Dresselhaus, M. S., and H. Dai.** 2004. Carbon nanotubes: Continued innovations and challenges. MRS Bulletin **29:**237-239.

36. **Du, Z. W., H. R. Li, and T. Y. Gu.** 2007. A state of the art review on microbial fuel cells: A promising technology for wastewater treatment and bioenergy. Biotechnology Advances **25:**464-482.

37. **Dubiel, M., C. H. Hsu, C. C. Chien, F. Mansfeld, and D. K. Newman.** 2002. Microbial iron respiration can protect steel from corrosion. Applied and Environmental Microbiology **68:**1440-1445.

38. **Fan, Y. Z., H. Q. Hu, and H. Liu.** 2007. Enhanced Coulombic efficiency and power density of air-cathode microbial fuel cells with an improved cell configuration. Journal of Power Sources **171:**348-354.

39. **Francetic, O., D. Belin, C. Badaut, and A. P. Pugsley.** 2000. Expression of the endogenous type II secretion pathway in *Escherichia coli* leads to chitinase secretion. EMBO Journal **19:**6697-6703.

40. **Francis, R. T., and R. R. Becker.** 1984. Specific indication of hemoproteins in polyacrylamide gels using a double-staining process. Analytical Biochemistry **136:**509-514.

41. **Futai, M., and H. Kanazawa.** 1983. Structure and function of proton-translocating adenosine triphosphatase (F_OF_1) - Biochemical and molecular biological approaches. Microbiological Reviews **47:**285-312.

42. **Gorby, Y. A., S. Yanina, J. S. McLean, K. M. Rosso, D. Moyles, A. Dohnalkova, T. J. Beveridge, I. S. Chang, B. H. Kim, K. S. Kim, D. E. Culley, S. B. Reed, M. F. Romine, D. A. Saffarini, E. A. Hill, L. Shi, D. A. Elias, D. W. Kennedy, G. Pinchuk, K. Watanabe, S. Ishii, B. Logan, K. H. Nealson, and J. K. Fredrickson.** 2006. Electrically conductive bacterial nanowires produced by *Shewanella oneidensis* strain MR-1 and other microorganisms. Proceedings of the National Academy of Sciences of the United States of America **103:**11358-63.

43. **Gralnick, J. A., and D. K. Newman.** 2007. Extracellular respiration. Molecular Microbiology **65:**1-11.

44. **Harlow, E., and D. Lane.** 1988. Antibodies: A Laboratory Manual. Cold Spring Harbor Laboratory Press, Cold Spring Harbor, NY.

45. **He, S. Y., C. Schoedel, A. K. Chatterjee, and A. Collmer.** 1991. Extracellular secretion of pectate lyase by the *Erwinia chrysanthemi* Out pathway is dependent upon Sec-mediated export across the inner membrane. Journal of Bacteriology **173:**4310-4317.

46. **Hermolin, J., and R. H. Fillingame.** 1995. Assembly of F_O sector of *Escherichia coli* H^+ ATP synthase - Interdependence of subunit insertion into the membrane. Journal of Biological Chemistry **270:**2815-2817.

47. **Hernandez, M. E., A. Kappler, and D. K. Newman.** 2004. Phenazines and other redox-active antibiotics promote microbial mineral reduction. Applied and Environmental Microbiology **70:**921-928.

48. **Higuchi, M., M. Shimada, Y. Yamamoto, T. Hayashi, T. Koga, and Y. Kamio.** 1993. Identification of two distinct NADH oxidases corresponding to H_2O_2-forming oxidase and H_2O-forming oxidase induced in *Streptococcus mutans*. Journal of General Microbiology **139:**2343-2351.

49. **Holmes, D. E., D. R. Bond, R. A. O'Neill, C. E. Reimers, L. R. Tender, and D. R. Lovley.** 2004. Microbial communities associated with electrodes harvesting electricity from a variety of aquatic sediments. Microbial Ecology **48:**178-190.

50. **Jantama, K., M. J. Haupt, S. A. Svoronos, X. L. Zhang, J. C. Moore, K. T. Shanmugam, and L. O. Ingram.** 2008. Combining metabolic engineering and metabolic evolution to develop nonrecombinant strains of *Escherichia coli* C that produce succinate and malate. Biotechnology and Bioengineering **99:**1140-1153.

51. **Jantama, K., X. Zhang, J. C. Moore, K. T. Shanmugam, S. A. Svoronos, and L. O. Ingram.** 2008. Eliminating side products and increasing succinate yields in engineered strains of *Escherichia coli* C. Biotechnology and Bioengineering **101:**881-893.

52. **Jensen, P. R., and O. Michelsen.** 1992. Carbon and energy metabolism of ATP mutants of *Escherichia coli*. Journal of Bacteriology **174:**7635-7641.

53. **Jurtshuk, P., and J. K. Liu.** 1983. Cytochrome oxidase analyses of *Bacillus* strains - Existence of oxidase-positive species. International Journal of Systematic Bacteriology **33:**887-891.

54. **Kajie, S., R. Ideta, I. Yamato, and Y. Anraku.** 1991. Molecular cloning and DNA sequence of *dniR*, a gene affecting anaerobic expression of the *Escherichia coli* hexaheme nitrite reductase. FEMS Microbiology Letters **83:**205-211.

55. **Karu, A. E., Y. Sakaki, H. Echols, and S. Linn.** 1975. Gamma protein specified by bacteriophage Lambda - Structure and inhibitory activity for *recBC* enzyme of *Escherichia coli*. Journal of Biological Chemistry **250:**7377-7387.

56. **Kashefi, K., and D. R. Lovley.** 2000. Reduction of Fe(III), Mn(IV), and toxic metals at 100 degrees C by *Pyrobaculum islandicum*. Applied and Environmental Microbiology **66:**1050-1056.

57. **Katz, E., B. Filanovsky, and I. Willner.** 1999. A biofuel cell based on two immiscible solvents and glucose oxidase and microperoxidase-11 monolayer-functionalized electrodes. New Journal of Chemistry **23:**481-487.

58. **Kelly, I.** 2003. The design of a robotic predator: The SlugBot. Robotica **21:**399-406.

59. **Kim, B. H., H. J. Kim, M. S. Hyun, and D. H. Park.** 1999. Direct electrode reaction of Fe(III)-reducing bacterium, *Shewanella putrefaciens*. Journal of Microbiology and Biotechnology **9:**127-131.

60. **Kim, B. H., H. S. Park, H. J. Kim, G. T. Kim, I. S. Chang, J. Lee, and N. T. Phung.** 2004. Enrichment of microbial community generating electricity using a fuel cell-type electrochemical cell. Applied Microbiology and Biotechnology **63:**672-681.

61. **Kim, G. T., G. Webster, J. W. T. Wimpenny, B. H. Kim, H. J. Kim, and A. J. Weightman.** 2006. Bacterial community structure, compartmentalization and activity in a microbial fuel cell. Journal of Applied Microbiology **101:**698-710.

62. **Kim, Y., L. O. Ingram, and K. T. Shanmugam.** 2008. Dihydrolipoamide dehydrogenase mutation alters the NADH sensitivity of pyruvate dehydrogenase complex of *Escherichia coli* K-12. Journal of Bacteriology **190:**3851-3858.

63. **Koebmann, B. J., H. V. Westerhoff, J. L. Snoep, D. Nilsson, and P. R. Jensen.** 2002. The glycolytic flux in *Escherichia coli* is controlled by the demand for ATP. Journal of Bacteriology **184:**3909-3916.

64. **Kolker, E., A. F. Picone, M. Y. Galperin, M. F. Romine, R. Higdon, K. S. Makarova, N. Kolker, G. A. Anderson, X. Y. Qiu, K. J. Auberry, G. Babnigg, A. S. Beliaev, P. Edlefsen, D. A. Elias, Y. A. Gorby, T. Holzman, J. A. Klappenbach, K. T. Konstantinidis, M. L. Land, M. S. Lipton, L. A. McCue, M. Monroe, L. Pasa-Tolic, G. Pinchuk, S. Purvine, M. H. Serres, S. Tsapin, B. A. Zakrajsek, J. H. Zhou, F. W. Larimer, C. E. Lawrence, M. Riley, F. R. Collart, J. R. Yates, R. D. Smith, C. S. Giometti, K. H. Nealson, J. K. Fredrickson, and J. M. Tiedje.** 2005. Global profiling of *Shewanella oneidensis* MR-1: Expression of hypothetical genes and improved functional annotations. Proceedings of the National Academy of Sciences of the United States of America **102:**2099-2104.

65. **Laemmli, U. K.** 1970. Cleavage of structural proteins during assembly of head of bacteriophage T4. Nature **227:**680-685.

66. **Lee, E. C., D. G. Yu, J. M. de Velasco, L. Tessarollo, D. A. Swing, D. L. Court, N. A. Jenkins, and N. G. Copeland.** 2001. A highly efficient *Escherichia coli*-based chromosome engineering system adapted for recombinogenic targeting and subcloning of BAC DNA. Genomics **73:**56-65.

67. **Liao, J. C., Y. P. Chao, and R. Patnaik.** 1994. Alteration of the biochemical valves in the central metabolism of *Escherichia coli*. Biochemical Engineering VIII **745:**21-34.

68. **Litster, S., and G. McLean.** 2004. PEM fuel cell electrodes. Journal of Power Sources **130:**61-76.

69. **Logan, B., S. Cheng, V. Watson, and G. Estadt.** 2007. Graphite fiber brush anodes for increased power production in air-cathode microbial fuel cells. Environmental Science & Technology **41:**3341-3346.

70. **Logan, B. E.** 2009. Exoelectrogenic bacteria that power microbial fuel cells. Nature Reviews Microbiology **7:**375-381.

71. **Logan, B. E.** 2007. Microbial Fuel Cells. John Wiley & Sons, Hoboken.

72. **Logan, B. E., B. Hamelers, R. Rozendal, U. Schrorder, J. Keller, S. Freguia, P. Aelterman, W. Verstraete, and K. Rabaey.** 2006. Microbial fuel cells: Methodology and technology. Environmental Science & Technology **40:**5181-5192.

73. **Logan, B. E., and J. M. Regan.** 2006. Electricity-producing bacterial communities in microbial fuel cells. Trends in Microbiology **14:**512-518.

74. **Lovley, D. R.** 2006. Bug juice: harvesting electricity with microorganisms. Nat Rev Microbiol **4:**497-508.

75. **Lovley, D. R.** 1993. Dissimilatory Metal Reduction. Annual Review of Microbiology **47:**263-290.

76. **Luli, G. W., and W. R. Strohl.** 1990. Comparison of growth, acetate production, and acetate inhibition of *Escherichia coli* strains in batch and fed-batch fermentations. Applied and Environmental Microbiology **56:**1004-1011.

77. **Malpica, R., B. Franco, C. Rodriguez, O. Kwon, and D. Georgellis.** 2004. Identification of a quinone-sensitive redox switch in the ArcB sensor kinase. Proceedings of the National Academy of Sciences of the United States of America **101:**13318-13323.

78. **Marsili, E., D. B. Baron, I. D. Shikhare, D. Coursolle, J. A. Gralnick, and D. R. Bond.** 2008. *Shewanella* secretes flavins that mediate extracellular electron transfer. Proceedings of the National Academy of Sciences of the United States of America **105:**3968-3973.

79. **Martinez-Morales, F., A. C. Borges, K. Martinez, K. T. Shanmugam, and L. O. Ingram.** 1999. Chromosomal integration of heterologous DNA in *Escherichia coli* with precise removal of markers and replicons used during construction. Journal of Bacteriology **181:**7143-7148.

80. **Matsumoto, J., M. Higuchi, M. Shimada, Y. Yamamoto, and Y. Kamio.** 1996. Molecular cloning and sequence analysis of the gene encoding the H_2O-forming NADH oxidase from *Streptococcus mutans*. Bioscience Biotechnology and Biochemistry **60:**39-43.

81. **Matsushita, K., T. Ohnishi, and H. R. Kaback.** 1987. NADH-ubiquinone oxidoreductases of the *Escherichia coli* aerobic respiratory chain. Biochemistry **26:**7732-7737.

82. **McLachlin, D. T., A. M. Coveny, S. M. Clark, and S. D. Dunn.** 2000. Site-directed cross-linking of b to the alpha, beta, and a subunits of the *Escherichia coli* ATP synthase. Journal of Biological Chemistry **275:**17571-17577.

83. **Miller, K.** 2004. Waste Not. *In* T. Phillips (ed.), NASA News: Technology. Science@NASA.

84. **Mohan, Y., S. M. M. Kumar, and D. Das.** 2008. Electricity generation using microbial fuel cells. International Journal of Hydrogen Energy **33:**423-426.

85. **Nealson, K. H., A. Belz, and B. McKee.** 2002. Breathing metals as a way of life: geobiology in action. Antonie Van Leeuwenhoek International Journal of General and Molecular Microbiology **81:**215-222.

86. **Noda, S., Y. Takezawa, T. Mizutani, T. Asakura, E. Nishiumi, K. Onoe, M. Wada, F. Tomita, K. Matsushita, and A. Yokota.** 2006. Alterations of cellular physiology in *Escherichia coli* in response to oxidative phosphorylation impaired by defective F_1 ATPase. Journal of Bacteriology **188:**6869-6876.

87. **Noji, H., R. Yasuda, M. Yoshida, and K. Kinosita.** 1997. Direct observation of the rotation of F_1-ATPase. Nature **386:**299-302.

88. **Noll, K.** 2006. Microbial Fuel Cells, p. 277-296. *In* N. Sammes (ed.), Fuel Cell Technology. Springer London, London.

89. **Ogasawara, H., Y. Ishida, K. Yamada, K. Yamamoto, and A. Ishihama.** 2007. PdhR (pyruvate dehydrogenase complex regulator) controls the respiratory electron transport system in *Escherichia coli*. Journal of Bacteriology **189:**5534-5541.

90. **Ozaki, Y., T. Suzuki, Y. Kuruma, T. Ueda, and M. Yoshida.** 2008. UncI protein can mediate ring-assembly of c subunits of F_OF_1-ATP synthase *in vitro*. Biochemical and Biophysical Research Communications **367:**663-666.

91. **Patnaik, R., W. D. Roof, R. F. Young, and J. C. Liao.** 1992. Stimulation of glucose catabolism in *Escherichia coli* by a potential futile cycle. Journal of Bacteriology **174:**7527-7532.

92. **Pham, T. H., K. Rabaey, P. Aelterman, P. Clauwaert, L. De Schamphelaire, N. Boon, and W. Verstraete.** 2006. Microbial fuel cells in relation to conventional anaerobic digestion technology. Engineering in Life Sciences **6:**285-292.

93. **Phung, N. T., J. Lee, K. H. Kang, I. S. Chang, G. M. Gadd, and B. H. Kim.** 2004. Analysis of microbial diversity in oligotrophic microbial fuel cells using 16S rDNA sequences. FEMS Microbiology Letters **233:**77-82.

94. **Pitts, K. E., P. S. Dobbin, F. Reyes-Ramirez, A. J. Thomson, D. J. Richardson, and H. E. Seward.** 2003. Characterization of the *Shewanella oneidensis* MR-1 decaheme cytochrome MtrA. Journal of Biological Chemistry **278:**27758-27765.

95. **Posfai, G., M. D. Koob, H. A. Kirkpatrick, and F. R. Blattner.** 1997. Versatile insertion plasmids for targeted genome manipulations in bacteria: Isolation, deletion, and rescue of the pathogenicity island LEE of the *Escherichia coli* O157:H7 genome. Journal of Bacteriology **179:**4426-4428.

96. **Potter, M. C.** 1911. Electrical effects accompanying the decomposition of organic compounds. Proceedings of the Royal Society of London Series B-Containing Papers of a Biological Character **84:**260-276.

97. **Qiao, Y., C. M. Li, S. J. Bao, Z. S. Lu, and Y. H. Hong.** 2008. Direct electrochemistry and electrocatalytic mechanism of evolved *Escherichia coli* cells in microbial fuel cells. Chemical Communications**:**1290-1292.

98. **Rabaey, K., N. Boon, M. Hofte, and W. Verstraete.** 2005. Microbial phenazine production enhances electron transfer in biofuel cells. Environmental Science & Technology **39:**3401-3408.

99. **Rabaey, K., N. Boon, S. D. Siciliano, M. Verhaege, and W. Verstraete.** 2004. Biofuel cells select for microbial consortia that self-mediate electron transfer. Applied and Environmental Microbiology **70:**5373-5382.

100. **Rabaey, K., P. Clauwaert, P. Aelterman, and W. Verstraete.** 2005. Tubular microbial fuel cells for efficient electricity generation. Environmental Science & Technology **39:**8077-8082.

101. **Ringeisen, B. R., E. Henderson, P. K. Wu, J. Pietron, R. Ray, B. Little, J. C. Biffinger, and J. M. Jones-Meehan.** 2006. High power density from a miniature microbial fuel cell using *Shewanella oneidensis* DSP10. Environmental Science & Technology **40:**2629-2634.

102. **Ross, D. E., S. S. Ruebush, S. L. Brantley, R. S. Hartshorne, T. A. Clarke, D. J. Richardson, and M. Tien.** 2007. Characterization of protein-protein interactions involved in iron reduction by *Shewanella oneidensis* MR-1. Applied and Environmental Microbiology **73:**5797-5808.

103. **Sambrook, J., E. F. Fritsch, and T. Maniatis.** 1989. Molecular cloning: A laboratory manual, 2nd ed, vol. I. Cold Spring Harbor Press, Cold Spring Harbor, N.Y.

104. **Sauer, U., F. Canonaco, S. Heri, A. Perrenoud, and E. Fischer.** 2004. The soluble and membrane-bound transhydrogenases UdhA and PntAB have divergent functions in NADPH metabolism of *Escherichia coli*. Journal of Biological Chemistry **279:**6613-6619.

105. **Seitarides, T., C. Athanasiou, and A. Zabanlotou.** 2008. Modular biomass gasification-based solid oxide fuel cells (SOFC) for sustainable development. Renewable & Sustainable Energy Reviews **12:**1251-1276.

106. **Shi, L., B. W. Chen, Z. M. Wang, D. A. Elias, M. U. Mayer, Y. A. Gorby, S. Ni, B. H. Lower, D. W. Kennedy, D. S. Wunschel, H. M. Mottaz, M. J. Marshall, E. A. Hill, A. S. Beliaev, J. M. Zachara, J. K. Fredrickson, and T. C. Squier.** 2006. Isolation of a high-affinity functional protein complex between OmcA and MtrC: Two outer membrane decaheme *c*-type cytochromes of *Shewanella oneidensis* MR-1. Journal of Bacteriology **188:**4705-4714.

107. **Shi, L., S. Deng, M. J. Marshall, Z. M. Wang, D. W. Kennedy, A. C. Dohnalkova, H. M. Mottaz, E. A. Hill, Y. A. Gorby, A. S. Beliaev, D. J. Richardson, J. M. Zachara, and J. K. Fredrickson.** 2008. Direct involvement of type II secretion system in extracellular translocation of *Shewanella oneidensis* outer membrane cytochromes MtrC and OmcA. Journal of Bacteriology **190:**5512-5516.

108. **Shi, L., T. C. Squier, J. M. Zachara, and J. K. Fredrickson.** 2007. Respiration of metal (hydr)oxides by *Shewanella* and *Geobacter*: a key role for multihaem *c*-type cytochromes. Molecular Microbiology **65:**12-20.

109. **Singh, A., M. D. Lynch, and R. T. Gill.** 2009. Genes restoring redox balance in fermentation-deficient *E. coli* NZN111. Metabolic Engineering **11:**347-354.

110. **Sinha, P. K., J. Torres-Bacete, E. Nakamaru-Ogiso, N. Castro-Guerrero, A. Matsuno-Yagi, and T. Yagi.** 2009. Critical roles of subunit NuoH (ND1) in the assembly of peripheral subunits with the membrane domain of *Escherichia coli* NDH-1. Journal of Biological Chemistry **284:**9814-9823.

111. **Smith, J. J., and G. A. McFeters.** 1997. Mechanisms of INT (2-(4-iodophenyl)-3-(4-nitrophenyl)-5-phenyl tetrazolium chloride), and CTC (5-cyano-2,3-ditolyl tetrazolium chloride) reduction in *Escherichia coli* K-12. Journal of Microbiological Methods **29:**161-175.

112. **Sorgen, P. L., T. L. Caviston, R. C. Perry, and B. D. Cain.** 1998. Deletions in the second stalk of F_1F_O-ATP synthase in *Escherichia coli*. Journal of Biological Chemistry **273:**27873-27878.

113. **Steed, P. R., and R. H. Fillingame.** 2009. Aqueous Accessibility to the Transmembrane Regions of Subunit c of the *Escherichia coli* F_1F_O ATP Synthase. Journal of Biological Chemistry **284:**23243-23250.

114. **Tauschek, M., R. J. Gorrell, R. A. Strugnell, and R. M. Robins-Browne.** 2002. Identification of a protein secretory pathway for the secretion of heat-labile enterotoxin by an enterotoxigenic strain of *Escherichia coli*. Proceedings of the National Academy of Sciences of the United States of America **99:**7066-7071.

115. **Tender, L. M., C. E. Reimers, H. A. Stecher, D. E. Holmes, D. R. Bond, D. A. Lowy, K. Pilobello, S. J. Fertig, and D. R. Lovley.** 2002. Harnessing microbially generated power on the seafloor. Nature Biotechnology **20:**821-825.

116. **Thomason, L., D. L. Court, M. Bubunenko, N. Constantino, H. Wilson, S. Datta, and A. Oppenheim.** 2005. Recombineering: Genetic Engineering in Bacteria Using Homologous Recombination, p. 1.16.1-1.16.21. *In* F. M. Ausubel, R. Brent, R. E. Klingston, D. D. Moore, J. G. Deidman, J. A. Smith, and K. Struhl (ed.), Current Protocols in Molecular Biology. John Wiley & Sons Inc., New York.

117. **Thony-Meyer, L., F. Fischer, P. Kunzler, D. Ritz, and H. Hennecke.** 1995. *Escherichia coli* genes required for cytochrome *c* maturation. Journal of Bacteriology **177:**4321-4326.

118. **Unden, G., and J. Bongaerts.** 1997. Alternative respiratory pathways of *Escherichia coli*: Energetics and transcriptional regulation in response to electron acceptors. Biochimica Et Biophysica Acta-Bioenergetics **1320:**217-234.

119. **Underwood, S. A., M. L. Buszko, K. T. Shanmugam, and L. O. Ingram.** 2002. Flux through citrate synthase limits the growth of ethanologenic *Escherichia coli* KO11 during xylose fermentation. Applied and Environmental Microbiology **68:**1071-1081.

120. **Underwood, S. A., S. Zhou, T. B. Causey, L. P. Yomano, K. T. Shanmugam, and L. O. Ingram.** 2002. Genetic changes to optimize carbon partitioning between ethanol and biosynthesis in ethanologenic *Escherichia coli*. Applied and Environmental Microbiology **68:**6263-6272.

121. **Valentini, G., M. Stoppini, M. L. Speranza, M. Malcovati, and G. Ferri.** 1991. Bacterial pyruvate kinases have a shorter N-terminal domain. Biological Chemistry Hoppe-Seyler **372:**91-93.

122. **van Hees, W.** 1965. A bacterial methane fuel cell. Journal of the Electrochemical Society **112:**258-262.

123. **Veit, A., T. Polen, and V. F. Wendisch.** 2007. Global gene expression analysis of glucose overflow metabolism in *Escherichia coli* and reduction of aerobic acetate formation. Applied Microbiology and Biotechnology **74:**406-421.

124. **Vemuri, G. N., E. Altman, D. P. Sangurdekar, A. B. Khodursky, and M. A. Eiteman.** 2006. Overflow metabolism in *Escherichia coli* during steady-state growth: Transcriptional regulation and effect of the redox ratio. Applied and Environmental Microbiology **72:**3653-3661.

125. **Vemuri, G. N., M. A. Eiteman, and E. Altman.** 2006. Increased recombinant protein production in *Escherichia coli* strains with overexpressed water-forming NADH oxidase and a deleted ArcA regulatory protein. Biotechnology and Bioengineering **94:**538-542.

126. **Venkateswaran, K., D. P. Moser, M. E. Dollhopf, D. P. Lies, D. A. Saffarini, B. J. MacGregor, D. B. Ringelberg, D. C. White, M. Nishijima, H. Sano, J. Burghardt, E. Stackebrandt, and K. H. Nealson.** 1999. Polyphasic taxonomy of the genus *Shewanella* and description of *Shewanella oneidensis* sp. nov. International Journal of Systematic Bacteriology **49:**705-724.

127. **Vetter, D., B. J. Andrews, L. Robertsbeatty, and P. D. Sadowski.** 1983. Site-specific recombination of yeast 2-micron DNA *in vitro*. Proceedings of the National Academy of Sciences of the United States of America-Biological Sciences **80:**7284-7288.

128. **von Canstein, H., J. Ogawa, S. Shimizu, and J. R. Lloyd.** 2008. Secretion of flavins by *Shewanella* species and their role in extracellular electron transfer. Applied and Environmental Microbiology **74:**615-623.

129. **Wang, Y. F., S. Tsujimura, S. S. Cheng, and K. Kano.** 2007. Self-excreted mediator from *Escherichia coli* K-12 for electron transfer to carbon electrodes. Applied Microbiology and Biotechnology **76:**1439-1446.

130. **Weber, J.** 2006. ATP synthase: Subunit-subunit interactions in the stator stalk. Biochimica Et Biophysica Acta-Bioenergetics **1757:**1162-1170.

131. **Wilkinson, S.** 2000. "Gastrobots" - Benefits and challenges of microbial fuel cells in food powered robot applications. Autonomous Robots **9:**99-111.

132. **Wilkinson, S.** 2001. Hungry for success - future directions in gastrobotics research. Industrial Robot-an International Journal **28:**213-219.

133. **Willner, I., Y. M. Yan, B. Willner, and R. Tel-Vered.** 2009. Integrated enzyme-based biofuel cells-A review. Fuel Cells **9:**7-24.

134. **Wood, B. E., L. P. Yomano, S. W. York, and L. O. Ingram.** 2005. Development of industrial medium required elimination of the 2,3-butanediol fermentation pathway to maintain ethanol yield in an ethanologenic strain of *Klebsiella oxytoca*. Biotechnology Progress **21:**1366-1372.

135. **Yokota, A., M. Henmi, N. Takaoka, C. Hayashi, Y. Takezawa, Y. Fukumori, and F. Tomita.** 1997. Enhancement of glucose metabolism in a pyruvic acid-hyperproducing *Escherichia coli* mutant defective in F_1 ATPase activity. Journal of Fermentation and Bioengineering **83:**132-138.

136. **Zhang, T., C. Z. Cui, S. L. Chen, X. P. Ai, H. X. Yang, S. Ping, and Z. R. Peng.** 2006. A novel mediatorless microbial fuel cell based on direct biocatalysis of *Escherichia coli*. Chemical Communications**:**2257-2259.

137. **Zhang, X., K. Jantama, J. C. Moore, K. T. Shanmugam, and L. O. Ingram.** 2007. Production of L-alanine by metabolically engineered *Escherichia coli*. Applied Microbiology and Biotechnology **77:**355-366.

138. **Zhao, F., R. C. T. Slade, and J. R. Varcoe.** 2009. Techniques for the study and development of microbial fuel cells: an electrochemical perspective. Chemical Society Reviews **38:**1926-1939.

139. **Zhou, S., L. O. Ingram, K. T. Shanmugam, L. Yomano, T. B. Grabar, and J. C. Moore.** 2006. Materials and methods for efficient lactic acid production. US, Application number 11/501,137.

140. **Zilberstein, D., V. Agmon, S. Schuldiner, and E. Padan.** 1984. *Escherichia coli* intracellular pH, membrane potential, and cell growth. Journal of Bacteriology **158:**246-252.

141. **Zuo, Y., S. Cheng, D. Call, and B. E. Logan.** 2007. Tubular membrane cathodes for scalable power generation in microbial fuel cells. Environmental Science & Technology **41:**3347-3353.

BIOGRAPHICAL SKETCH

Jonathan Moore was born in Concord, Massachusetts in 1974. His family moved to Santa Barbara, California in 1983 and in 1992, Jonathan moved to La Jolla to attend the University of California, San Diego. Jonathan graduated from UC San Diego, Revelle College, with a Bachelor of Arts degree in biochemistry and cell biology in 1996. After receiving his undergraduate degree, Jonathan started a career in the biotechnology industry in the San Diego area. He worked as a researcher at Diversa Corporation until 2003, when his interest in renewable energy led him to join the the laboratory of Dr. Lonnie O. Ingram as a graduate student in the Department of Microbiology and Cell Science at the University of Florida.